Development of Nanosized zeolites for converting Methanol to olefins

BY

Anas Karrar Jamil

A Thesis Presented to the
DEANSHIP OF GRADUATE STUDIES

KING FAHD UNIVERSITY OF PETROLEUM & MINERALS
DHAHRAN, SAUDI ARABIA

In Partial Fulfillment of the
Requirements for the Degree of

MASTER OF SCIENCE

In

CHEMICAL ENGINEERING

April 2014

KING FAHD UNIVERSITY OF PETROLEUM & MINERALS

DHAHRAN - 31261, SAUDI ARABIA

DEANSHIP OF GRADUATE STUDIES

This thesis, written by Anas Karrar Jamil Abdelrahman under the direction his thesis advisor and approved by his thesis committee, has been presented and accepted by the Dean of Graduate Studies, in partial fulfillment of the requirements for the degree of **MASTER OF SCIENCE IN CHEMICAL ENGINEERING.**

A. Al Amer

Dr. Adnan M. Jarallah Al-Amer
(Advisor)

Oki Muraza

Dr. Oki Muraza
(Co-Advisor)

Mozahar Hossain

Dr. Mohammad Mozahar Hossain
(Member)

Shaikh Abdur Razzak

Dr. Abdur Razzak Shaikh
(Member)

Dr. Zuhair Omar Malaibari
(Member)

Dr. Usamah A. Al-Mubaiyedh
Department Chairman

Dr. Salam A. Zummo
Dean of Graduate Studies

17/4/14
Date

This work is dedicated with all my heart to:
My darling mother (Mabroka) and father (Karrar)
Whose sincere prayers, sacrifice, and support made this work possible.
Sisters (Einas, Lina and Elaf) and brother (Othman)
For their motivation and encouragement

ACKNOWLEDGMENTS

I would like to express my acknowledgment to my supervisors, Prof. Adnan M. Jarallah Al-Amer and co-supervisor Dr. Oki Muraza. I would like also to extent my acknowledgment to my MS thesis committee members Dr. Mohammed Mozahar Hossain, Dr. Shaikh Abdur Razzak and, Dr. Zuhair Omar Malaibari as I deeply appreciate their contributions.

My sincere appreciation is also for Dr. Zain Hassan Abdallah Yamani, Director of Center of Research Excellence in Nanotechnology (CENT) and to all scientists, lab team in CENT where the experiments have been performed. I would like to thank the Chairman of Chemical Engineering Department Dr.Usamah A. Al-Mubaiyedh and the entire faculty and staff. I would like to acknowledge the funding provided by King Abdulaziz City for Science and Technology (KACST) through the Science & Technology Unit in Center of Research Excellence in Nanotechnology at King Fahd University of Petroleum & Minerals (KFUPM) for supporting this work as part of the National Science, Technology and Innovation Plan. I thank the project collaborator, Prof. Toshiyuki Yokoi from Tokyo Institute of Technology For the appreciated help and collaborations. I would like to express my sincere gratitude to Dr. Mohammed Mozahar Hossain for his discussions and comments throughout my MS thesis preparation.

My special thanks are given to Mr. Jerwin C. Separa who helped me in the SEM analyses, and Dr. Mohammed M. Hossain and Mr. Abdalwadood for their assistances in the NH3-TPD analysis.

At last but not at least, I would like to acknowledge the full scholarship from King Fahd University of Petroleum and Minerals.

TABLE OF CONTENTS

LIST OF TABLES

LIST OF FIGURES

ABSTRACT

Full Name : [Anas Karrar Jamil Abdelrahman]

Thesis Title : [Development of nanosized zeolites for converting methanol to olefins]

Major Field : [Chemical Engineering]

Date of Degree : [April 2014]

Commercial zeolites used for methanol to olefins (MTO) reaction suffer from serious problems of fast deactivation and poor selectivity. One of the effective methods to overcome these problems is by fabrication of nanoscale high selective catalysts.

To reduce the diffusion limitation in the MTO reaction, nanoscale crystal sizes of one-dimensional pore ZSM-22 zeolite has been developed. The prepared catalysts were characterized and tested in a model reaction with mass-transfer limitation, namely the methanol to olefins (MTO) conversion reaction.

Nanocrystalline zeolite ZSM-22 with TON frameworks have been synthesized using conventional autoclave and microwave assisted hydrothermal methods. The effect of different synthesis parameters, such as crystallization temperature, time, and water content on the crystal size, surface area has been studied. The effect of adding surfactant and co-solvent on the ZSM-22 crystal size, morphology and crystallinity had been studied in details. The synthesized zeolites used in this work were characterized using a variety of methods, including powder X-ray diffraction (XRD), scanning electron microscope (SEM), transmission electron microscope (TEM), N_2 adsorption–desorption

measurements (BET measurement), temperature programmed desorption (TPD) and infra-red Spectroscopy (FT-IR).

The prepared ZSM-22 zeolite was tested for the methanol to olefins reaction (MTO), Weight hourly space velocity (WHSV) of 1.03 g. $g^{-}1.h^{-1}$ was found to be suitable in the MTO reaction, temperature range of 350 - 450 ^{o}C was used; most of the experiments were done at 450 ^{o}C. MTO reaction over ZSM-22 nanocrystals exhibited a high selectivity for propylene and light olefins. At 100% methanol conversion, the selectivity to $C_2^{=}$ - $C_4^{=}$ olefins was 87% with 53% selectivity of propylene. Very low amounts of heavier compounds, paraffin's 4% and heavier olefins 6%, were detected. By reducing the crystal size of ZSM-22 zeolite, deactivation rate can be reduced and high selectivity to propylene can be maintained. ZSM-22 crystal size of 100 nm was almost free of diffusion resistance, 300 nm was in the transition period, while 1000 nm was suffering from serious diffusional problems resulted in high deactivation rates.

ملخص الرسالة

الاسم الكامل: أنس كرار جميل عبدالرحمن

عنوان الرسالة: تطويرالحفازات النانوية لتحويل الميثانول الى الوفينات

التخصص: الهندسة الكيميائية

تاريخ الدرجة العلمية: جمادي الاول ١٤٣٥هـ الموافق / مارس ٢٠١٤م

المواد الحفازة المستعملة في تفاعل تحويل الميثانول الى الوفينات تعاني من مشكلات سرعة الانخماد والافتقار الى الانتقائية المطلوبة للمنتج المراد انتاجه. احدى الوسائل المقترحة لحل هذه المشاكل عن طريق تصنيع حفاز ذو انتقائية عالية وحجم بلورات متناهية الصغر.

تم تطوير مادة حفازة من نوع الزيولايت بخاصية المسام ذات بعد واحد مع التركيز على تصغير حجم البلورة الى المستوى النانوي وبذللك يتم ضمان التخلص من مشكلة محدودية الانتشار اثناء التفاعل الكيميائي. تم اختبار المادة الحفازة المجهزة في تفاعل تحويل الميثانول الى الوفينات.

تم تصنيع المادة الحفزية (ZSM-22) نانوية الحجم عن طريق استعمال الفرن العادي والفرن المحسن باستعمال تقنية الاشعة ذات الموجات القصيرة. تم دراسة تاثير العوامل الموثرة على تصنيع البلورة مثل حرارة وزمن التبلور,كمية الماء المتحوى في البلورة.

تم اجراء دراسة تفصيلية على تاثير عوامل الفعالية السطحية (surfactant) والمذيب المصاحب (co-solvent) على حجم ,شكل, تبلور البلورة الناتجة. تم تطبيق العديد من الاجهزة الوصفية لتحديد خواص بلورة المادة الحفازة (ZSM-22). على سبيل المثال تقنية الاشعة السينية (XRD), المجهر الالكتروني المسحي (SEM) ,المجهر الالكتروني النفاذي (TEM) ,جهاز قياس السطح (BET) وجهازي قياس المواقع الحمضية الكمي (TPD) والنوعي (FT-IR). من خلال اجراء التجارب على المفاعل تم التوصل الى ان معدل التغذية (1.03) هو الانسب. تم اجراء التجارب على درجات حرارة مختلفة في المدى (450-350) درجة مئوية. وجد ان المادة الحفازة نانوية الحجم لها مقدرة اعلى على مقاومة الانخماد اثناء التفاعل مصحوب بي انتقائية عالية تجاه المنتج المطلوب البروبيلين

(propylene). كانت الانتقائية نحو الوفينات (87%) ونحو البروبيلين (% 53), في حين ان الانتقائية نحو المواد الاثقل الغير مرغوبة قليلة جدا (6%). من خلال انموذج ثيلي (Thiele Modulus) تم التوصل الى ان البلورة ذات الحجم الصغير (100 nm) خالية من عوائق الانتشار اثناء التفاعل في حين ان البلورة متوسطة الحجم (300 nm) اظهرت مقاومة اقل والبلورة كبيرة الحجم (1000 nm) تعاني بشكل كبير من مشكلة انتشار المواد المتفاعلة والناتجة في المادة الحفازة وبالتالي معدل اخماد عالي كما هو متوقع.

CHAPTER 1

INTRODUCTION

The catalysts used so far in the existed technologies for converting methanol to light olefins suffer from serious deficiencies. SAPO-34 used in UOP/Hydro MTO (methanol-to-olefins) technology has narrow pore opening combined with large cage inside the crystal, this feature lead to high deactivation rate and selectivity towards ethylene more than higher olefins such as propylene. On other hand, relatively large pore diameter in ZSM-5 catalyst, adopted by Lurgi's MTP (methanol-to-propylene) process, resulted in low selectivity towards olefins [1].

One-dimensional pore zeolites with medium pore opening, such as such as ZSM-12, ZSM-22, ZSM-23, ZSM-48, and ferrierite [2, 4] have been studied for typical shape-selective reactions such as naphtha cracking to produce light olefins like propylene [1]. ZSM-22 is an one-dimensional pore zeolite with pore diameter of 0.46 nm × 0.57 nm [5, 8] classified as medium-pore molecular sieve [4]. The one dimensional pore system and the pore opening size make ZSM-22 highly selective for propylene and produce high propylene / ethylene (P/E) ratio [1].

However, ZSM-22 crystals tend to grow as a bundle of needles with length normally higher than 1μm and high aspect ratio (crystal length/crystal diameter) of 10 [3, 6, 7]. Owing to this lengthy needle-like nature of ZSM-22 crystals, rapid deactivation rate

caused by blocking of pores by the large coke molecules, as consequence mass transfer of reactants and product inside catalyst pore are hampered. The strategy to overcome this rapid deactivation rate is by increasing mass transfer by either fabrication of hierarchical catalyst by making mesoporosity in catalyst crystal or reducing the diffusional conduits. In this work, the focus will be on the second option, which is scaling down the crystal size into nanoscale. Beside the main mass transfer enhancement, product selectivity and catalyst life time will inevitably be improved as consequence of increasing the number of pore mouths.

The aim of this work was to provide insight into how the crystal size of the catalyst used affects the catalyst stability and selectivity. For this purpose, ZSM-22 zeolite was synthesized, characterized and applied in catalytic tests of methanol conversion. While this material is not recognized yet as a commercial MTP catalyst, the one dimensional pore and the pores size of the ZSM-22 zeolite make it potential as a model catalyst in the methanol conversion reaction with high selectivity towards light olefins.

To obtain nanosized ZSM-22 zeolite crystals, various techniques have been adopted. In the first part of this work, we started by using conventional hydrothermal synthesis, variations in parameters such as water content, template concentration, Si/Al ratio and the effect dynamic synthesis have been investigated and highlighted in details. Secondly, the influence of using microwave assisted hydrothermal method, crystal growth inhibiter and crystal growth modifiers have been studied. The properties of synthesized ZSM-22 zeolites have been checked using different techniques such powder X - Ray Diffraction (XRD), scanning electron microscopy (SEM), N2 adsorption - desorption measurements (BET measurement), infrared spectroscopy (FTIR), transmission electron microscope

(TEM), temperature programmed desorption (TPD). The last part of this thesis is dedicated to the catalytic testing of our synthesized nanosized zeolites in methanol to propylene reaction, supported with comprehensive analysis of the crystal size effect via Thiele modulus and deactivation studies.

CHAPTER 2

LITERATURE REVIEW

2.1 Background

Demand on light olefins such as propylene is increasing, while propylene produced by the conventional methods such as steam cracking (SC), fluid catalytic cracking (FCC) and propane dehydrogenation may not be enough to meet the rising demand. Conversion of methanol to olefins with special attention to propylene can be used to increase propylene production.

The cost of light olefins is increasing dramatically and it is expected to continue this trend in the future [2, 3]. These light olefins are used in petrochemical industries such as in polymers manufacturing. Due to the increased demand of polypropylene, there is an increasing a shortage in propylene supply as shown in Figure 2-1. This figure shows that conventional ways (steam and fluid catalytic cracking of relevant hydrocarbon feedstocks) for producing olefins will not be able to meet the demands on propylene in the near future.

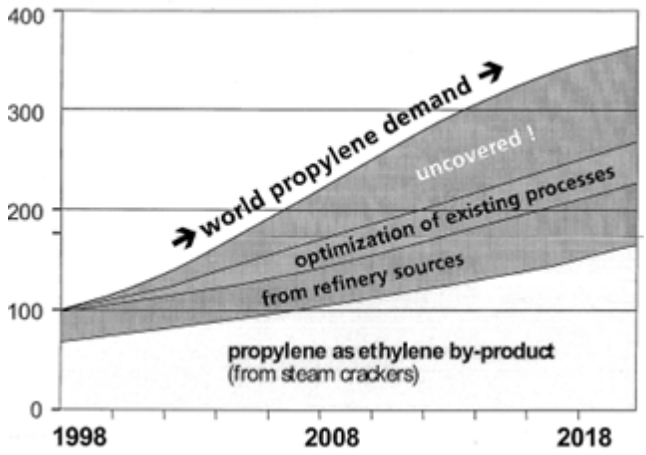

Figure 2-1. Propylene world demand gap [54]

2.2 Methanol production in Saudi Arabia

Saudi Arabia has the largest methanol producer plant Ar-Razi plant produces 1.7 MM mton/year and that represent about 85 % of the methanol produced in the Middle East [4]. Giant companies are contributed in the methanol industry in Saudi Arabia, such as, Mitsubishi Gas Chemicals Co. Inc., Saudi International Petrochemical Company, Japan-Arabia Methanol Company Limited, Saudi International Petrochemical Company (SIPC) and the Saudi Methanol Company.

2.3 Methanol production process

The production of methanol from synthesis gas is a well-established industrial process. Methanol production plant consists from three main parts; in the first section of the plant,

natural gas (methane) is converted into synthesis gas (Syngas) ($CO + H_2$). Secondly, the synthesis gas is converted to methanol. Methanol is purified and hydrogen is recycled.

In a typical plant, methanol production is carried out in two steps. The first step is to convert the feedstock natural gas into a synthesis gas stream consisting of CO, CO_2, H_2O and hydrogen. This is usually accomplished by the steam reforming of natural gas. The second step is the catalytic synthesis of methanol from the synthesis gas. Each of these steps can be carried out in a number of ways and various technologies offer a spectrum of possibilities which may be most suitable for any desired application.

$$CH_4 + H_2O \leftrightarrow CO + 3\,H_2$$

$$CO + 2\,H_2 \leftrightarrow CH_3OH$$

2.4 Methanol to olefins

Historically, the methanol-to-hydrocarbons technology was aimed to produce high quality gasoline. Thereafter, this process was used to produce other types of valuable chemicals such as light olefins. Light olefins discovered as intermediate products in the methanol to gasoline reaction. Thereafter research efforts shifted to producing light olefins instead.

It is well known that methanol demands are low, in the meantime, it is more profitable to convert methanol to high value products. Depending on market demands, methanol can

be converted to either gasoline (MTG) or olefins (MTO), by using different types of catalysts and using optimized operation conditions. The general reaction path of the methanol conversion to hydrocarbons is shown in the reaction below (Equation (2-1) [5].

$$2CH_3OH \overset{-nH_2O/+nH_2O}{\Longleftrightarrow} CH_3OCH_3 \overset{-H_2O}{\longrightarrow} C_2^{=} - C_5^{=} \rightarrow \text{paraffins, aromatics, } C_6^{+} \text{ olefins} \qquad \textbf{(2-1)}$$

In the methanol to hydrocarbon reaction, methanol passes three main steps first it is dehydrated to dimethyl ether (DME) in a reversible reaction. The resulted dimethyl ether (DME) is then further converted to produce light olefins. Finally, the olefins are converted by polycondensation and alkylation reactions to gasoline which is mainly paraffins, aromatics, naphthenes and higher olefins, as shown in Figure 2-2.

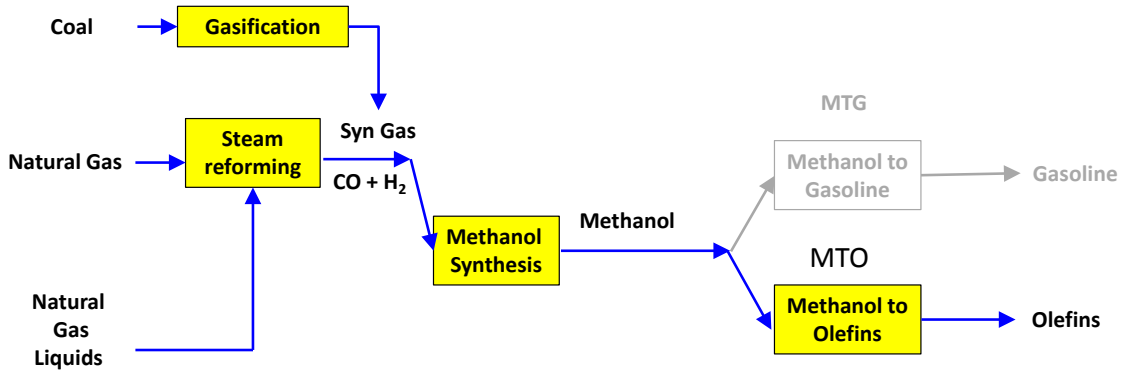

Figure 2-2. Different routes from methanol to hydrocarbons [6].

There are two available technologies used, the first process which is the UOP/Hydro MTO (methanol-to-olefins) technology depends on the product-shape-selective UOP MTO-100 catalyst which is molecular sieve silicoaluminophosphate (SAPO) [6]. The other one is Lurgi's MTP (methanol-to-propylene) process based on catalyst produced by Süd-Chemie, MTPROP (ZSM-5 catalyst) [5]. In general, the advantage of The MTH technology is the flexibility. By changing process conditions and/or the catalysts used,

the products selectivity can be shifted depending on the markets demands the process may produce light alkenes (methanol to olefins– MTO, or methanol to propylene – MTP), or high octane gasoline (MTG) [7].

2.5 Zeolites

Zeolites were discovered by Swedish mineralogist Axel Fredrik Cronstedt [8]. Zeolites are aluminosilicate crystalline materials contain microspores that make them extremely important materials in the modern industries applications. Zeolites consist from the most abundant elements in the earth's crust (Si, Al and O) (see Figure 2-3).

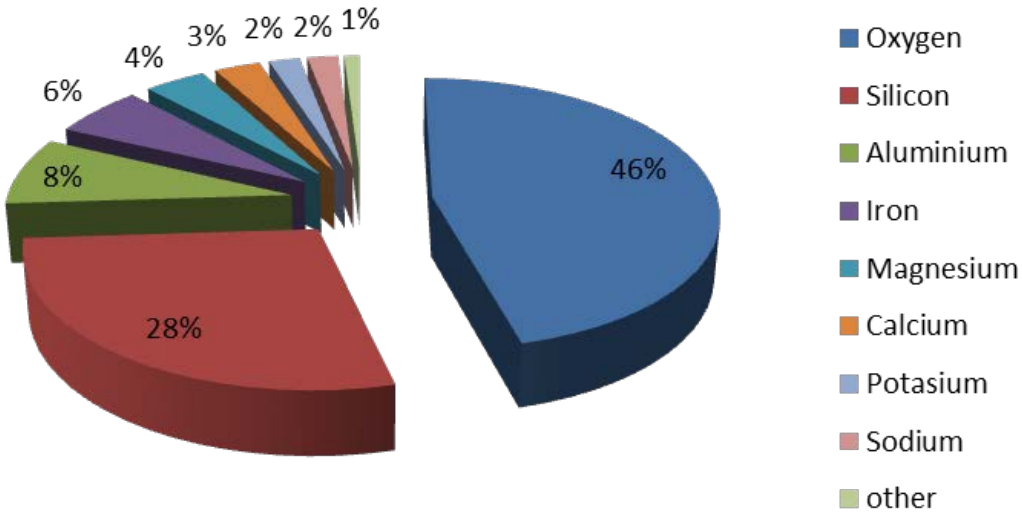

Figure 2-3. Important elements of the earth crust [9].

The elementary building block of the zeolite is the tetrahedral TO_4 where T is either Si or Al atoms. Generally the zeolite can be described by the following formula [8].

$M_{n/m}^{m+}$	$[Si_{1-n}Al_nO_2]$	nH_2O
extraframework cations	Framework	Sorbed phase

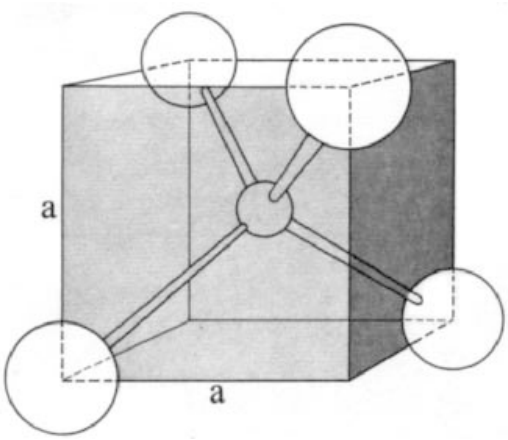

Figure 2-4. Basic structure of zeolite frameworks [10]

Owing to the ability of zeolites to exchange ions, zeolites have tremendous ability as catalyst, adsorbent and ion-exchanger. Another criterion of the zeolitic material is the micropores structure of the crystal resulted in different kind of zeolites topology and hence different industrial applications. What makes zeolites different from other catalysts materials is their pore size uniformity. For each type of zeolite, the pore size is constant. Depending on the pore size zeolite can be classified into three categories; macro-pore with pore size larger than 50 nm, mesopores with 50 nm > pore size > 2 nm and micro-pore with pore size smaller than 2 nm [11]. Based on the pore opening size, zeolite can be classified into three categories; small pore with eight-membered-rings (8 MR), medium pore with ten-membered rings (10 MR) and large pore with twelve-membered-rings (12 MR). These criteria allow zeolites to have the shape selectivity.

Zeolite structure can be described based on smaller units called secondary building units (SBUs). So far, there are about 19 SBUs, as shown in Figure 2-5 below.

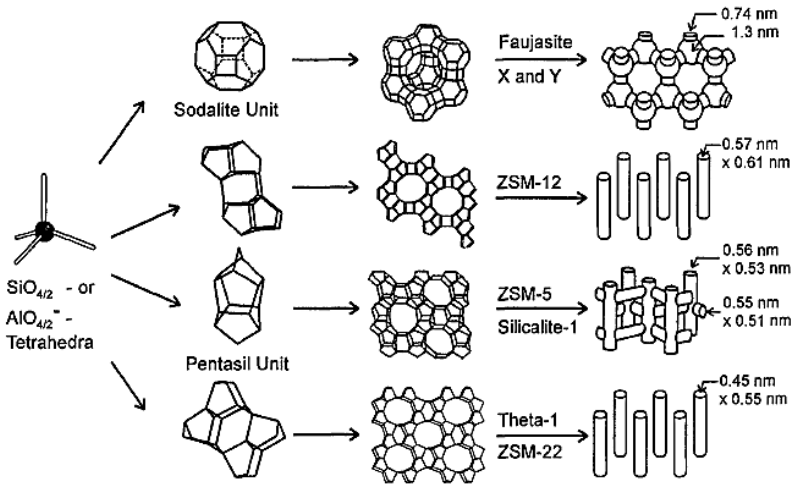

Figure 2-5. Zeolites framework structure and pore size [11].

One of the most important properties of zeolites is their acidity, the zeolite activity and selectivity based on its acidity situation [12], the proper way to describe the zeolite based on the acidity criteria is by determine the acidity type (Lewis or Brønsted), acid cites density, strength distribution and location of these acid cites. As it will be described later many techniques are used to describe our zeolite acidity.

Shape selectivity is other important criteria for zeolites as catalysts and molecular sieves. Shape selectivity could be towards reactant, only reactant with specific kinetic diameter could enter while the other higher reactants are not allowed. The selectivity could also be applied for the products.

Another selectivity based on the diffusional length of the catalyst, reaction where the intermediate product enters in series of reactions could be controlled by increasing or decreasing the diffusional length via tuning the crystal size. With small crystal length, reactant reacts and escapes easily. However, in long channels, the reactant will attracted by many active sites producing other products.

2.6 Synthesis of zeolites

As already well known, zeolites are available in nature and already widespread uses. However the need for zeolites with specific criteria like pore size, surface area crystal size required some kind of intervention. Fundamental steps for synthesizing zeolites crystals [10]: reactant mixture, nucleation and crystal growth.

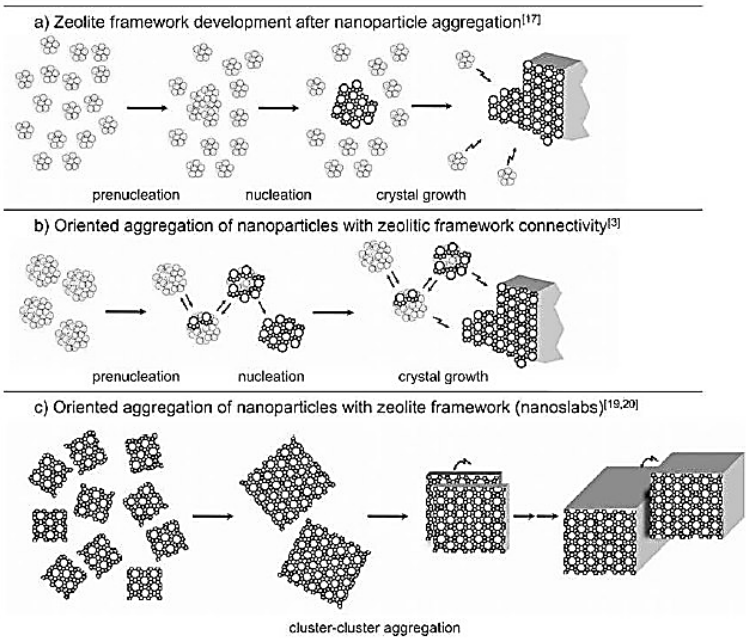

Figure 2-6. Fundamental steps for synthesizing zeolites crystals [13].

Figure 2-6 and Figure 2-7 explain more the aforementioned zeolites synthesis steps and describe how the zeolite crystal is formed. The reactant mixtures affected by the following variable in the synthesis of zeolites [10]: temperature, alkalinity (pH) and chemical composition.

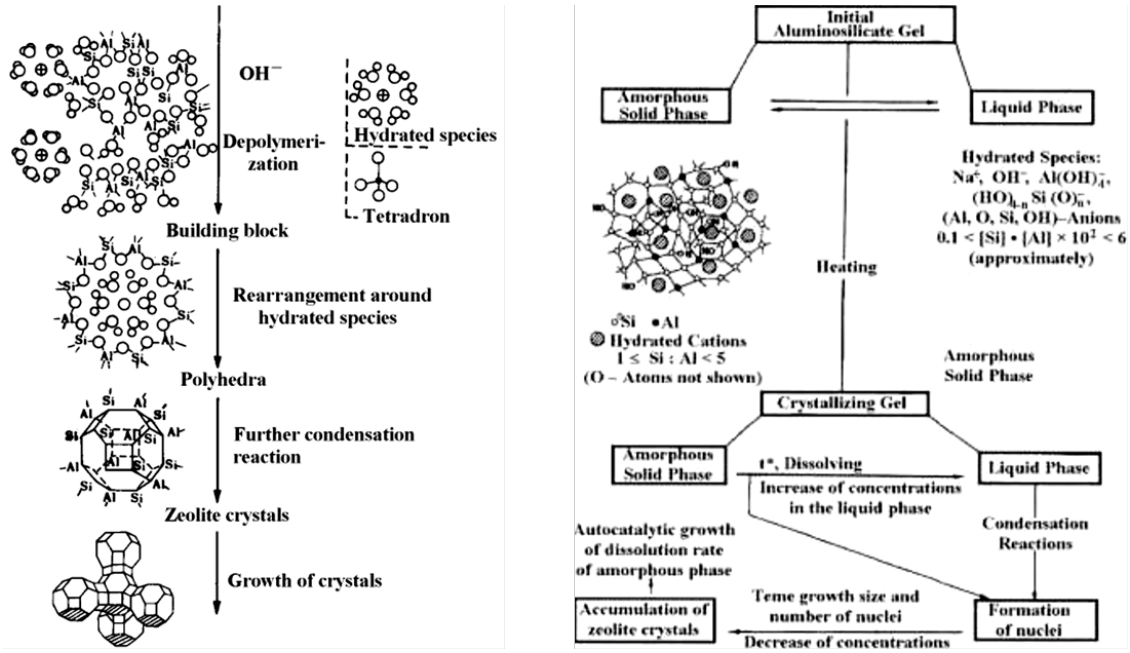

Figure 2-7. Schematic illustrations of the solution-mediated transport.[10]

2.7 Molecular Sieves

The main characteristic of molecular sieves used in methanol to olefins is the pore opening of zeolites, which is small enough to set shape selectivity towards products. The small-pore molecular sieves studied in the MTO process can be classified into three categories depending on their pore opening sizes, (a) small pore openings, less than 0.45 nm, such as chabazite, erionite, zeolite T, ZK-5, ZSM-34, zeolite A, SAPO-17, SAPO-34, and SAPO-44, (b) medium pore openings, 0.5 to 0.6 nm, such as ZSM-5, ZSM-11, ZSM-48 and EU-2 and (c) large pore opening, greater than 0.6 , such as mordenite, X and Y zeolite, SAPO-5, MeAPO-5, and MAPO-5. Zeolites such as, Offretite, Zeolite T, ZSM-34 and clinoptilolite, with pores partially blocked by large cations or structural dislocations show sorption properties similar to those with small-pore openings less than 0.45 nm [14].

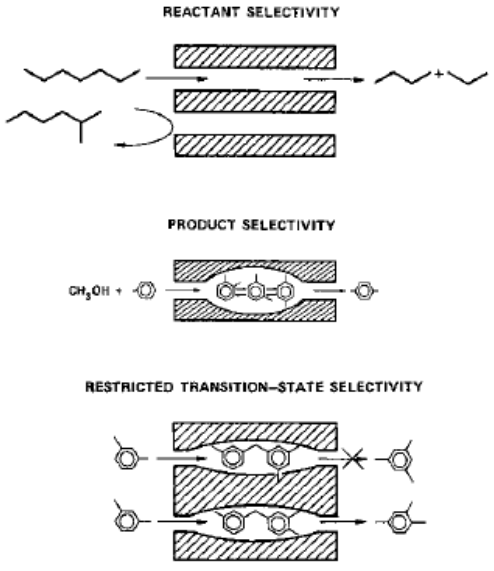

Figure 2-8. Different shape selectivities of molecular sieves [8].

Molecular sieves pore openings are smaller than the kinetic diameter of branched and aromatic molecules, but large enough to permit the access of linear molecules.

Figure 2-8 demonstrates the concept of molecular sieves shape selectivity. Hence only alcohols, normal alkanes (linear paraffins) and normal alkenes (olefins) are handled but no aromatics, branched alkanes and alkenes (isomers) can either diffuse in or diffuse out.

2.8 One-dimensional pore system with 10-member ring zeolites

In this section we describe 10-ring zeolites, medium-pore size molecular sieve that can be used in conversion of methanol to hydrocarbons. This group of zeolites have Constraint Index (CI) about 1-12 [15]. Figure 2-9 shows three different sizes of pore openings, small pore size with 8-rings, example of this classification is zeolite A, medium pore size with10-rings, ZSM-5 is the most famous member of this group and finally the large pore opening with 12-rings such as zeolite X and Y as shown in Figure 2-9. Beside aluminosilicate zeolites, medium pore group includes metallosilicates, such as silicoaluminophosphates SAPOs [15] such as SAPO-11, SAPO-31, and SAPO-41[16]. More descriptions about one dimensional pore zeolites with different topologies and pore openings are described in details in Appendix A .

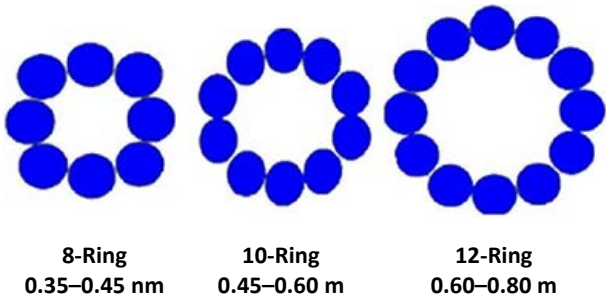

Figure 2-9. Examples of different zeolites pore openings [17].

Medium pore zeolite can have 3D pore opening system in which pores intersect with each other such as ZSM-5 [18], ZSM-11 [19], and MCM-22 [20]. Also medium pore zeolites can be one-dimensional pore system without intersection among the pores conduits, examples of this group include ZSM-22 [21], ZSM-23 [22], ZSM-35 [23], ZSM-57 [24], ferrierite [25], and ZSM-48 [26].

We will focus on the one-dimensional pore zeolites with 10-ring pore opening, as it includes our proposed catalyst. 10-ring pore opening classified as medium pore size with opening in the range of 0.5 to 0.7 nm [15]. These openings allow molecules such as n-hexane, 3-methylpentane, benzene and p-xylene to be adsorbed inside the pore freely [15].

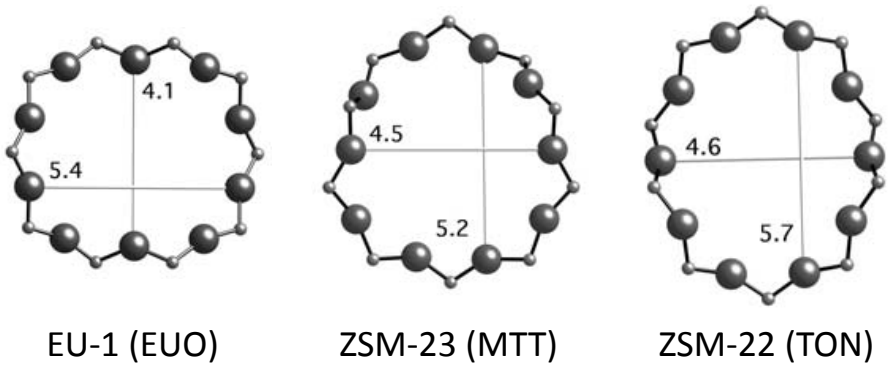

Figure 2-10. Some important 10-ring one-dimensional zeolites [17].

On other hand, very small amounts of aromatics were detected when using these 10-ring one-dimensional pore zeolites this property help a lot in producing environmental friend gasoline [15]. Some of the 10-ring one-dimensional pore zeolites catalytic applications are summarized Figure 2-10 and Table 2.8-1.

Table 2-1. List of some one-dimensional 10-member ring zeolites and examples of their applications.

Zeolite	Ring shape	Main channel (nm)	Unit Cell (T-atoms)	Maximum diameter [a] (nm)	Application	Ref
ZSM-22 (TON)	elliptical	0.46 × 0.57	24	0.571	hydro-isomerization	[27-30]
					hydrocracking	[21, 31]
					crude oil catalytic dewaxing	[32]
					naphtha catalytic cracking	[33]
					isomerization of xylene	[28]
					olefins cracking	[34]
ZSM-23 (MTT)	teardrop	0.45 × 0.52	24	0.619	isomerization of xylene	[28]
					C_4 alkanes Catalytic cracking	[35]
					Alkylation of aromatic	[36]
					olefins cracking	[34, 37]
ZSM-48 (MRE)	cylindrical	0.53 × 0.56	24	0.636	hydro-isomerization	[38]
					catalytic de-waxing	[39]
					methanol to olefins	[40]
					olefins cracking	[37, 41]

EU-1 (EUO)	zig-zag	0.41 × 0.54	112	0.700	catalytic dewaxing	[42]
					hydroconversion	[43]
					isomerization of aromatics	[28, 44]
					catalytic cracking	[42]
					hydrodesulphurization, hydrodenitrification	[42]

[a] Maximum diameter of a sphere that can be included inside the largest opening

2.9 ZSM-22

ZSM-22 is a medium-pore zeolite with high silica to alumina ratio. The framework consists of 5, 6- and 10-rings with TON framework. The TON framework family includes ZSM-22, Theta-l, Nu-10, KZ-2, and ISI-1 [45-47]. The pore structure of ZSM-22 with TON framework is linear one-dimensional (non-interconnecting) with 10-membered ring openings with effective pore size of 0.46×0.57 nm, which is smaller than the pore size of ZSM-11 and ZSM-5, [21, 48, 49]. Figure 2-11 below show the unit cell of ZSM-22 as drawn by Materials Studio 6.0.

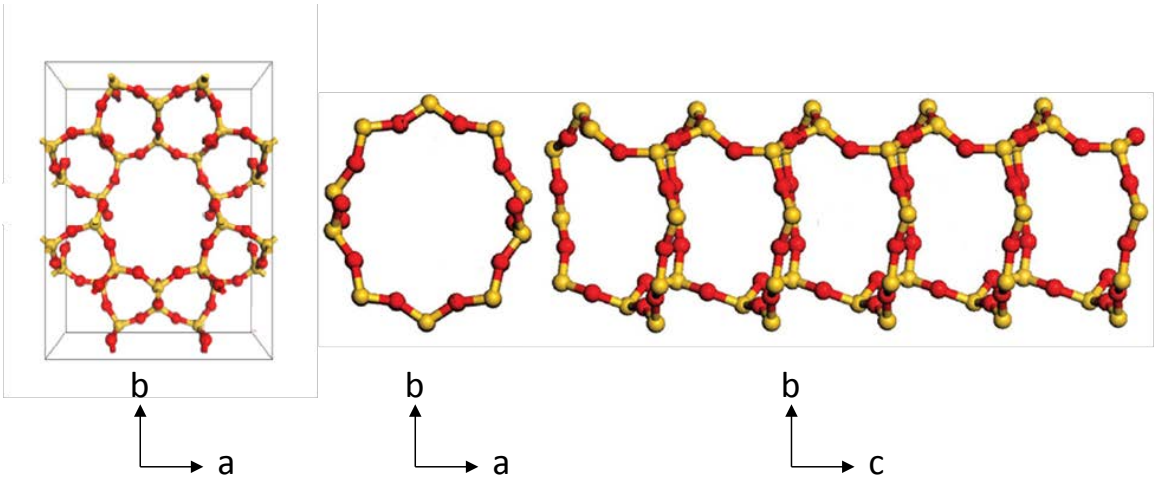

Figure 2-11. ZSM-22 crystal unit cell structure.

Because of ZSM-22 shape selectivity, it has high potential for many shape selective reactions such as isomerization [27-30], hydrocracking [21, 31], dewaxing of the crude oil [32], naphtha cracking [33] and methanol-to-olefins [50] (see Table 2.8-1).

2.10 Mass transport inside the catalyst

In heterogeneous catalysis, catalyst pellets are usually porous solids, in order to increase active sites and surface area available for reaction and adsorption. Molecules of reactants or products have to penetrate via external resistance of the layer around the pellet and then diffuse in and out from the catalyst crystal as shown in Figure 2-12.

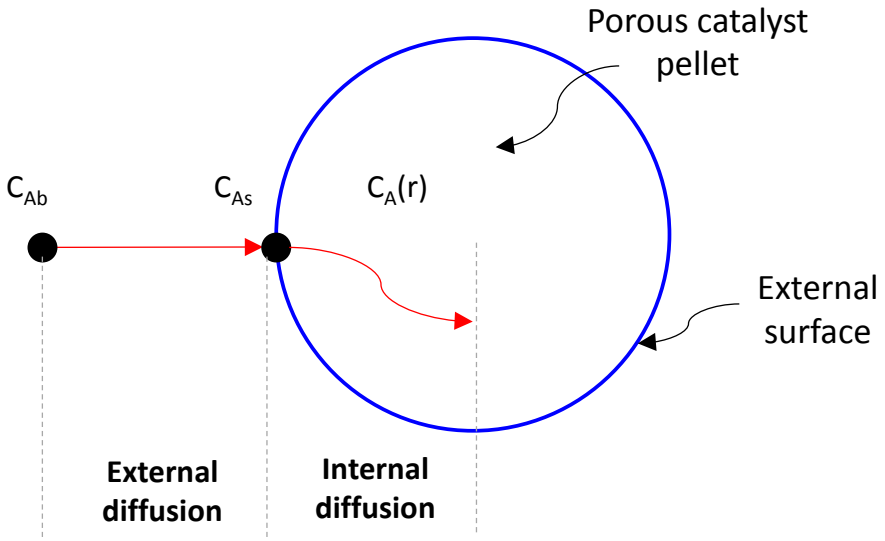

Figure 2-12. Reaction steps for a catalyst pellet [51]

Figure 2-12, shows the main reaction steps in heterogeneous catalysis. Unless the temperature is very low, diffusion of molecules inside the catalyst pellets is the responsible from obstructing the reaction rate [52]. High temperature stimulates pressure difference across pore insuring the mass flow [52].

Dimension of the pore opening determine the type of molecules diffusion. For the case of very large pore diameter in comparison with the diffusing molecules, molecules transportation is mainly governed by molecule-molecule collision since the probability of

collusions among the molecules is by far higher than collisions with pore wall. With small opening the diffusion is governed by collusion between molecules and the pore wall, this case is called Knudsen diffusion. In the case of very narrow pore opening molecules diffuse via configuration diffusion as shown in Figure 2-13.

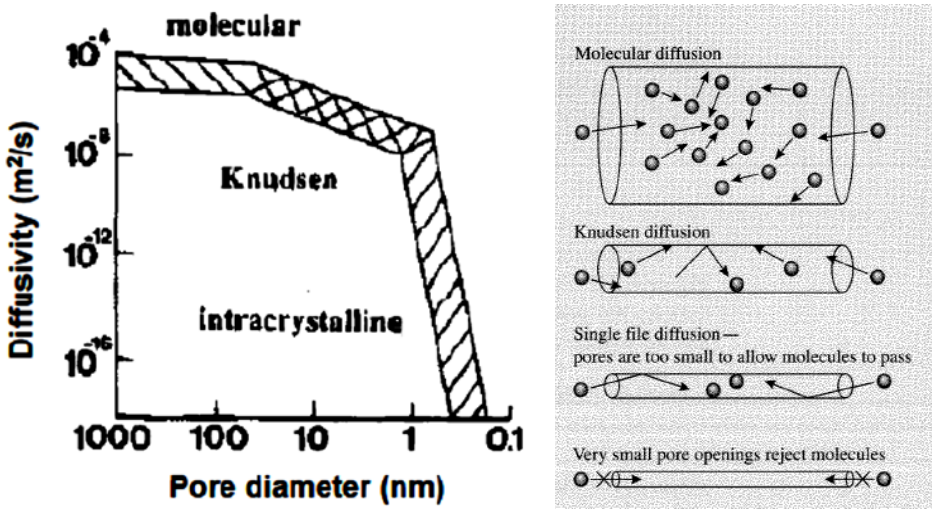

Figure 2-13. Relation between pore diameter and typical diffusivities illustrating diffusion regimes[51].

The pores inside the catalyst are not as simple as shown in Figure 2-13 . However, they are arbitrary zigzagged with varied cross section areas (see Figure 2-14); an effective diffusion coefficient is needed to calculate the average diffusion.

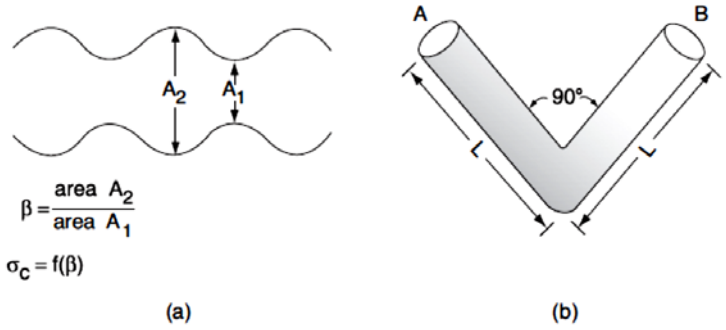

Figure 2-14.(a) Pore constriction; (b) pore tortuosity [51].

$$D_e = \frac{D_{AB}\phi_p\sigma_c}{\tilde{\tau}} \quad \textbf{(2-2)}$$

Where:

$$\tilde{\tau} = \text{tortusity} = \frac{\text{Actual distance a molcule travels between two points}}{\text{Shortest distance between those two points}}$$

$$\phi_p = pellet\ porosity = \frac{Volume\ of\ void\ space}{Total\ volume(voids\ and\ solids)}$$

σ_c = constriction factor

Thiele modulus (ϕ_n) is used to determine whether the reaction is limited by the internal diffusion or the reaction kinetics.

The quantity ϕ_n^2 is a measure of the ratio of "a" surface reaction rate to "a" rate of diffusion through the catalyst pellet:

$$\phi_n^2 = \frac{K_n R^2 C_{As}^{n-1}}{D_e} = \frac{\text{"a" } surface\ reaction\ rate}{\text{"a" } diffusion\ rate} \quad \textbf{(2-3)}$$

As it is clear from Equation (2-3) [53], internal diffusion is the limiting step when the Thiele modulus (ϕ) is large (> 4) [53]. On the other hand, the reaction is limited by the surface reaction when the Thiele modulus (ϕ) is small (< 0.4) [53].

Internal Effectiveness Factor indicate the how internal diffusion and surface reaction limiting the reaction rate [53]:

$$\eta = \frac{\text{Actual overall rate of reaction}}{\begin{array}{c}Rate\ of\ reaction\ that\ would\ result\ if\ entire\ interior\ surface \\ were\ exposed\ to\ the\ external\ surface\ conditions\end{array}} \quad \textbf{(2-4)}$$

Table 2-2. Influence of catalyst pellet shape on the effectiveness factor [53].

Pellet shape	Internal Effectiveness Factor (η)
Sphere	$\eta = \frac{1}{\phi}\left[\frac{1}{\tanh 3\,\phi} - \frac{1}{3\,\phi}\right]$
Cylinder	$\eta = \frac{1}{\phi}\frac{I_1(2\phi)}{I_0(2\phi)}$
Slab	$\eta = \frac{\tanh\ \phi}{\phi}$

2.11 Deactivation

As mentioned earlier, small-pore molecular sieves have high selectivity for linear small hydrocarbons, however, this selectivity lead to drawback of relatively rapid deactivation during the reaction. The big cavities inside zeolite are accused to be responsible for this rapid deactivation. The reason for that is because of the shape selectivity properties, aromatic and branched compounds that formed inside those big cavities cannot diffuse back because of their large kinetic diameters in comparison with pore-opening size. As a result, those large molecules isolate active sites by forming carbonaceous deposits. Hence, deactivation by coke may be by both depositing on the acid sites as well as blockage of pore openings. It is also important to note that the rate of deactivation is directly proportional to catalyst acidity. In some cases, deactivation by coke may be permanent due to structural degradation during regeneration. The selectivity toward light olefins and olefins /aromatic ratio on the medium opening pore zeolites catalysts, ZSM-

11, ZSM-48 and Zeolite EU-2 were relatively high in comparison with ZSM-5, yet their deactivation rate is extremely rapid [1, 42, 54]. This highly deactivation rates hamper the catalytic performance of the medium pore size one dimensional zeolites like ZSM-22 and make the reaction controlled by the diffusional resistance [7].

2.12 Kinetics models of MTH reaction

Kinetics of the reaction needs to be studied carefully, since it determines which catalyst is suitable based on many variables. Several models have been proposed to explain the shape selectivity of zeolites for methanol to hydrocarbons reaction.

2.12.1 Dessau's MTH reaction mechanism

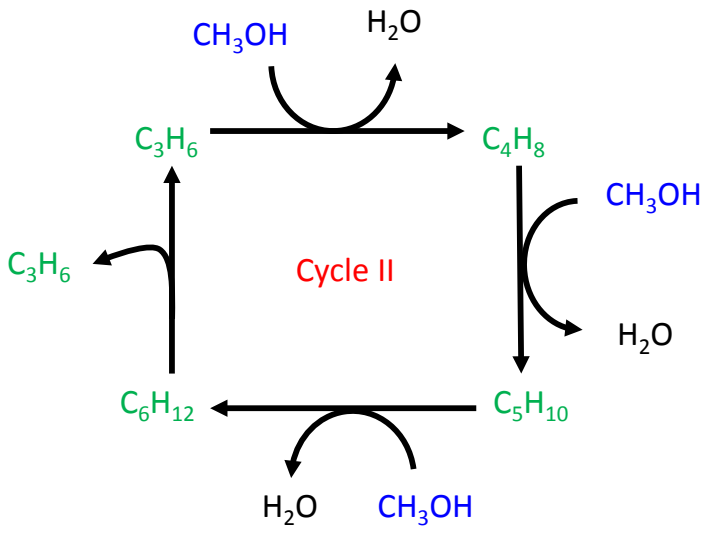

Figure 2-15. Dassau's mechanism [55].

According to this mechanism, trace amounts of impurities could start up the MTH reaction. Those impurities could be in the methanol feed, in the carrier gas or in the solid

catalyst itself [56]. In this mechanism the reaction is co-catalyzed by the presence of alkenes [57, 58]. Alkene molecule is methylated repeatedly by methanol molecules and forms larger alkenes which then undergo cracking reaction. The cracking products may either reacts again with methanol or desorb from the catalyst. However, this mechanism does not explain the appearance of aromatics in the products.

2.12.2 Hydrocarbon pool mechanism

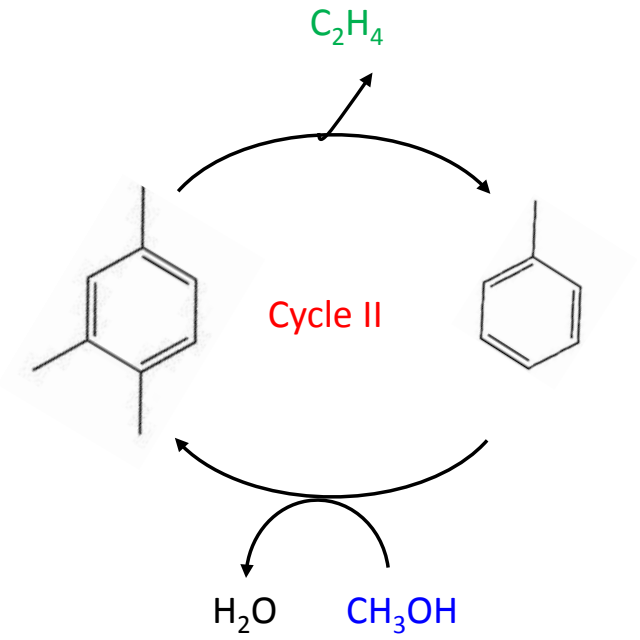

Figure 2-16. Hydrocarbon pool mechanism [55].

Trapped large organics form a hydrocarbon pool which act as a catalytic scaffold. As shown in Figure 2-16, the trapped aromatics, are mainly methylated benzene molecules (polymethylbenzenes) act as reaction centers for the MTH reaction [55]. These species are methylated repeatedly with methanol molecules to produce light alkene, mainly

ethylene and propylene. Depending on the catalyst topology different aromatic species can act as hydrocarbon pool species [59, 60]. Hence, the activity of the methylbenzene hydrocarbon pool species is also dependent on the catalyst topology. It is important to note that the alkenes formed from the hydrocarbon pool are controlled by the identity of the methylbenzene intermediate involved. Narrow pores H-ZSM-5 zeolite enforced them to contain the lower methylbenzenes as active intermediates than the higher methylbenzenes [61, 62] which favor producing mainly ethylene and some of propylene [61]. Ethylene would be formed from converting trimethylbenzenes to methylbenzenes (see Figure 2-16). For catalysts such as H-SAPO-34 and H-Beta that have large space enough to form the higher methylbenzene intermediates such like penta and hexamethylbenzene, propene and butenes are favored to form [62].

Figure 2-17. Hexamethylbenzene and pentamethylbenzene

Note that the accessibility/activity of the hydrocarbon pool species decreases with increasing catalyst deactivation, and they will transform into deactivation products.

2.12.3 Mixed mechanism (dual cycle concept)

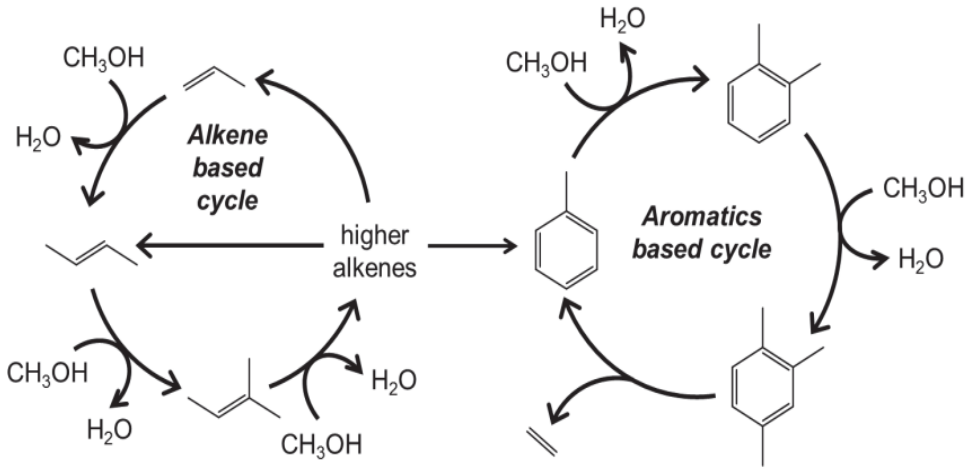

Figure 2-18. Cycle I: Hydrocarbon pool mechanism, Cycle II: Dessau's mechanism [63].

Both mechanisms operate simultaneously, cycle I produces ethane while cycle II produces C3+ alkenes, with minor amounts of ethylene. [55] dual cycle mechanism is explain the methanol conversion over ZSM-5[55, 63].

Unlike ZSM-5, SAPO-34, and beta catalysts, the space in the H-ZSM-22 catalyst channels preventing the formation of aromatic compounds those are required for hydrocarbon pool mechanism. Specific catalyst topology favors specific product(s) formation via alkene cracking and methylation. Hence, understanding variables that govern the reaction selectivity is vital for selectivity control. Reaction mechanism is highlighted as one parameter that controls selectivity in the MTH reaction over zeolite material.

2.13 ZSM-22 zeolite as a MTO catalyst

Until recent years, ZSM-22 (TON) was believed to be inefficient catalyst for methanol to olefins reaction [64-66]. The narrow space inside pores of ZSM-22 crystals was believed insufficient for relatively large molecules that were responsible from stimulating hydrocarbon pool mechanism [64, 67].

On other hand, other researchers reported that ZSM-22 is a light olefins producers via methylation cracking mechanism (Dassau's mechanism) [55, 68-70].

2.13.1 Olefins selectivity

ZSM-22 has only one dimensional 10 member ring channels with no intersections and the largest space which ZSM-22 can offer is 0.57 × 0.46 nm [49].

Considering the channel of ZSM-22 was too narrow for the reaction following the mechanism of hydrocarbon pool, the methanol conversion more possibly went through the olefin methylation and cracking route, hence high selectivity towards propylene combined with low yield of ethylene in comparison [71]. However, it is reported that ZSM-22 have high selectivity towards heavy olefins like pentene and hexene without any selectivity towards aromatics [70]. Possible explanation for that is the conventional ZSM-22 crystal length long enough for the formation of higher olefins via the olefins methylation reaction.

2.13.2 Effect of zeolite topologies in MTO reaction

Methanol conversion may follow aromatic based hydrocarbon pool mechanism and or olefin methylation-cracking mechanism depends on the topology of the catalyst used. The main reaction mechanism over SAPO-34 and ZSM-12 is the hydrocarbon pool [67]. In ZSM-5, the methanol conversion both follow the hydro-carbon pool mechanism and the olefin methylation-cracking route. Aromatics or olefins addition could improve the methanol conversion following hydrocarbon pool mechanism or methylation-cracking route respectively [65]. For ZSM-22, the tubular shape of the pores suppresses the hydrocarbons pool mechanism allowing methylation-cracking route to dominate. **Error! Reference source not found.** below illustrate topology of some zeolites used in methanol to olefins reaction.

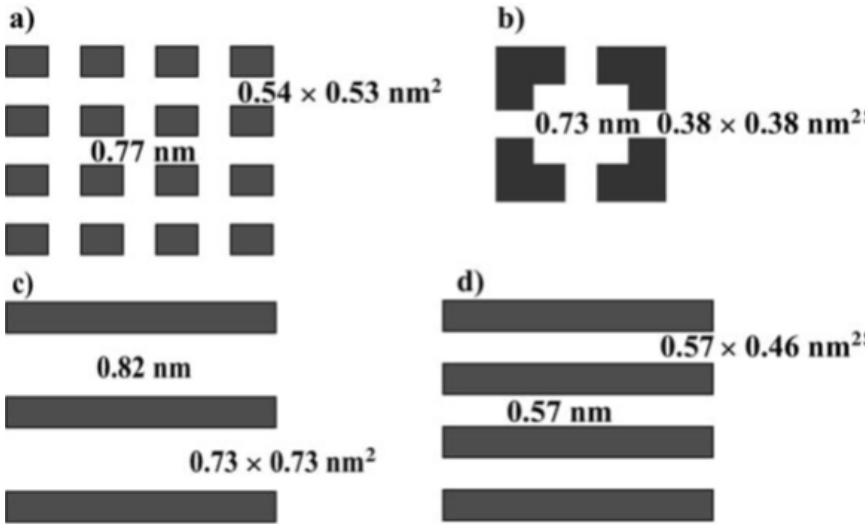

Figure 2-19. Illustration of zeolite pore structures: (a) MEL structure of ZSM-11; (b) CHA structure of SAPO-34; (c) AFI structure of SAPO-5; and (d) TON structure of ZSM-22 [33].

2.13.3 ZSM-22 zeolite acidity

The weak and medium acid sites usually assigned as silanol groups ” Brønsted acidity” at the external surface or at lattice defects and OH groups bonded to the extra-framework aluminum species [67]. The strong acid ”Lewis acidity” resulted from the framework tetrahedral aluminum species [67]. Some of the olefins were produced over ZSM-22 due to acid cites (Brønsted acidity) on the external surfaces and the pore mouth of ZSM-22 crystal [72, 73] via the hydrocarbon pool mechanism [72, 73]. However it is suggested by Teketel et al. that the aforementioned hydrocarbon pool mechanism does not work inside ZSM-22 crystal pores [55].

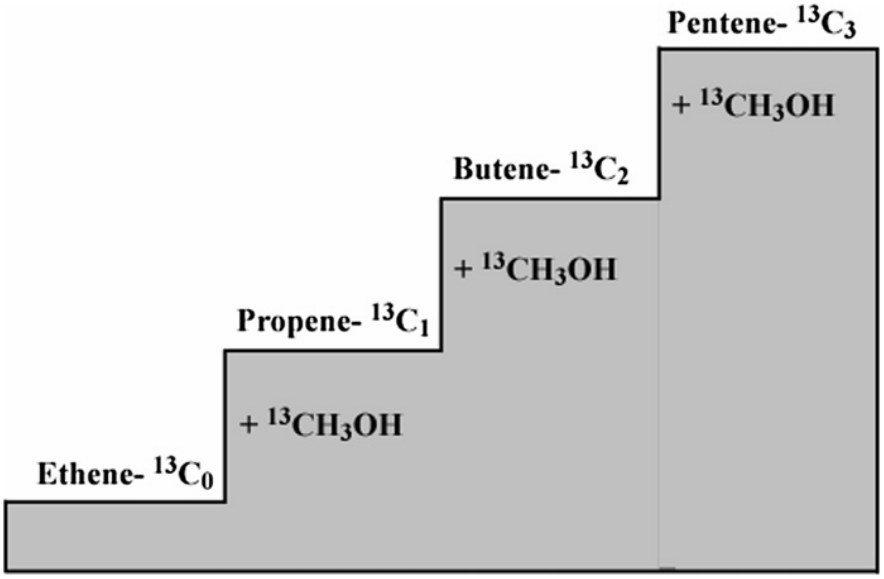

Figure 2-20. Schematic illustration of ethylene homologation sequence [32].

In MTO reaction Brønsted acidity is responsible from dehydration reactions, as well as Homologation and methylation of olefins as shown in Figure 2-20 [67], on other hand Lewis acidity is responsible from cracking of larger olefins into light olefins.

2.13.4 Deactivation of ZSM-22 zeolite crystals

ZSM-22 zeolite with only 1-dimensional channels that are easy to be blocked by the coke species [72]. As consequence of that, active sites accessibility and mass-transport are decreased resulted in higher deactivation rates compared to ZSM-5. With coke deposition, the stronger acidic sites were easier to be covered by the coke and as a result the cracking of higher olefins was suppressed [65]. These were responsible for the increase in heavier olefin production, the low efficiency in methanol conversion and the production of lighter olefin.

ZSM-5 cannot provide enough spaces for the formation of coke species larger than tetra-methylbenzenes, and this was believed to be the reason of the long life time of ZSM-5 for methanol conversion [63, 70, 74, 75]. ZSM-22 has pore size similar to ZSM-5. However ZSM-22 deactivated quickly in comparison with ZSM-5 and this probably due to the 3-D pore structure of ZSM-5 [72].

Deactivated H-ZSM-22 contains lower coke species in comparison with the similar one-dimensional zeolite H-ZSM-12 [67], hence, we can postulate from the zeolites pore shapes and sizes that the coke ”aromatics molecules” deposited on the pore mouth of ZSM-22 crystal and crystal surface. Even aromatic species like toluene can be methylated to produce trimethylbenzene over the surface of the deactivated ZSM-22 crystals which is likely can’t be produced inside the pore [67]. Supporting to our hypothesis Li et al. related the fast deactivation of ZSM-22 crystals on MTO reaction due to the pore blocking by coke species [70] this hypothesis is in agreement with Wei et al. results [73].

2.14 Synthesis of conventional ZSM-22 zeolite

Conventional ZSM-22 is needle-like shape crystals with one-dimensional channels (ca. 0.46- 0.57 nm aperture) oriented along the [001] direction [47, 49], and with the particles size in the range of 0.5- 2 microns [33, 76, 77]. The performance of ZSM-22 as shape-selective catalysis in the oil refinery and petrochemicals industries depends mainly on their crystal size, morphology (length/diameter). Conventional ZSM-22 has a severe diffusion resistance and to overcome this problem both crystal length and aspect ratio should be decreased.

The required crystallization time for conventional hydrothermal synthesis of ZSM-22 is longer than 48 h [28, 30, 33, 78]. Fast synthesis can be achieved by using microwave as a heating source of for the crystallization of ZSM-22 zeolite. As reported by Hayasaka et al., the synthesis of ZSM-22 can be divided into nucleation step followed by crystallization, and then the formed crystals are aggregated together as time progressed [79]. In order to produce small uniform particles length, the aging time should be prolonged. Meanwhile, crystallization time should be shortened to reduce the severity of agglomeration.

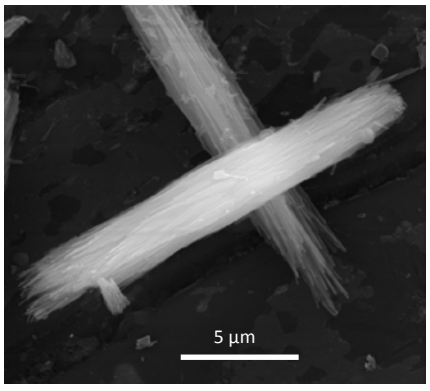

Figure 2-21. Conventional ZSM-22 crystal shape.

2.15 Size and shape control of zeolite catalysts

Conventional zeolite crystals (micron size), especially with one dimensional pore; suffer from serious diffusional limitation that hamper the reaction rate. In one pore dimensional zeolites like ZSM-22, reducing crystals size will lead to reduce pore length and subsequently shorter diffusion length [7], In addition to that, reducing particles size will also improve the catalyst activity via preventing pore blocking and coke deposition [80, 81]. Tuning the particle size from micron to nanoscale affects the reaction selectivity; since the shorter diffusional length allows better access to acid sites. While longer diffusional length gives the chance for larger products to form. Hence, the shorter diffusional length by either reducing crystal size or the aspect ratio (length/diameter) is very essential to obtain better stability against deactivation in catalytic cracking reactions. long diffusional length is applicable in some reactions, which need long path to achieve the desired products such as in methylation of olefins [14] and other applications in detergents and photonics [82-84].

2.16 Synthesis of nanosized ZSM-22 zeolite crystals

2.16.1 Microwave synthesis of zeolites

Synthesis of nanosized material by using microwave assisted hydrothermal synthesis (MAHyS) has been reported elsewhere [85-89]. Recently, many zeolites have been synthesized using MAHyS such as ZSM-5 (MFI) [85, 90-93], ZSM-12 (MTW) [87], Beta (BEA) [94], zeolite-Y (FAU) [85, 95], zeolite-L (LTL) [85], and zeolite-A (LTA) [85, 93, 96]. The high rate of heat transfer rate by radiation in the synthesis solution gives the

advantage of rapid zeolite synthesis [32]. The as-synthesized ZSM-22 particles by MAHyS were small and uniform, nevertheless they were severely agglomerated which reflect the high agglomeration rate of ZSM-22 particles. One of the effective techniques used to reduce the agglomeration rate is by using non-ionic surfactants [80].

2.16.2 Zeolite growth modifiers

This part of the research is devoted to synthesize nanosized ZSM-22 zeolites with less agglomeration as a catalyst in mass-transfer limited reactions like the conversion of methanol to light olefins. Investigating the catalytic performance advantage of reducing agglomeration rates of the nano ZSM-22 is an essential part of this research. In order to achieve our main goal we reduced the agglomeration rate of ZSM-22 zeolite crystals. Low agglomeration rate combined with small and uniform crystal size were optimized by changing surfactant concentrations in the zeolites synthesize the solution. We report a surfactant-microwave method as a powerful technique to synthesize ZSM-22 nanocrystals with uniform size and less aggregation. The non-ionic surfactant used in this study was polyoxyethylene with a chain length of 10 with HLB value of ca.12.

2.16.3 Surfactants as an agglomeration preventer

Synthesis of nanosized material by using microwave assisted hydrothermal synthesis (MAHyS) has been reported elsewhere [85-89]. Recently, many zeolites have been synthesized using MAHyS such as ZSM-5 (MFI) [85, 90-93], ZSM-12 (MTW) [87], Beta (BEA) [94], zeolite-Y (FAU) [85, 95], zeolite-L (LTL) [85], and zeolite-A (LTA) [85, 93, 96]. The high rate of heat transfer rate by radiation in the synthesis solution gives the

advantage of rapid zeolite synthesis [32]. The as-synthesized ZSM-22 particles by MAHyS were small and uniform, nevertheless they were severely agglomerated which reflect the high agglomeration rate of ZSM-22 particles. One of the effective techniques used to reduce the agglomeration rate is by using non-ionic surfactants [80]. In this work, we investigated the effect of polyoxyethylene with oxyethylene chain length of 10 under microwave irradiation. Over the last two decades, an increasing interest can be observed for using non-ionic surfactants in the zeolites synthesis such as in ZSM-5 (MFI) [80], mordenite (MOR) [80] ferrierite (FER) [97] and zeolite A (LTA) [98] for the purposes of crystallinity enhancements as well as controlling of zeolites particles size and morphology [80, 97, 98]. We used nonionic surfactant as agglomeration preventer for zeolites nanocrystals, Nasacar et al. found that crystal size of zeolite A were reduced with smallest size of 50 nm by adding surfactants with hydrophilic-lipophilic balance (HLB) of 8.6 to 10 [99], HLB is an index to measure surfactant solubility in water depending on the balance between the surfactant hydrophilic and hydrophobic groups [100, 101]. Surfactant with HLB value ca.10 gave good results for nanosilica synthesis as reported by Arriagada et al. [102] and by Che et al. [103] for zeolite A. Suitable surfactant HLB value depends on the type of targeted zeolite. Normally, the HLB value selected is in the range of 8.6 and 15 [99, 102, 104, 105]. We chose polyoxyethylene oxide (PEO) as surfactant among the other non-ionic surfactants because of their relatively cheapness and they are environment friendly [97].

2.16.4 Alcohols and diols as crystal growth modifiers

Many alcohols, diols and other organic solvents have been incorporated in zeolite syntheses, for instance, methanol, ethanol, propanol, iso-propanol, glycol, ethylene glycol, propylene glycols, urea, acetone and mixture thereof [76, 77, 106, 107]. Those organic solvents have been added to the synthesis mixture of zeolite for the following purposes: (i) to reduce crystal size of zeolites (ii) to reduce the utilization of organic structure directing agent (OSDA) with seeds of the desired zeolite [107], (iii) to inhibit or stimulate co-crystallization [106]. Accordingly, addition of organic additives is promising approach to control the crystal size of nanosodalite zeolites with low aspect ratio [106].

The application of ethanol on enhancing the synthesis of many zeolites has been reported elsewhere, for instance, in zeolite Y (FAU), silicalite-1, ZSM-5 (MFI), sodalite (SOD) and zeolite L (LTL) [77, 106, 108, 109]. Addition of ethanol to the synthesis solution decreased the crystal size of ZSM-5 from 60 nm to 15 nm [110]. Coupled effect of ethanol and urea controlled the crystal size of sodalite (SOD) zeolite [106]. In the presence of ethanol, SOD crystals with size less than 100 nm were produced while using ethanol-urea mixture in the synthesis mixture further reduced the SOD crystal size. Meanwhile, synthesis of SOD crystals in acetone-water system resulted nanosized SOD with the crystal size of 200 nm and impurities of zeolite A [106]. As reported by Gaona-Gómez and Cheng [111], ethanol can also be applied to reduce crystal aspect ratio of zeolite LTL, an aluminosilicate with one-dimensional (1D) pore system. Aluminosilicate-sodalite and all-silica sodalite were successfully synthesized by Bibby and co-workers in

the presence of ethylene glycol and propanol [112]. Generally, it is not only the type of alcohol or diol, which contribute to control the size and morphology of crystalline zeolites crystals but also the concentration of solvents may affect. This concentration can be in the range of 2 to 60 wt.% of total synthesis mixture, yet it is preferred to have the additive in the range of 2 to 4% [76, 77].

Micron-sized of sodalite crystals were produced when low concentration of ethanol was added to the SOD precursors, but when high concentration of ethanol was added, the nanosized sodalite zeolites were produced [109]. Kirker and co-workers reported the application of alcohols and diols in the synthesis of ZSM-22 [76, 77]. They reported utilization of ethylene glycol to synthesize ZSM-22 in the presence of 1,6 hexanediamine as a organic structured directing agent. In the same work, the conventional synthesis for ZSM-22 zeolite (in the absence of an alcohol or diol) produced ZSM-22 needle shape crystals with crystal length in range of 500 to ca. 2000 nm [76, 77]. Table 1 summarizes a comparison between conventional zeolites synthesis with modified synthesis in the presence of the crystal growth modifier.

Table 2-3. The co-solvent and conventional zeolites synthesis method reported earlier [76].

Parameters	Conventional ZSM-22 synthesis	Modified new ZSM-22 synthesis
Modifier (s)	-	ethylene-glycol
Temperature	at 80 to 210 °C	80 to 210 °C, preferably 130 °C to 210 °C
Time	6 to 3600 h	5 to 300 h
Size	Agglomerates of elongated crystals ca. 2000 nm.	≤ ca.1000 nm

It is important to note that the synthesis of some zeolites may be sensitive to the addition of the crystal growth modifier, for instance, diols may stimulate the appearance of impurities in zeolite L synthesis [111]. According to Gaona-Gómez and Cheng, the impurities appeared because of the growth modifier hydrophobicity, where growth modifier with moderate hydrophobicity prefers to form zeolite L rather than other competing phases. Hence, tri-ethylene glycol (with moderate hydrophobicity) was preferred in the synthesis of zeolite L rather than using low- or high- hydrophobicity solvents (such as diethylene glycol and ethylene glycol). Similar trend was reported in the addition of alcohols to zeolite synthesis. Ethanol was preferred than methanol and n-butanol in the preparation of zeolite L [111]. Kirker et.al reported that addition of crystal growth modifier method suppressed the co-crystallization of ZSM-5 in the synthesis of ZSM-23 (MTT), however, the similar effect was not observed in the synthesis of ZSM-22 (TON) [77].

Table 2-4. Some co-solvents reported in the synthesis of one-dimensional pore zeolites (MTT, TON, and LTL) and SOD.

Zeolite	Framework	Tested co-solvent	Reference
ZSM-22	TON	ethylene glycol	[76, 77]
ZSM-23	MTT	ethanol, n-propanol	[76, 77]
		iso-propanol 1,2 ethanediol	
		mixture of (0.9 ethanol/0.1 methanol)	
sodalite	SOD	ethanol, urea, acetone	[106, 109]
zeolite L	LTL	ethylene glycol, diethylene glycol, triethylene glycol	[108]

CHAPTER 3

OBJECTIVES OF STUDY

Methanol to olefins (MTO) reaction is controlled by internal diffusion [7]. Diffusion plays an important role on both selectivity and activity of catalysts used in MTO reaction. Reaction rate depends on the catalyst effectiveness factor which is a function of the Thiele modulus as shown in Equation (3-1) [7]:

$$k_e = k\,\eta$$

$$\eta = \frac{3}{\phi}\left[1 - \frac{1}{\tanh\phi}\right] \qquad \textbf{(3-1)}$$

$$\phi = R\sqrt{k/D}$$

The diffusion limitation occurs on the intracrstalline scale. In the Thiele modulus, intracrystalline diffusivity is redefined with respect to the adsorbed phase concentration (see Equation (3-2)), including the dimensionless adsorption equilibrium constant (K):

$$\phi_s = R\sqrt{k/D_{eff}} = \sqrt{\frac{R^2}{D}\cdot\frac{k}{K}} \qquad \textbf{(3-2)}$$

Both intrinsic rates constant (k) and the effective diffusivity (D_{eff}) can be extracted from measurements of the reaction rate with different size fractions of the zeolite crystals.

3.1 Strategies for increasing catalyst effectiveness

In fact there are two strategies to increase the catalyst effectiveness. The first strategy is by increasing molecules diffusivity which is gotten by increasing the pore diameter (wide pore). However, this will be on the expense of the shape-selective properties of the zeolites. A high yield of light olefins requires crystal length long enough to convert the formed DME in the first step of the reaction to olefins in the second step of the MTO reaction (see Equation (2-1)). To insure the formation of olefins, the ratio of the Thiele module should be large [113]:

$$\frac{\phi_2}{\phi_1} = \sqrt{\left(\frac{k_2}{k_1}\,\frac{D_{MeOH}}{D_{DME}}\right)} \gg 1 \qquad \textbf{(3-3)}$$

The second strategy is by reducing the mean diffusion path length (L) of catalyst. This can be pursued by either decreasing the crystal size or by the introduction of auxiliary pore system consisting of larger pores (mesopores). Since the kinetic diameter of DME molecule (0.585 nm) [114] is larger than the methanol molecule (0.44 nm) [115], the diffusivity ratio D_{MEOH}/D_{DME} increases by decreasing the effective opening pore size (see Equation (3-3)) [113]. More details about molecules critical diameter are shown in Table B-1 in Appendix B.

3.2 Objective and scope of study

- The main objective of this study is to obtain a catalyst with more light olefins selectivity “specifically propylene” and low deactivation rate.
- Nanosized one dimensional zeolite as a catalyst in the conversion of methanol to light olefins were developed and to characterized.
- Effect of adding non surfactant in ZSM-22 zeolite synthesis has been studied.
- Alcohols and diols were used as a co-solvent.
- Effect of co-solvents as crystal growth modifiers in ZSM-22 zeolite synthesis was studied.
- ZSM-22 zeolite with different crystal sizes and morphologies were synthesized.
- Effect of ZSM-22 zeolite crystal size was investigated using Thiele modulus and effectiveness factor.

CHAPTER 4

EXPERIMENTAL METHODS

4.1 Experimental: ZSM-22 synthesis

Aluminate solution was made by adding 0.9 g of aluminum sulfate octadecahydrate and 4.2 g of 1,6-diaminohexane (DAH) as template to 1.9 g of KOH and 44.2 g of deionized (DI) water. Silicate solution was prepared by adding 18 g of silica colloidal solution to 31 g DI water. The gel solution was prepared by adding silicate to aluminate solution. The gel was heated to 50^{o}C under continuous stirring at 250 RPM for 5 min before adding Brij-76, a polyoxyethylene surfactant with chain length of 10, at 105^{o}C. The initial molar composition of the prepared gel was: 1 Al_2O_3: 91.4 SiO_2: 26.5 K_2O: 27.4 DAH: 3202 H_2O:y Brij-76 (where y = 0, 5, 10, 15, 20 and 25 respectively). The gel was aged at 50^{o}C for 72 h. Synthesis was performed in a microwave lab station at 180^{o}C for 12 h. The calcined zeolites (K-ZSM-22) were transformed to NH_4-ZSM-22 by ion-exchanged with NH_4NO_3 (under microwave irradiation) then calcined to obtain H-ZSM-22.

4.2 CHARACTERIZATION OF ZSM-22 CRYSTALS

ZSM-22 catalysts were characterized using powder X-Ray Diffraction (XRD), X-ray fluorescence (XRF) , scanning electron microscopy (SEM), N_2 adsorption–desorption measurements (BET measurement), infrared spectroscopy (FTIR), transmission electron microscope (TEM) and temperature programmed desorption (TPD). Finally, the catalytic behavior of the resulted ZSM-22 crystals was investigated in a catalytic fixed bed reactor.

4.2.1 Powder X-ray Diffraction (XRD)

Crystallinity of the as-synthesized crystals were identified using X- ray diffraction using Rigaku x-ray diffractometer with a step size of 0.03^{o}, with Bragg-Brentano geometry, position sensitive detector and CuK α radiation (λ= 1.5406 Å). XRD data were analyzed using EVA 8.0 (Rigaku).

4.2.2 Scanning electron microscope (SEM)

The crystal size and shape were investigated using scanning electron microscopy. ZSM-22 crystals sample was spread on samples holder using volatile solvent like ethanol. Low acceleration voltage (15 kV) and spot size 3 were used for imaging. The equipment used was SEM-FIB Tescan Lyra.

4.2.3 Transmission electron microscope (TEM)

ZSM-22 catalyst was suspended in ethanol, and a drop of the mixture was spread and dried on porous carbon film sample cell. The dried specimens were analyzed using electron microscope; the TEM experiments were performed at Chemical & Environmental Engineering Department & Nanoscience Institute of Aragon (INA) University of Zaragoza Mariano, Spain.

4.2.4 N2 adsorption–desorption measurements (BET measurement)

The surface area of ZSM-22 catalysts was determined by nitrogen adsorption at a temperature of 77 K. About 60 mg of the catalysts were pretreated for 5 h prior to the

surface area measurements. The pretreatment was carried out by outgassing the catalysts at 80 °C for 1 h followed by 4 h at 300 °C.

4.2.5 X-ray fluorescence (XRF)

XRF was carried out using a Bruker MSL300 spectrometer. ZSM-2 zeolite in the powder form was used to analyze the elements included in our as-synthesized samples to determine and to confirm Si/Al of resulted ZSM-22 crystals.

4.3 Catalyst activity evaluation

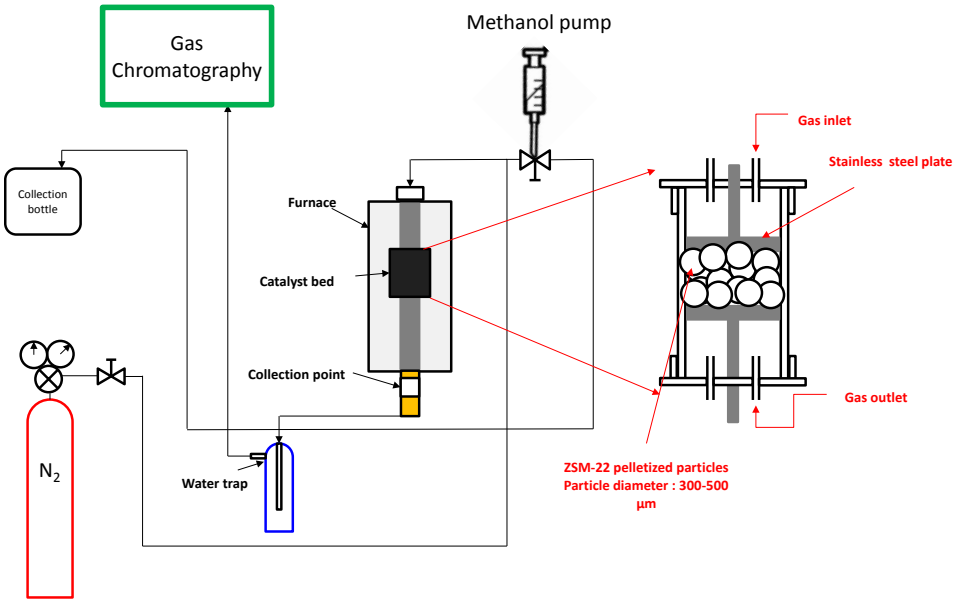

Figure 4-1. Schematic diagram of a fixed bed reaction system.

ZSM-22 zeolites were evaluated for the conversion of methanol to light olefins. Catalytic conversion of methanol was carried out over H-ZSM-22 catalysts in a fixed bed reactor made of stainless steel (ID: 9.8 mm and OD 12.7 mm) as shown in Figure 4-1, Catalyst weight was 100 mg pelletized and sieved in the range of 300 micron. Methanol was diluted by using helium (He) gas, the concentration of methanol was in the range of 2.5 % to 5% with W/F between 33 and 67 $g.h.mol^{-1}$. The catalyst testing reaction temperatures were varied between 350 - 500 °C. However, most of the experiments were performed at 450 °C. The reaction product was analyzed by two connected online gas chromatograph (GC, Shimadzu GC-2014).

$$MeOH\ conversion\ \% = \frac{[(MeOH\ in - MeOH\ in\ the\ products)mol \times 100]}{MeOH\ in(mol)} \quad \textbf{(4-1)}$$

$$Product\ selectivity\ \% = \frac{moles\ of\ the\ product\ produced * 100}{[(MeOH\ in - MeOH\ in\ the\ products)\ mol]} \quad \textbf{(4-2)}$$

CHAPTER 5

RESULTS AND DISCUSSION

5.1 Effect of microwave-assisted synthesis parameters on ZSM-22 crystal size and morphology

5.1.1 The most influential synthesis parameters

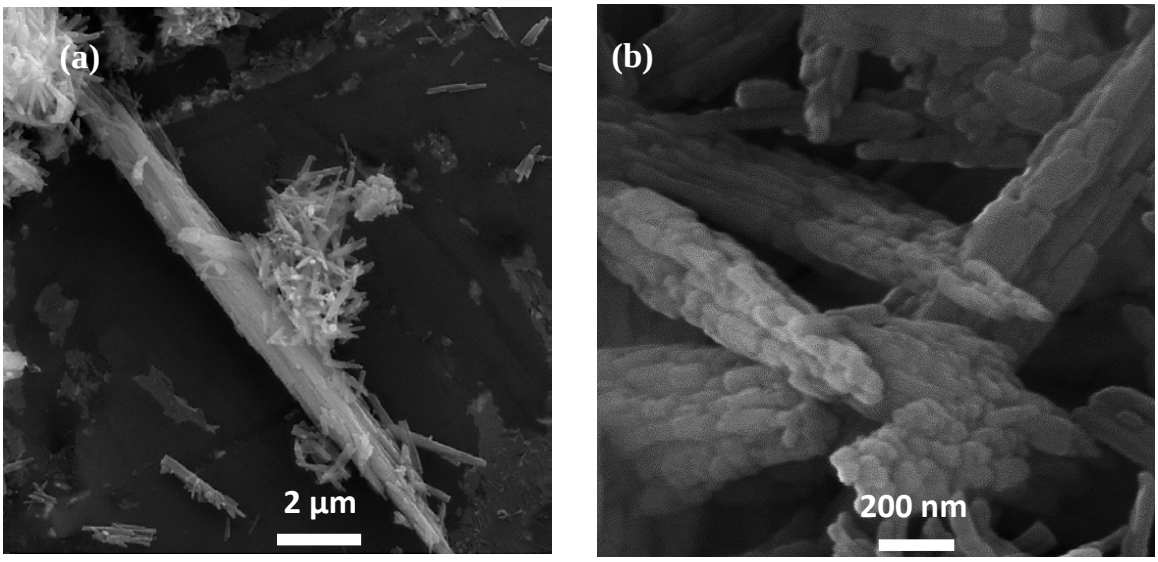

Figure 5-1. ZSM-22 crystals synthesized with different aging times.

Conventional ZSM-22 crystals have typical very high crystal-aspect-ratio (>10) [33]. Crystal aspect-ratio can be reduced from 10 to less than 5 by controlling the nucleation and the growth under microwave irradiation. Optimum aging time, crystallization time and temperature have been obtained to get pure and high crystalline ZSM-22 crystals

with reduced size and lower aspect-ratio. By variation of aging time from 2 to 84 h, we observed that the nucleation rate was favored by aging time (see Figure 5-1).

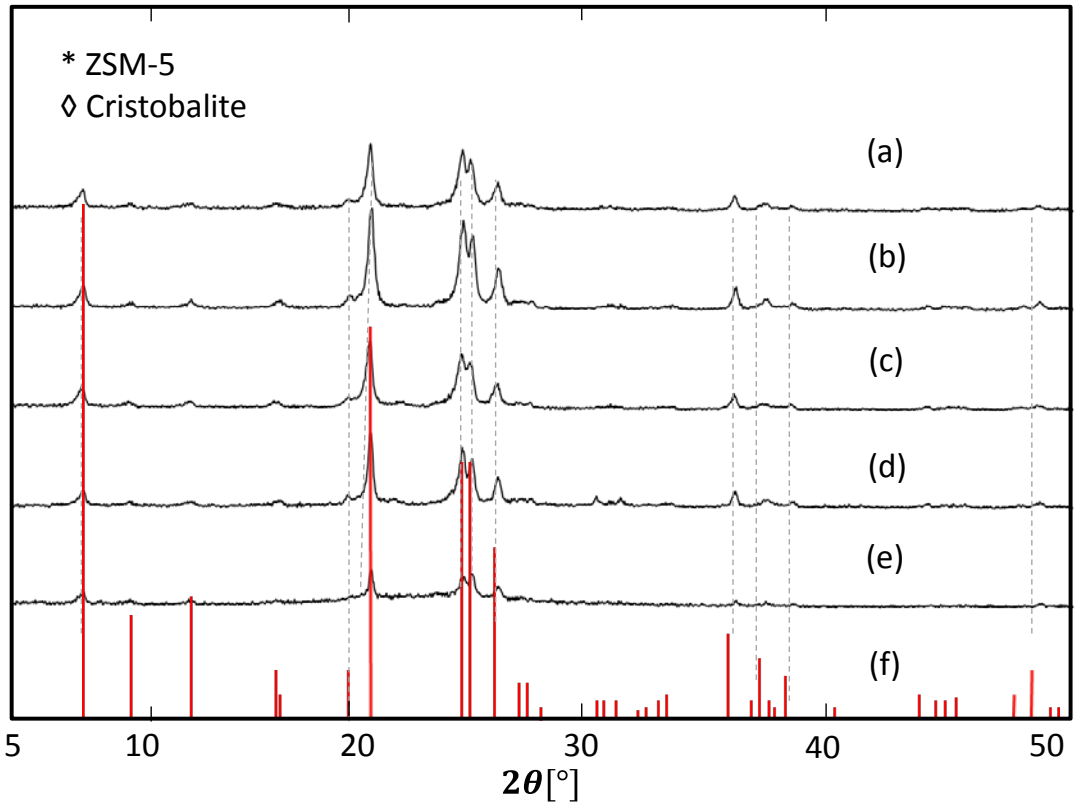

Figure 5-2. XRD patterns of ZSM-22 synthesized with different aging times by MAHyS: (a) 2 h, (b) 24, (c) 48, (d) 72 h, (e) 84 h, (f) standard's XRD.

However, excessive amount of nuclei resulted in low crystallinity since its need more crystallization time to be crystallized as shown in Figure 5-2. Crystals length decreased with increasing of aging time, which coincided with literature review [116-118].

Alfaro et al. reported that prolonging aging times decreased the LTA zeolites crystals lengths, which as consequence of increasing in the amount of nuclei created in the synthesis gel solution [117]. In agreement with these findings, zeolite Y [116] and ZSM-5 [118] crystal sizes were decreased noticeably by prolonging their aging times.

On the other hand, increasing crystallization time is undesired since it gives the chance for the particles to grow as well as stimulating other crystallization phases such as ZSM-5 as shown in Figure 5-3.

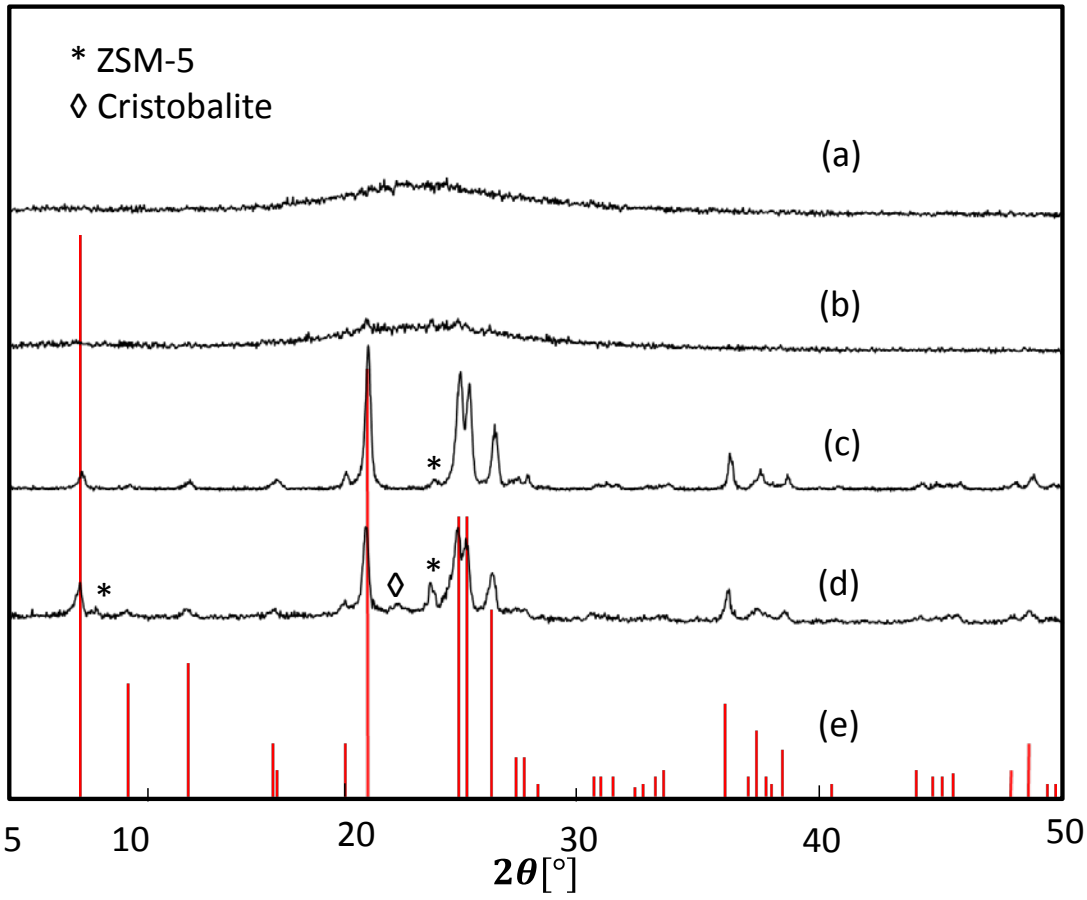

Figure 5-3. XRD patterns of ZSM-22 synthesized by using MAHyS with different crystallization times: (a) 3 h, (b) 6 h, (c) 12 h, (d) 18 h, (e) standard's XRD.

Eventually ZSM-22 with crystal length less than 100 nm was produced. However the crystals were agglomerated as shown in Figure 5-4 and Figure 5-5.

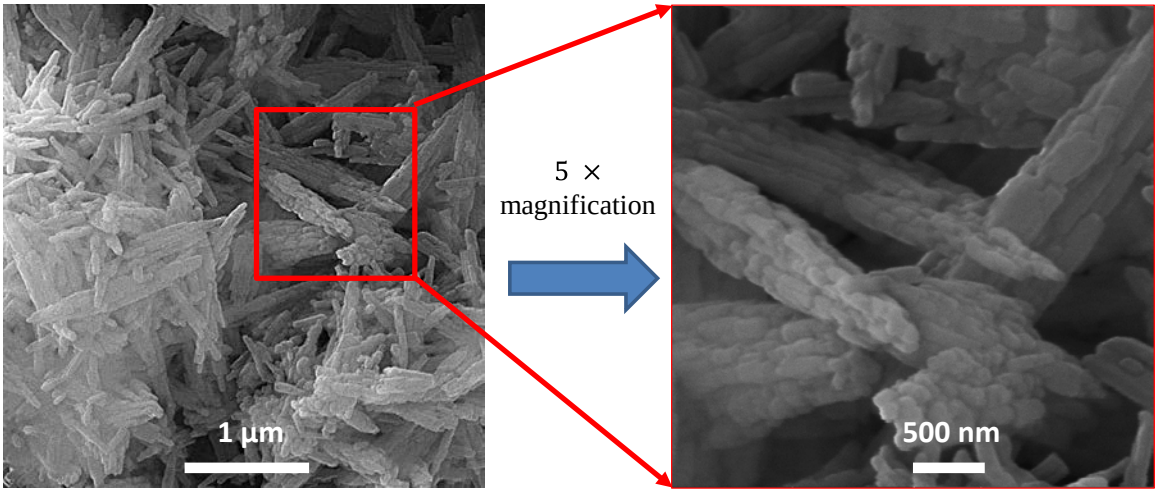

Figure 5-4. Fe-SEM images of Aggregated ZSM-22 nanocrystals synthesized by using MAHyS with Si/Al of 46 without surfactant (Brij-76).

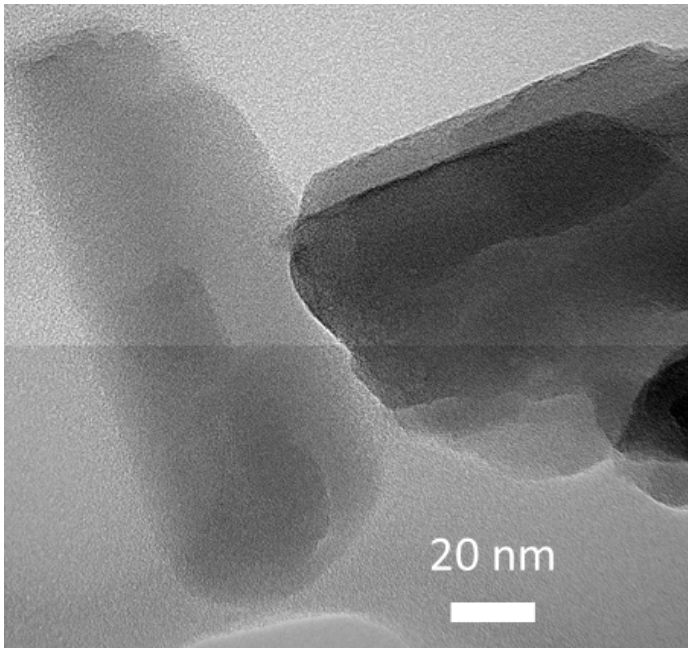

Figure 5-5. TEM image, confirming the size of single crystal synthesized under microwave radiation (MAHyS) for 12 h after aging time of 72 h.

5.1.2 Effect of Brij-76 /Al ratio

As noticed from Figure 5-6, crystallinity phase of ZSM-22 was not affected by addition of Brij-76 surfactant. On other hand, adding nonionic surfactant improved the crystallinity of other one-dimensional zeolite, ferrierite (FER) as reported elsewhere [97].

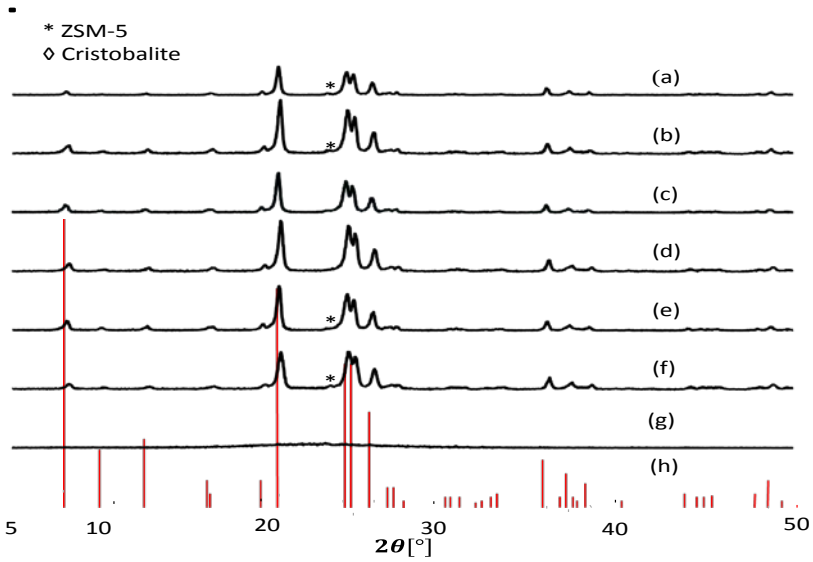

Figure 5-6. XRD patterns of ZSM-22 synthesized by using MAHys with Si/Al of 46 and different Brij-76/Al mole ratios: (a) 0, (b) 2.5, (c) 5, (d) 7.5, (e) 10, (f) 15, (g) 20, (h) standard's XRD.

Table 5.1.2-1. Effect of Brij/Al ratio on ZSM-22 size and morphology synthesized by MAHyS.

Si/Al (-)	Brij/Al (-)	Length (L) (nm)	Diameter (D) (nm)	Aspect ratio L/D
46	0	94	60	1.6
46	2.5	95	60	1.6
46	5	133	60	2.2
46	10	190	70	2.7

Table 5.1.2-1 below, shows that the agglomeration rate was reduced noticeably by adding a small quantity of surfactant (Brij-76/Al = 2.5). However, adding more surfactant (Brij-76/Al $\geq$ 5) increased the length of crystals. Crystal size and morphology depended on the surfactant amount, with increasing surfactant concentration; crystal length was not changed linearly. However, the crystal increased significantly by adding more surfactant from Brij-76/Al of 2.5 to 10 as shown in Table 5.1.2-1. Khomane et al. reported similar behavior by adding non-ionic surfactant with polyethylene oxide (PEO) chains (Tween) to zeolite ferrierite (FER) [97].

Table 5-1. Effect of Brij/Al ratio on ZSM-22 size and morphology synthesized by MAHyS.

Si/Al (-)	Brij/Al (-)	Length (L) (nm)	Diameter (D) (nm)	Aspect ratio L/D
46	0	94	60	1.6
46	2.5	95	60	1.6
46	5	133	60	2.2
46	10	190	70	2.7

5.1.3 Effect of Si/Al ratio

In this section, the initial gels were prepared with different Si/Al ratio. Variation of Si/Al ratio changed the acidity and the surface area of the ZSM-22 crystals. Our discussion here is limited to the effect of Si/Al on crystallinity, size and morphology.

The XRD patterns in Figure 5-7 shows that ZSM-22 crystallinity increased with the increasing of Si/Al, these results supported previous report of Hincapie et al. for MOR zeolite [119]. Other reports found different trend for ZSM-23 zeolite [120].

Hu and co-workers reported that decreasing Si/Al ratios for ZSM-5 (MFI), zeolite Beta (BEA) and zeolite L (LTL), lead to increase the crystals lengths which as consequence of decreasing in the amount of nuclei created in the synthesis gel solution [121]. Notably different from those findings, we observed the increase of ZSM-22 crystals length by increasing Si/Al ratio as shown in Figure 5-7. This finding is in agreement with other reports [119, 120, 122].

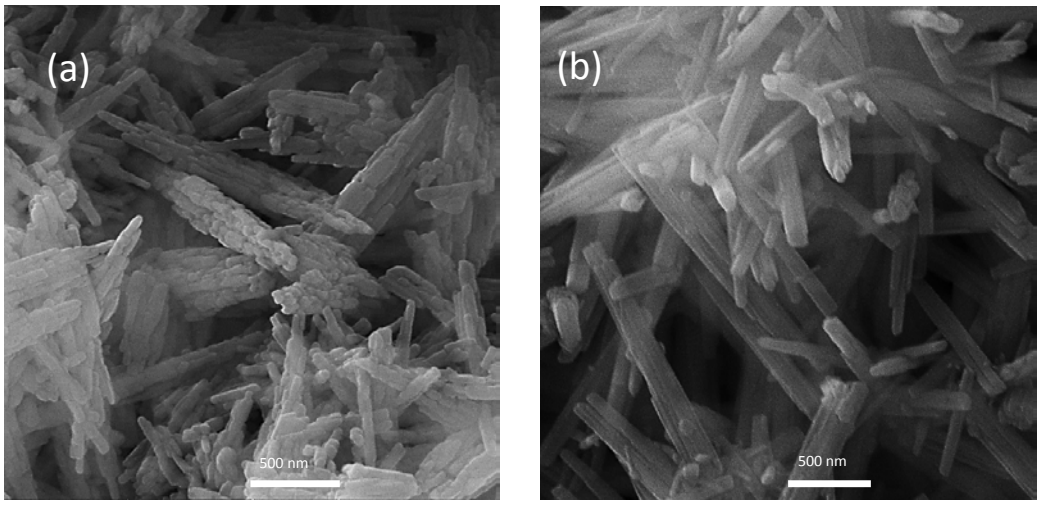

Figure 5-7. FE-SEM of ZSM-22 zeolite synthesized by MAHyS with different Si/Al ratios.

5.1.4 Effect of adding surfactant on agglomeration

Introduction of surfactant molecules with the surfaces of zeolite nuclei favored the nucleation process of the zeolite [80, 97]. In addition, the presence of surfactant suppressed the agglomeration of the zeolite crystals. Therefore, careful selection of surfactant type as well as surfactant concentration are crucial parameters to control the nucleation and growth of zeolite phases [97].

As shown in Figure 5-8, the chemical structure of polyoxyethylene (10) stearyl ether (Brij-76) consists from large hydrophilic head attached to a short hydrophobic chain, the head contains 10 units. On the other side of the surfactant is The hydrophobic tail , which is an alkyl group with 18 carbon atoms.

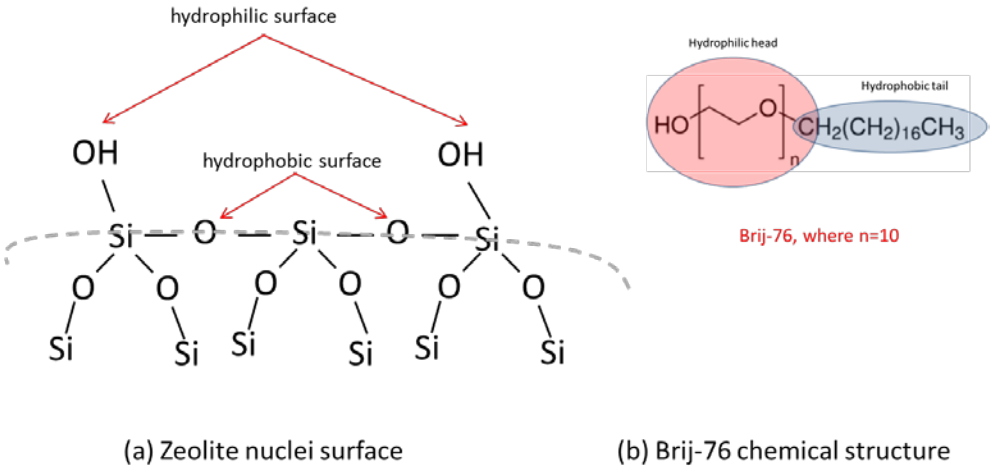

Figure 5-8. Chemical structure of zeolites nuclei and the nonionic surfactant Brij-76 in MAHyS.

The hydrophilic head is the part of the surfactant molecules that adsorbed on surface of zeolite nuclei [80, 97]. From Figure 5-8 (a) the zeolite nuclei surface is composed of hydrophilic silanol groups (-O-Si-OH) and hydrophobic (-Si-O-Si-) surfaces. Figure 5-8 (b) shows that the hydrophilic heads of surfactant stabilize the nuclei since they adsorb on the silanol and (-Si-O-Si-) [80]. As consequence, the nucleation process was favored [80].

Griffin's method [100, 101] was used to calculate the HLB for Brij-76 surfactant, we found that the HLB is 12 which can be classified as hydrophilic surfactant (above 10). According to Griffin's method, if the surfactant HLB is higher than 10 the surfactant is soluble in water as hydrophilic part of the surfactant is larger than the hydrophobic one [100, 101]. Surfactant with HLB below10 is not suitable for surfactant-microwave method.

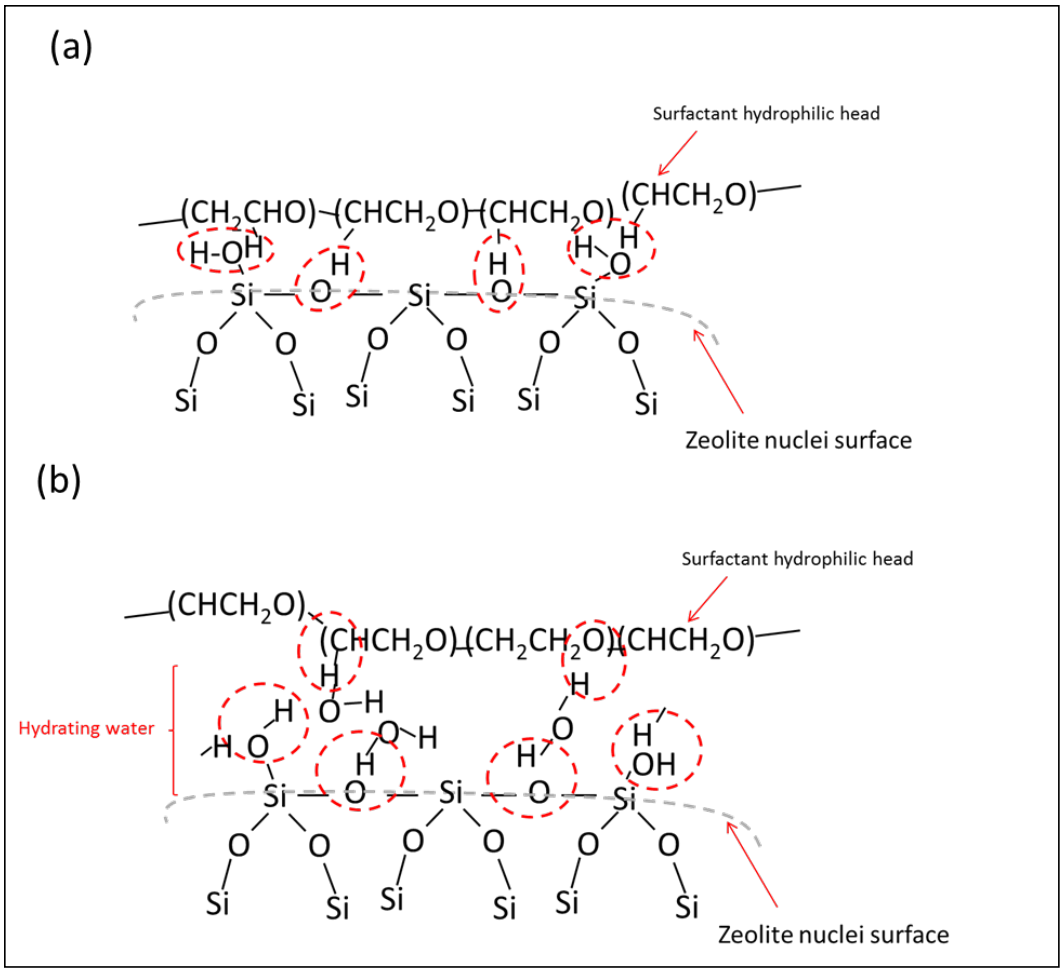

Figure 5-9. Mechanisms of the nonionic surfactant Brij-76 adsorption on ZSM-22 zeolite nuclei in MAHyS.

Brij-76 molecules are arranged in such way that the hydrophobic tails oriented inside while hydrophilic heads outside as layer as shown in Figure 5-9 [97]. The hydrophilic shell (POE molecules) interacted with zeolites nuclei [97]. The agglomeration rate of nanosized ZSM-22 crystals was reduced when we added the surfactant. We proposed a schematic illustration for the effect of adding surfactant as shown in Figure 5-10. Surfactant added with a small amount was effective in reducing the agglomeration rate of nanosized ZSM-22 crystals produced by microwave irradiation.

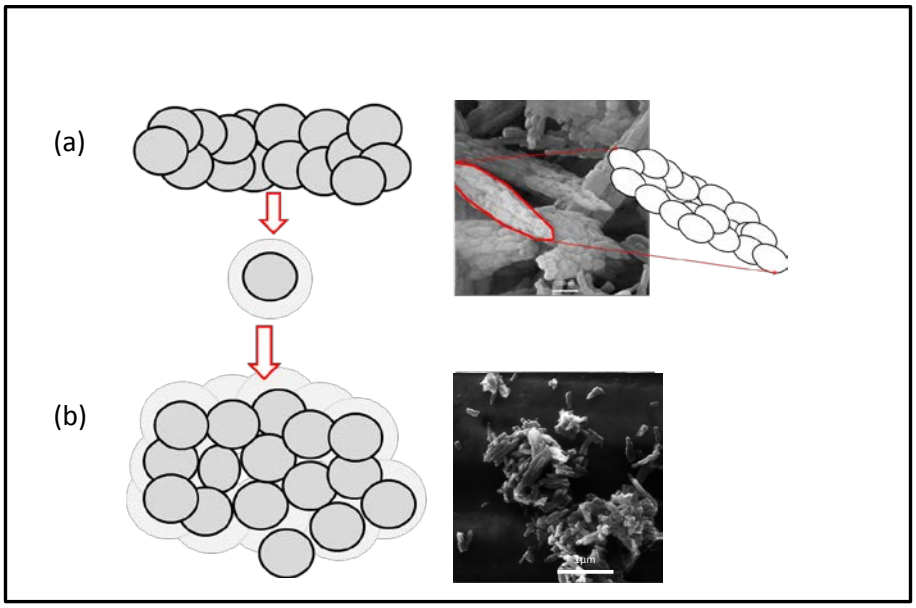

Figure 5-10. Systematic illustration of the effect of adding surfactant on ZSM-22 synthesized by using MAHyS.

5.1.5 Effect of adding co-solvent on phase purity of ZSM-22 zeolite

In this section, alcohols with different carbon chain length and hydroxyl group (OH) such as, ethanol, 2-propanol, ethylene glycol and glycerol were used.

Detailed information about the effect of co-solvent identity on the size and morphology of ZSM-22 crystals were summarized in Table 5.1.5-1.

The sample without adding co-solvent ZSM-22 with purity of 93 % was produced. However when co-solvent was added, the formation of ZSM-5 phase was favored noticeably. The highest phase transformation was for glycerol followed by ethylene glycol, i-propanol consequently.

Apparently using moderate hydrophobicity co-solvent like ethanol (C/O=2) still ZSM-22 was the major phase in the produced crystals. While using lower and higher co-solvent

hydrophobicity will lead to favoring ZSM-5 formation (see Table 5.1.5-1). Similar results were observed for the synthesis of zeolite L [111].

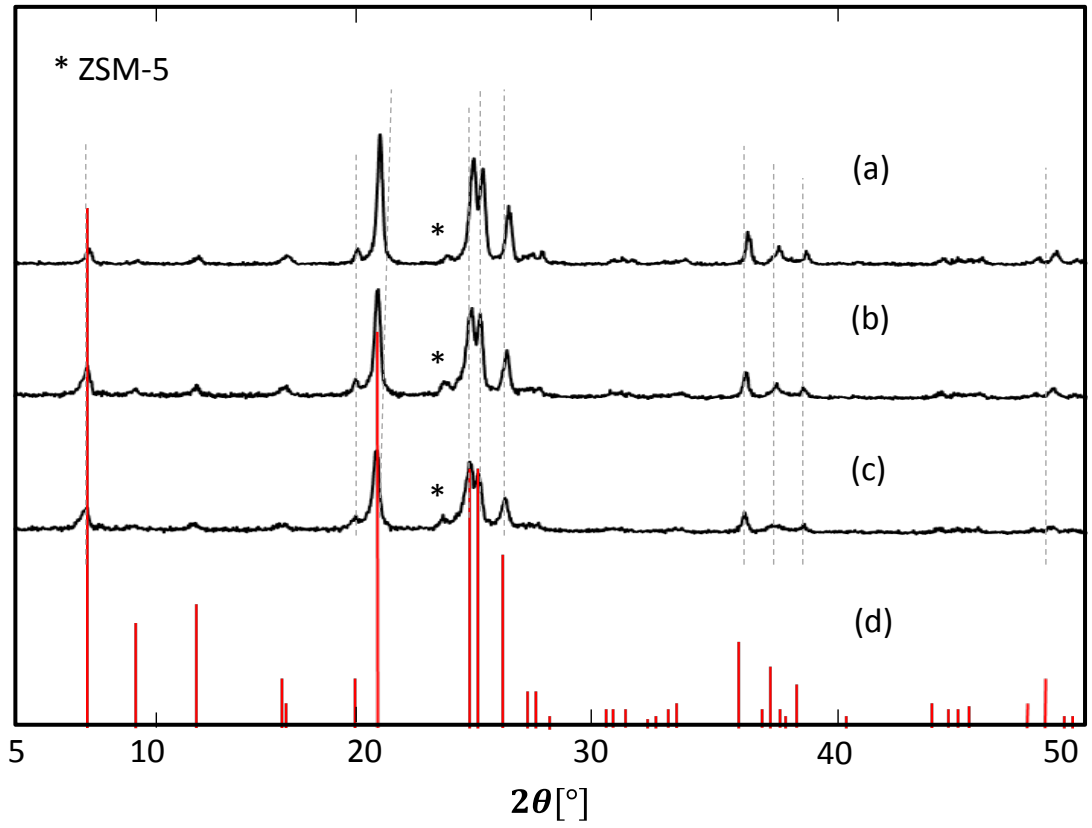

Figure 5-11. XRD patterns of ZSM-22 synthesized with different EtOH/Al ratios: (a) 0, (b) 1.25, (c) 2.5, (d) standard's XRD.

Table 5-2. The summary of the co-solvent used and morphologies of the as-synthesized ZSM-22 crystals.

Co-solvent	Formula	Molar mass ($g.mol^{-1}$)	C/O (-)	Morphology of product	Phases (%)	
					ZSM-22	ZSM-5
-	-	-	-	Agglomerated nano crystal	93	07
ethanol	C_2H_6O	46.07	2	Single elongated crystals	89	11
i-propanol	C_3H_8O	60.01	3	Single elongated crystals	21	79
ethylene glycol	$C_2H_6O_2$	62.07	1	Single elongated crystals	19	81
glycerol	$C_3H_8O_3$	92.09	1	Single elongated crystals	05	95

1- ZSM-22 crystals synthesized with Si/Al:46 and co-solvent/ Al ratio: 0.25.
2- Crystallinity phases of as-synthesized crsytals calculated from XRD based on the highest peak of each phase

5.1.6 Effect of ethanol concentration on crystal growth

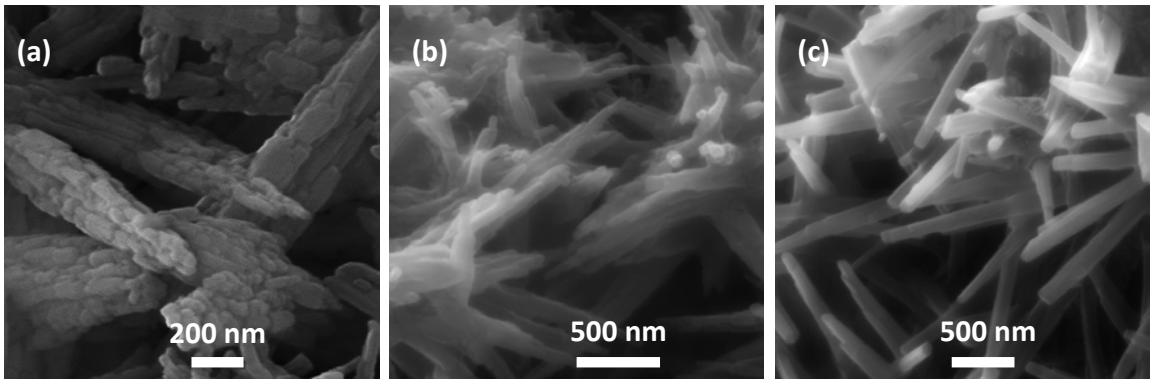

Figure 5-12. SEM of ZSM-22 synthesized with Si/Al of 46, EtOH/Al ratio in MAHyS: (a) 0, (b) 1.25, (c) 2.5.

Figure 5-11 shows X-ray patterns of ZSM-22 synthesized in the presence of ethanol as crystal growth modifier. Larger crystals were grown with high concenteration of ethanol. The presence of ZSM-5, an unwanted product, was favored by ethanol adding ethanol. The SEM and TEM images in Figure 5-4 and Figure 5-5 show the length of ZSM-22 crystal was approximately 100 nm, the crystals were stacked to form agglomerates. With adding ethanol, the crystal length increased until it reached micro length 1000 nm with EtOH/Al of 2.5. Apparently, addition of co-solvent promotes the crystal growth in the length direction as shown Figure 5-12 in and summarized in Table 5.1.6-1.

Table 5-3. Summary of morphology changes of ZSM-22 synthesized with ethanol as a growth modifier.

EtOH/Al ratio (-)	**Morphology (-)**	**Crystal diameter (nm)**	**Crystal Length (nm)**	**Phases (%)**		**Cyrstallinity [1,2] (%)**
				ZSM-22	**ZSM-5**	
-	Agglomerated nano crystal	< 100	< 100	93	07	100
0.25	Single elongated crystals	100	450	89	11	89
1.25	Single elongated crystals	100	600	86	14	86
2.5	Single elongated crystals	100	1000	80	20	66

[1] First samples used as reference for the crystallinity calculations.
[2] Crystallinity of as-synthesized crystals calculated from XRD based on the highest peak of each sample.

To better understand the influence of the growth modifiers used on the crystallinity of the produced ZSM-22 crystals, other solvents were applied in ZSM-22 synthesis. As shown in Figure 5-13, addition of glycerol favored the nucleation of ZSM-5. However, adding glycerol made ZSM-5 the dominant phase while ethanol ZSM-5 percentage was 20% as maximum.

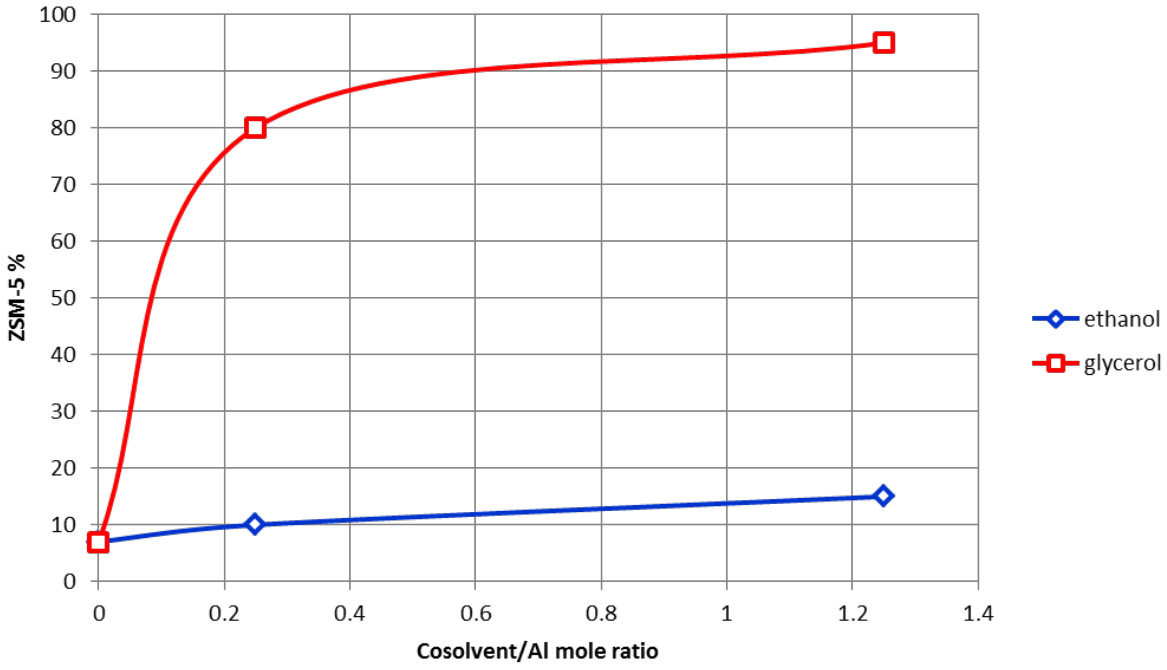

Figure 5-13. Effect of co-solvent on co-crystallization of ZSM-22 crystals in MAHyS.

5.2 Effect of synthesis parameters on size and morphology under rotating autoclave

5.2.1 Static and dynamic synthesis of ZSM-22 zeolite

Different crystallization methods have been reported to synthesis ZSM-22; those methods are static synthesis (without mixing) [28, 76, 123, 124] or vertical stirring [28, 30, 33, 49, 88, 125-127], and even horizontal rotation [33, 78]. The conventional synthesis methods resulted in large particle sizes (ca. 2–5 μm) [33, 126, 128]. Smaller crystal size (ca. 1 μm) was reported by Masih et al. [129] using horizontal rotational oven at low rotation speed (20 rpm) supported by magnetic stirrer. It was reported that by using horizontal rotation with magnetic stirrers should be used to ensure homogenous mixing and to obtain pure ZSM-22 zeolite [129]. However, we found that was unnecessary if we slightly increase the rotation speed. Using 1,8-diaminooctane (DAO) as template resulted in relatively large crystals in comparison with 1,6-diaminohexane (DAH) [71, 129]. Rotational speed of 37 rpm using DAO as template for 72 - 96 h at 160 ^{o}C resulted in ZSM-22 crystals with size (ca. 2 μm) [71]. We chose 1,6-diamnohexane as it is available, cheap and effective in synthesizing ZSM-22 and it is reported that DAH gave smaller size than DAO in the same synthesis condition [33, 71, 129]. The crystallization temperature was fixed at 180 ^{o}C as an optimum temperature. We found that the variation of temperature did not affect the ZSM-22 crystal size. However, the crystallinity and impurities were affected noticeably by temperature difference as shown in Figure 5-14.

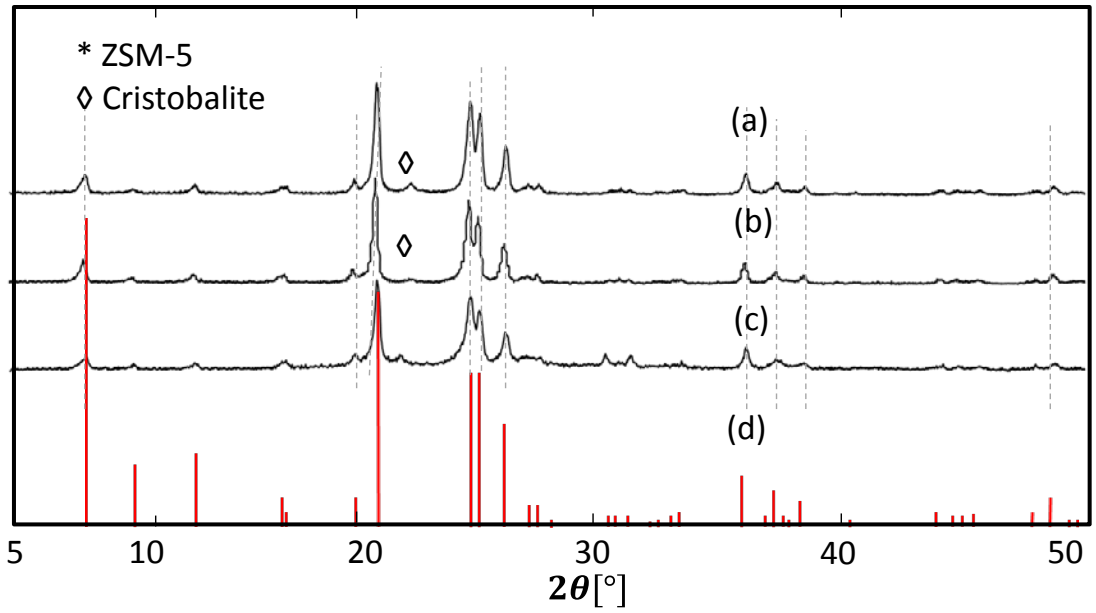

Figure 5-14. ZSM-22 crystals synthesized with different crystallization temperatures: (a) 200 °C, (b) 180 °C, (c) 160 °C, (d) standard's XRD.

5.2.2 Effect of speed in the horizontal rotation

Hydrothermal synthesis was carried out in the horizontal rotational system with different rotational speed in order to investigate the effect of dynamic synthesis in the presence of 1,6-diaminohexane. Static synthesis (see Figure 5-15) resulted in amorphous phase with initial peaks for ZSM-5. Rotation at 10 rpm resulted in low crystallinity ZSM-22 with impurity (ZSM-5). The presence of impurity can be suppressed by using higher rotational speed above 30 rpm (see Figure 5-16).

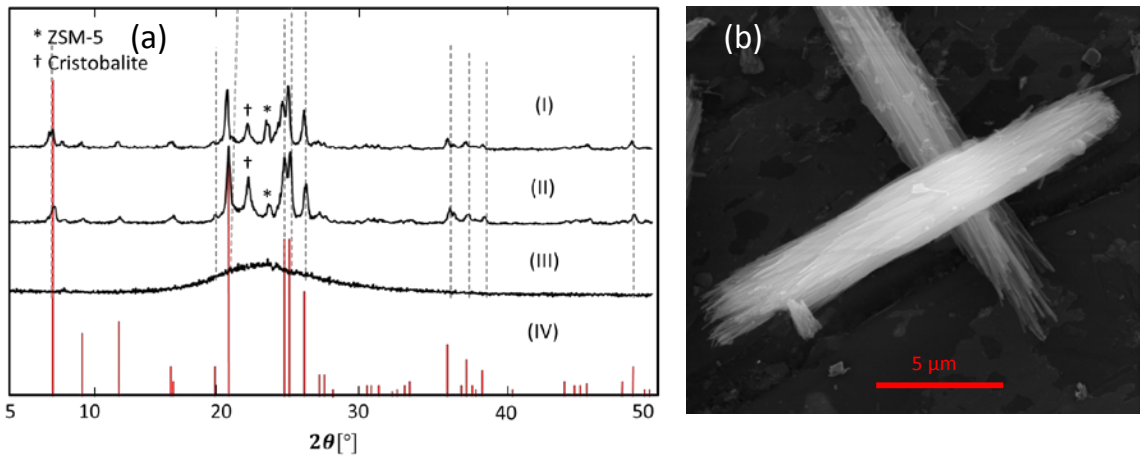

Figure 5-15. (a) XRD patterns of ZSM-22 synthesized via static autoclave: (I) 86 h, (II) 72 h, (III) 48, (IV) standard's XRD. (b) Large ZSM22 with size (ca. 20 µm) synthesized in 72 h.

Very slow rotation speed resulted in a poor mixing and induced the formation of impurity phase, low crystallinity and large crystal sizes. On the other hand, extremely high speed resulted in centrifugal effect and then again bad mixing [129]. Synthesis at rotation speed 20 rpm was not enough unless extra source of mixing is used to enhance the mixing process of the thick gel solution [129].

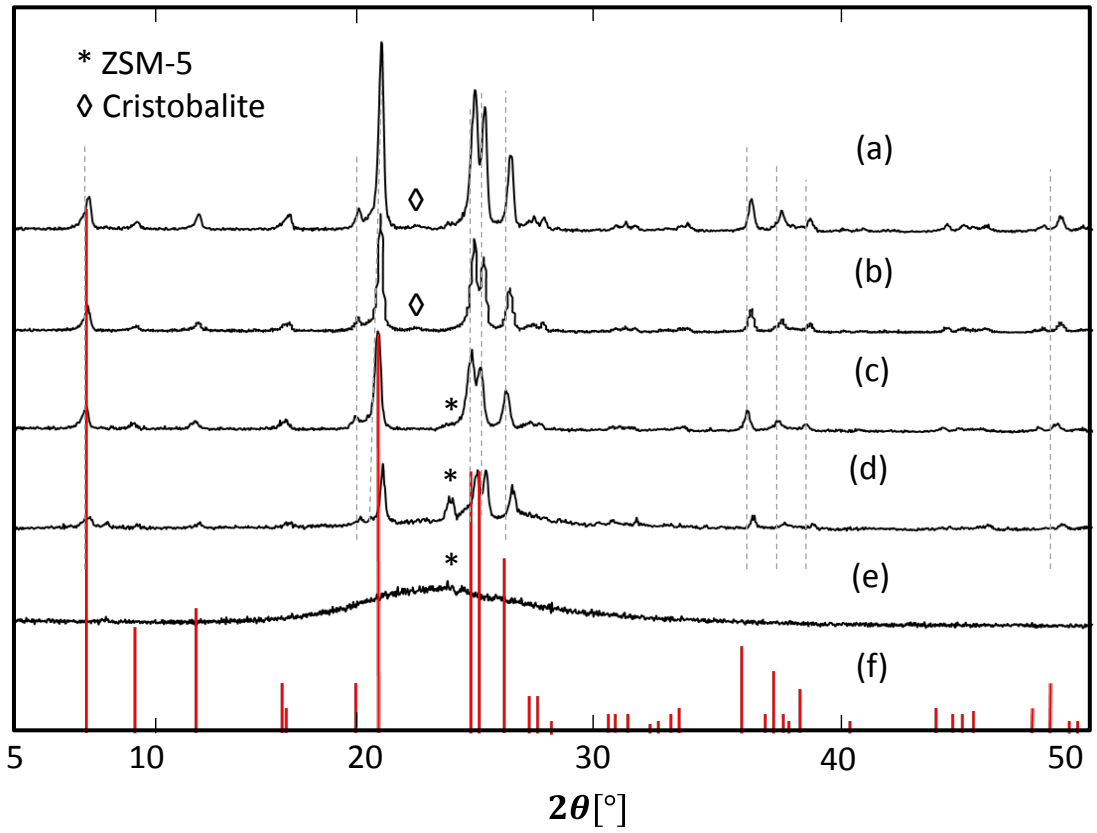

Figure 5-16. XRD patterns for the effect of horizontal rotation speed (rpm): (a) 70, (b) 50, (c) 30, (d) 10, (e) 0, (f) standard's XRD.

At rotational speed lower than 30 rpm the ZSM-22 crystal size was higher than 1 µm, increasing speed to 50 rpm resulted in nanosized crystals with size about 75 nm. Increasing velocity above 50 rpm did not affect the size but it increased the crystallinity noticeably. High crystallinity and pure nanosized ZSM-22 were obtained at rotational speed of 70 rpm as shown in Figure 5-16 and Figure 5-17.

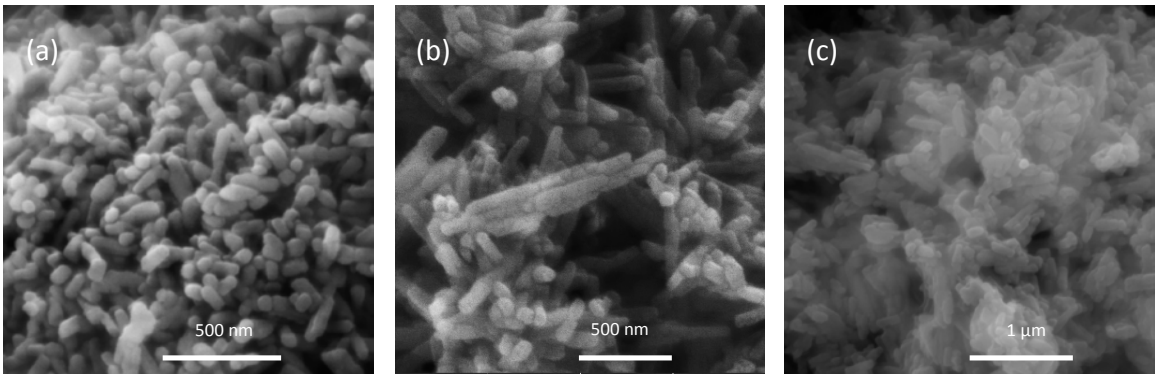

Figure 5-17. Effect of horizontal rotation speed (rpm): (a) 70, (b) 50, (c) 30

5.2.3 Influence of H_2O/SiO_2 ratio

As shown in Figure 5-18 and Figure 5-19, increasing the water content led to increase the crystallinity of ZSM-22 crystals. On other hand, decreasing water content leading to slightly increase in the ZSM-22 crystal size (see Figure 5-19.c) combined with reduction of the crystallinity (see Figure 5-18.c).

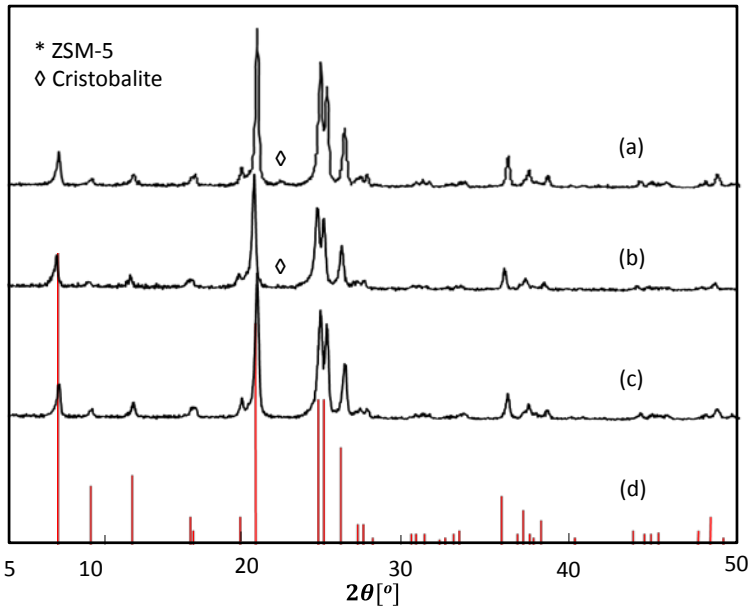

Figure 5-18. XRD patterns of ZSM-22 synthesized with changing water content (H_2O/SiO_2): (a) 43.8, (b) 35, (c) 26.3, (d) standard's XRD.

The nucleation and crystal growth of zeolites are highly effected by water content in the starting gel, since water fills cavities of zeolite which lead to key role in stabilizing the structure of zeolite [10]. In addition, changing water content affects the zeolite morphology, zeolite crystals with low aspect ratio may be produced by decreasing water content [108].

Zeolite crystal size is favored by increasing water content since the nucleation sites decreased in diluted solutions. By increasing water content, the alkalinity, silica/alumina species and solution saturation will decrease as consequence of diluting the starting gel [121]. A wide range of size distribution was originated from decreased dissolution and concentration of nutrient in the starting gel. For ZSM-5 zeolite, at relatively low water content (< 13.87) increasing water content affects size distribution while after increasing water content to 13.87 leads to increase crystal size and also affects size distribution. At high alkalinity, decreasing water content lead to increase in both crystal size and size distribution while at low alkalinity the only size distribution are mainly affected [121]. In this work, with (26.5 K_2O/ Al_2O_3) we found that decreasing water content increased size and distribution of resulted ZSM-22 crystal size as shown in Figure 5-19.a.

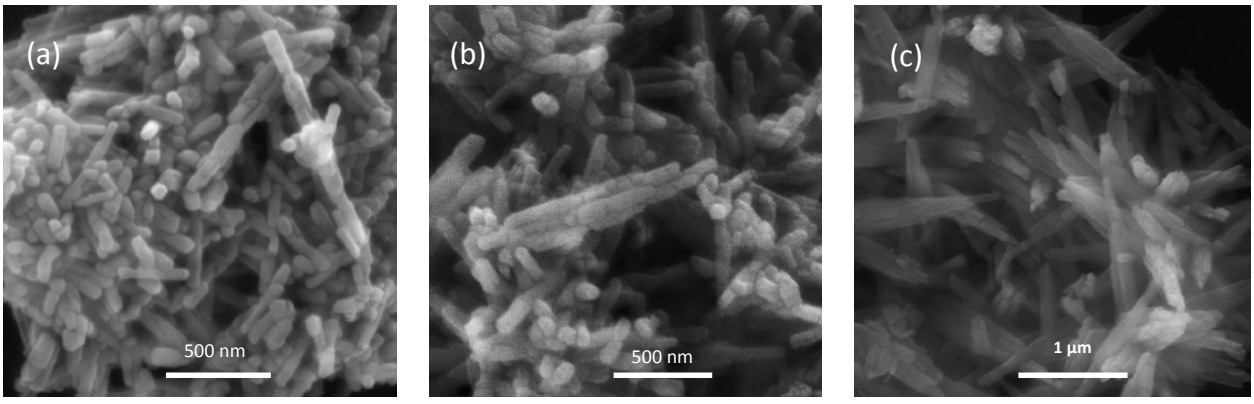

Figure 5-19. SEM shows the effect of changing water content (H_2O/SiO_2): (a) 43.8, (b) 35, (c) 26.3

5.2.4 Influence of Si/Al ratio

In this section, the initial gels were prepared with different Si/Al ratio (see Table 5.2.4-1). The effect of Si/Al on crystallinity, size and morphology were analyzed.

Table 5-4. Properties of the as-synthesized ZSM-22 with different Si/Al ratios.

Si/Al[a] (initial)	Product phase	Crystal size (nm)
30	ZSM-22	75 <
46	ZSM-22	75
80	ZSM-22+cristobalite	300
100	ZSM-22+cristobalite	20,000

[a] Si/Al calculated in the initial solution.

As shown in Table 5.2.4-1 and Figure 5-20 (a), by decreasing Si/Al ratio to 30 crystals size of ZSM-22 scaled down to lower than 75 nm.

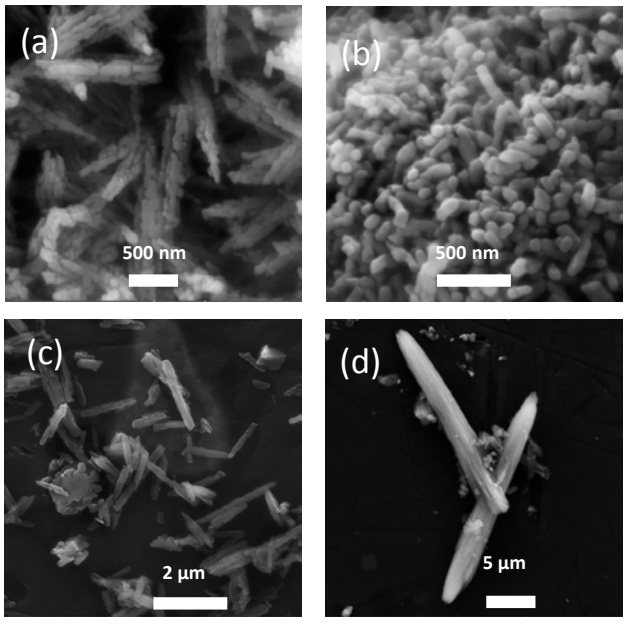

Figure 5-20. ZSM-22 crystals synthesized with different Si/Al ratios in the synthesis solution: (a) 30, (b) 46, (c) 80, (d) 100.

On other hand, increase Si/Al ratio led to increase the crystal size dramatically to about 20 μm at Si/Al ratio of 100, this result can be explained by the consequence of decreasing in the amount of nuclei created in the synthesis gel solution when increasing Si/Al and the vice versa [121]. These findings were in agreement with what reported in literature [119, 120, 122]. The crystals lengths of ZSM-5, BEA and zeolite LTL decreased with increasing Si/Al as reported by Hu et al. [121]. Noticeably different from those findings, as shown in Table 5.2.4-1 and Figure 5-20 we observed the increase of ZSM-22 crystals length by increasing Si/Al ratio. Increasing Si/Al in the synthesis gel increased the cristoblite phase in the resulted crystals.

5.2.5 Influence of DAH/SiO_2 ratio

As mentioned before, one of the factors that affect the ZSM-22 crystals size is the type of template used (see Table 5.2.5-1). SZM-5 crystal size and morphology were affected by the type of template used [130, 131].

Table 5-5. Overview of templates used to synthesize ZSM-22 zeolites.

Template	Ref.
1,6-diaminohexane	[30, 33, 128]
1,8-diaminooctane	[88, 125]
ethylpyridinium bromide	[21, 28]
diethylamine hydrochloride	[32, 78]
n-ethylpyridine	[21]
diethylamine	[32]

We focused our work on using 1, 6-diaminohexane (DAH) as template for synthesizing of ZSM-22 zeolite. Rotational synthesis system gave the advantage of reducing DAH/Si

ratio without the appearance of any impurities. Noticeably, decreasing DAH/Si decreased ZSM-22 crystal size as shown in Figure 5-21. Similar results were reported by Fouad et al. [130] and Sang et al. [131] for ZSM-5 synthesis. It was found that ZSM-5 crystal size increased by increasing template/Si ratio. On other hand, zeolite beta crystals were decreased by increasing template/Si ratios [132, 133].

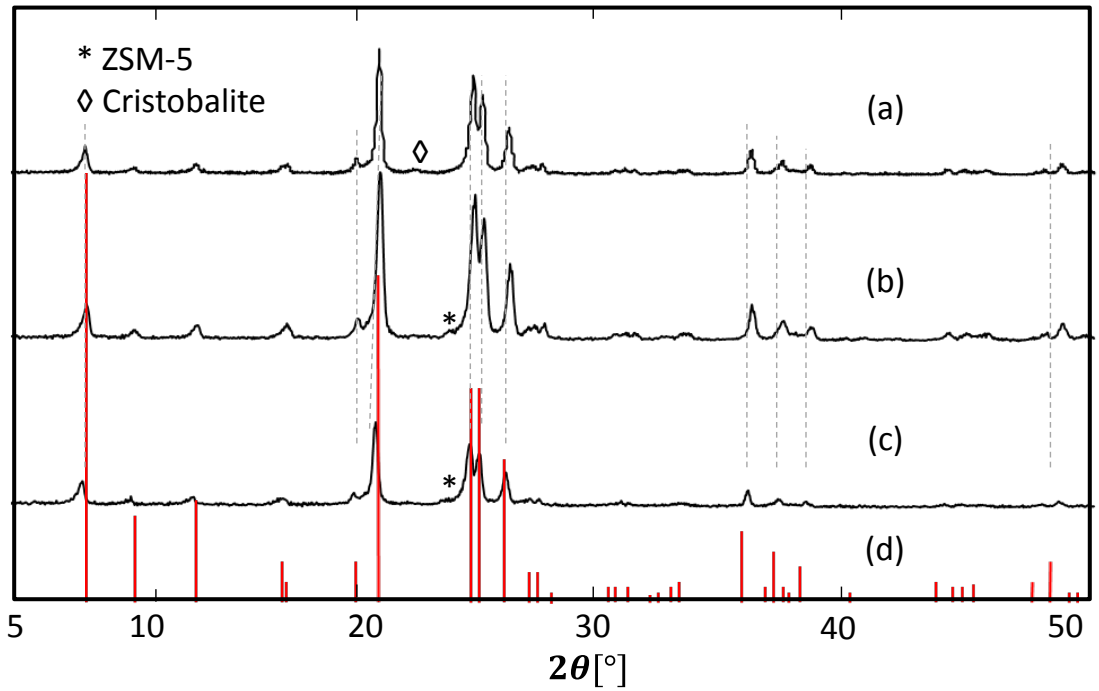

Figure 5-21. ZSM-22 crystals synthesized with different DAH/Si ratios: (a) 0.3, (b) 0.2, (c) 0.1, (d) standard's XRD.

With small amount of ethylene glycol (0.5 wt.%) in the initial gel the DAH/SiO_2 ratio could be reduced to 0.1 with slight effect on the crystallinity and nanoscale ZSM-22 crystals as shown in Figure 5-22.

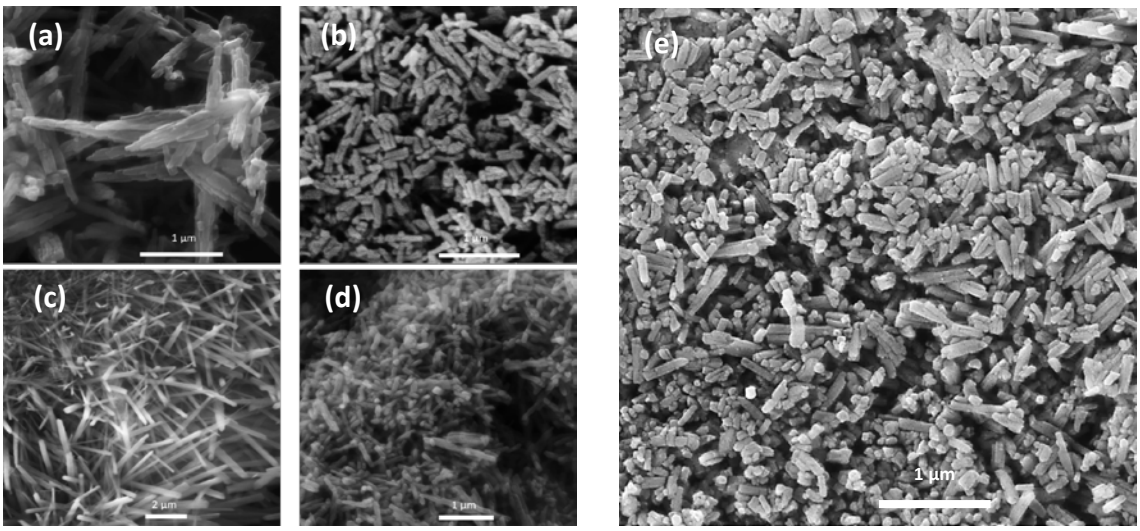

Figure 5-22. Crystals synthesized : (a) ethanol (5 wt.%) and 0.3 DAH/Si ,(b) ethanol (5 wt.%) and 0.2 DAH/Si ,(c) (20 wt.%) and 0.3 DAH/Si ,(d) (20 wt.%) and 0.2 DAH/Si , (e) ethylene glycol (0.5 wt. %) and 0.1 DAH/Si.

5.2.6 ZSM-22 zeolite co-crystallization phases

There are many reasons for the impurities to appear while synthesizing the targeted zeolites, such as whether the synthesis was a static or dynamic, velocity of stirring or rotation, synthesis temperature, synthesis time and even the template used. In order to avoid the appearance of impurities it is very necessary to understand crystalline structure of all potential crystallinity phases. Based on the unit cell, ZSM-5 (MFI) [134, 135] and ZSM-11 (MEL) [134-136] are denser (96 T-atoms) than ZSM-22 (only 24 T-atoms) [137], hence ideal environment to form ZSM-5 and ZSM-11 are the stagnant since it is need form relatively large unit cells (4 times of TON) [137], as shown in Figure 5-15. ZSM-5 formed with high percentage in stagnant synthesis and it increased with time. In Table 5.2.6-1, ZSM-22 zeolite synthesized at static condition with different crystallization times.

Table 5-6. Static synthesis of ZSM-22 zeolite.

Time [h]	ZSM-22 [%]	Cristobalite [%]	ZSM-5 [%]
72	56	31	13
96	53	25	22

On other hand, cristobalite is very sensible towards temperature, any increasing upper than 160 ^{o}C is in favor for cristobalite formation [138, 139]. However, temperature is necessary for the crystallization process in order to get high crystallinity zeolites (see Figure 5-14), to prevent the impurities with ZSM-22 phase such as ZSM-5, ZSM-11 and cristobalite, homogeneous mixing were required [88, 125, 129, 139]. The type of template used was also affecting the appearing of impurities. Without using any template pure cristobalite were gotten even with adding seeds up till to 1%. When 1,6-diaminohexane was used as template, ZSM-5 and cristobalite [30, 33, 128] may appear as co-crystallization phases, while using 1,8-diaminooctane ZSM-11 may appear [137]. We chose 1,6-diaminohexane as it is available, cheap and effective in synthesizing ZSM-22 zeolite and reported to give smaller size than 1,8-diamonooctane [33].

Generally during the synthesis of ZSM-22 zeolite, impurities were concentrated on dead zones (stagnant areas) like the walls and bottom of the Teflon liner in case of vertical rotation [139]. Using vertical stirring to synthesize ZSM-22 zeolite, impurity phases of cristobalite [139] and ZSM-5 [129] appeared even the case of using rigorous stirring. The impurity phases were concentrated more in the stagnant location near the wall and the bottom of the synthesis bottle [129]. Promoting the nucleation step and suppressing the

growth of zeolite crystal is the fundamental approach to obtain small zeolite crystals [79, 88]. By using hydrothermal synthesis with rotated autoclaves, nanometer-range ZSM-22 zeolite crystals with a diameter of 75 nm and a length of 75 nm (aspect ratio of 1.0) have been obtained. In this work, we used alcohols and diols as crystal growth modifier to induce nucleation and growth of zeolite crystals.

Table 5-7. Selected alcohols and diols used as co-solvents.

Co-solvent	Formula	Molar mass ($g\ mol^{-1}$)	Skeletal formula
ethanol	C_2H_6O	46.07	
n-propanol	C_3H_8O	60.01	
i-propanol	C_3H_8O	60.01	
ethylene glycol	$C_2H_6O_2$	62.07	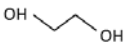
glycerol	$C_3H_8O_3$	92.09	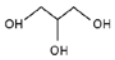
tri- ethylene glycol	$C_6H_{14}O_4$	150.17	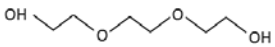
n-butanol	$C_4H_{10}O$	74.12	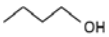
n-octanol	$C_8H_{18}O$	130.23	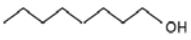

5.2.7 Effect of ethanol concentration

The XRD patterns in Figure 5-23 show the effect of ethanol addition on the product distribution. Small traces of cristobalite phase were observed from the sample synthesized in the absence of crystal growth modifiers (Figure 5-23.a). Interestingly, the cristobalite peaks disappeared when 5 wt.% of ethanol was added to the synthesis mixture. However, the unwanted cristobalite appeared again at higher concentration of co-solvent, when 10 wt.% of ethanol was added to the synthesis mixture.

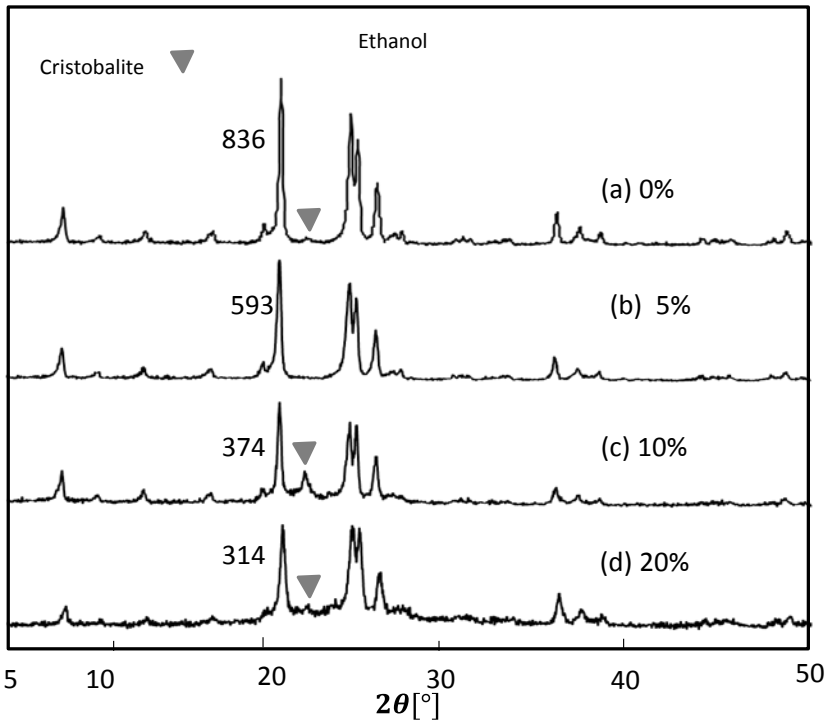

Figure 5-23. XRD patterns of ZSM-22 zeolite synthesized with different ethanol weight percent (wt. %).

Figure 5-24 shows that the FE-SEM images of ZSM-22 crystals. We can clearly observe the growth of ZSM-22 in the c-direction.

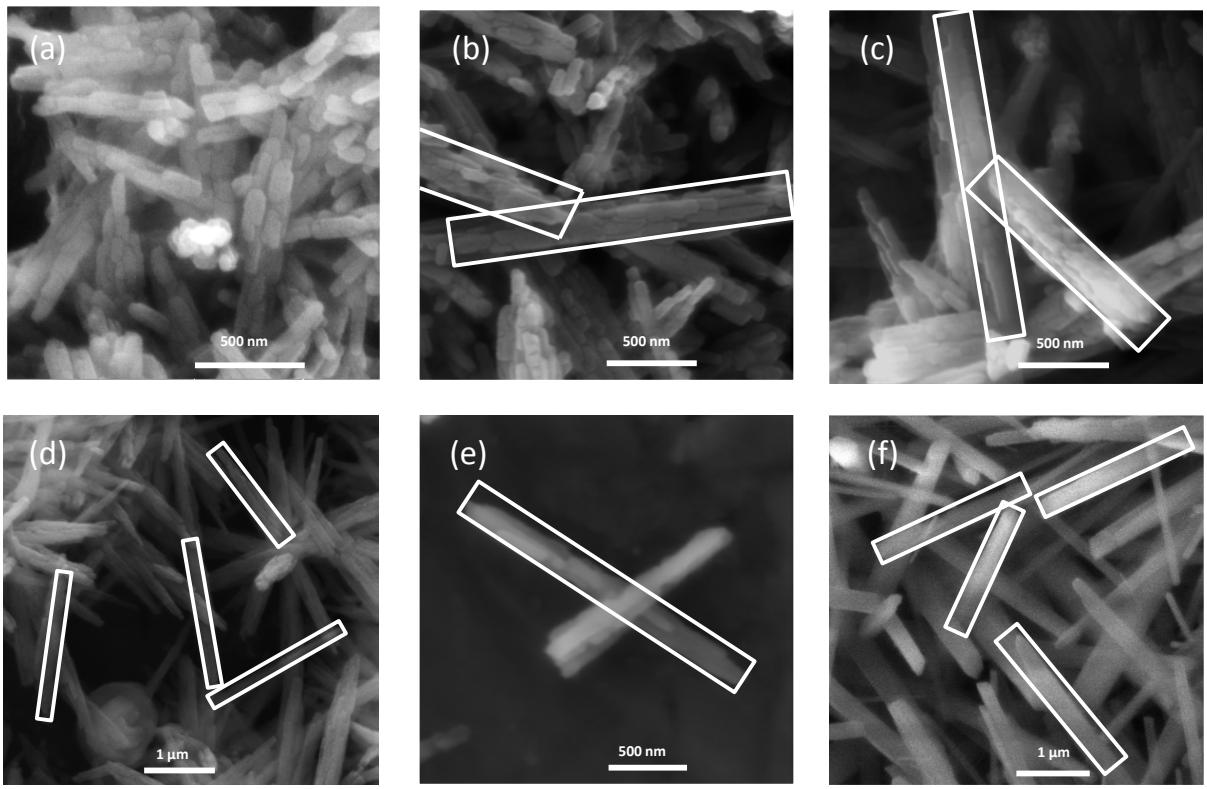

Figure 5-24. Size and morphology of ZSM-22 crystals synthesized with different weight percent (wt.%) of ethanol: (a) 0, (b) 2.5 (c) 5 (d) 7.5 (e) 10 (f) 20.

Figure 5-25 illustrates a possible growth mechanism of ZSM-22 crystals; the individual nanorods were attached together forming larger agglomerate when ethanol was added as a co-solvent. By increasing ethanol concentration in the synthesis mixture, the individual agglomerates increased in both length and diameter. The most significant increase was observed in the agglomerate length. By using a higher amount of ethanol (20 wt.%), the agglomerate became a unified large crystal. It is important to note that the unified crystal, became a longer when high concentrations of ethanol (>20 wt.%) was added as shown later in Figure 11.

Hayasaka and co-workers reported that the ZSM-22 nanorods attached and merged laterally with the increase of synthesis time [79].This the fused large crystals contain different Al orientation and hence provide different effect on the catalytic activity [79].

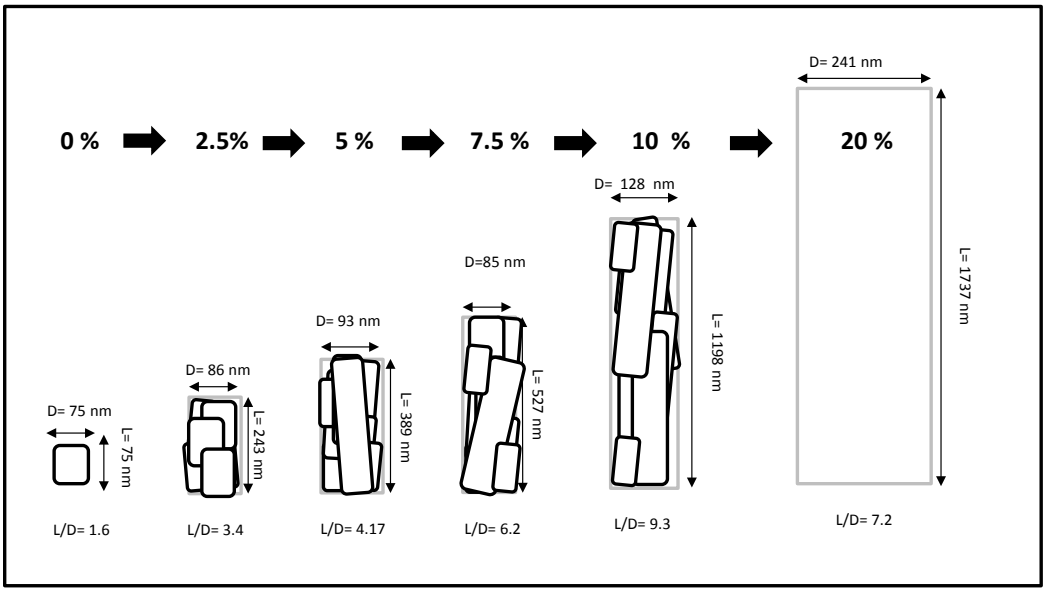

Figure 5-25. The effect of adding ethanol (EtOH (wt. %)) on the ZSM-22 morphology.

The nanorods were fused and attached together to form larger crystals as explained by the Ostwald ripening mechanism [140]. The formations of nanorods were favored kinetically since it was easier to form. Larger crystals were formed at the last stage of the phase formation unless it was transformed into another thermodynamically preferred phase [140, 141]. The effect of the co-solvent on the crystal growth is coinciding with Ostwald ripening mechanism. Co-solvents worked as an accelerator for the nanorods to be stabilized into the larger crystals.

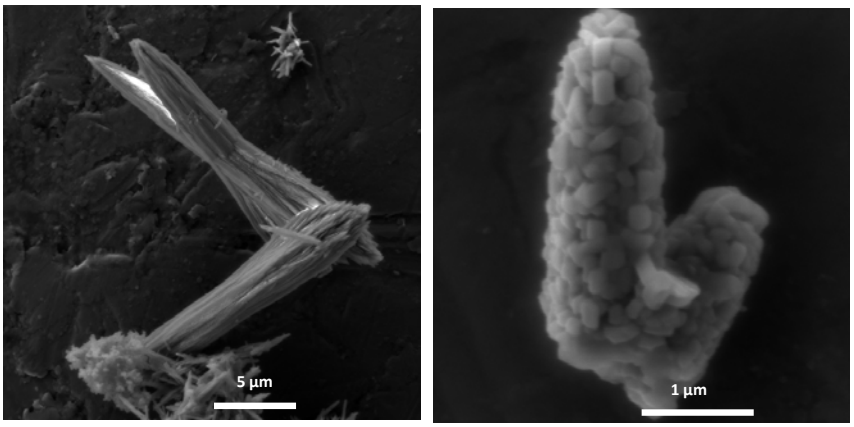

Figure 5-26. SEM micrographs of ZSM-22 synthesized with 10 wt.%.ethanol.

Wide crystal distribution was observed when 10 wt.% of ethanol was added to the synthesis mixture as presented in Figure 5-26. The non-uniformity of crystal sizes reported Gaona-Gómez and Cheng when ethanol was used as crystal growth modifier to synthesis LTL framework [111]. Lupulescu and coworkers reported that addition some co-solvents may stimulate similar phenomena [142].

5.2.8 Effect of propanol

With more hydrophobic solvent (1-propanol), it seems that the crystal growth modifier work more on reducing or preventing crystal length increasing. As shown in Figure 5-27, 1-propanol gave the smallest crystal and aspect ratio in comparison with the other crystal growth modifiers used.

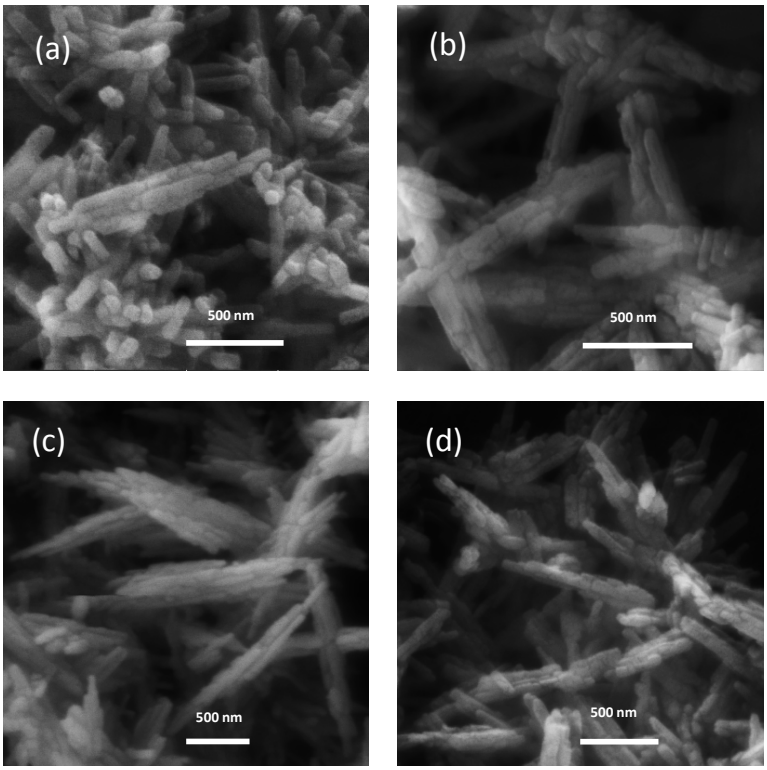

Figure 5-27. SEM micrographs of ZSM-22 synthesized in the presence of 0.5 wt.% co-solvents: (a) 1-propanol, (b) glycerol, (c) 2-propanol, (d) ethylene glycol.

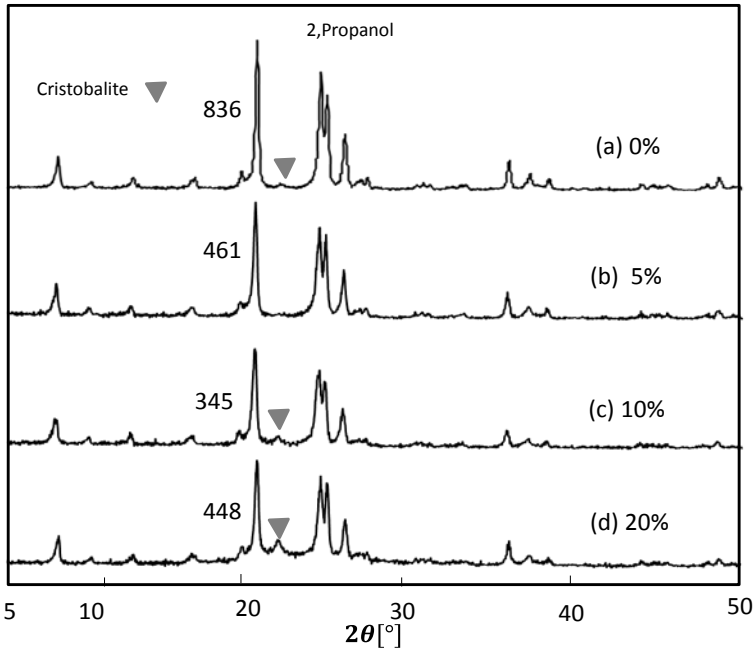

Figure 5-28. XRD patterns of ZSM-22 synthesized with different concentration of 2-propanol (wt. %): (a) 0, (b) 5, (c) 10, (d) 20.

It was noticed that the addition of isopropanol favor the agglomeration and orientation of ZSM-22 crystals and the formation of cristobalite impurity as showed in Figure 5-28 and Figure 5-29.

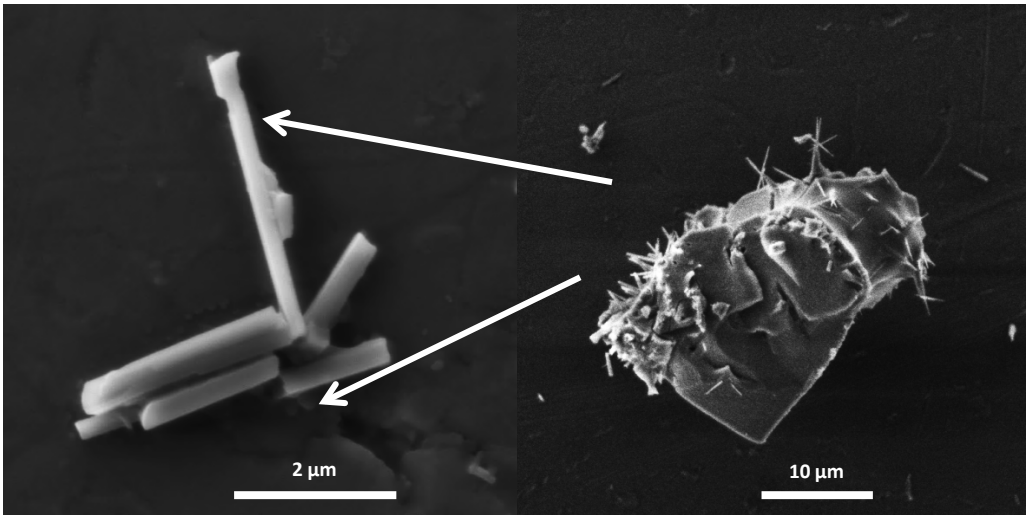

Figure 5-29. SEM of ZSM-22 synthesized with 20 wt.% of 2-propanol.

5.2.9 Effect of diols

The positive effect of the crystal growth modifier was observed when ethylene glycol was added to synthesis mixture. The presence of ethylene glycol suppressed the nucleation of cristobalite as shown from the XRD patterns in Figure 5-30.

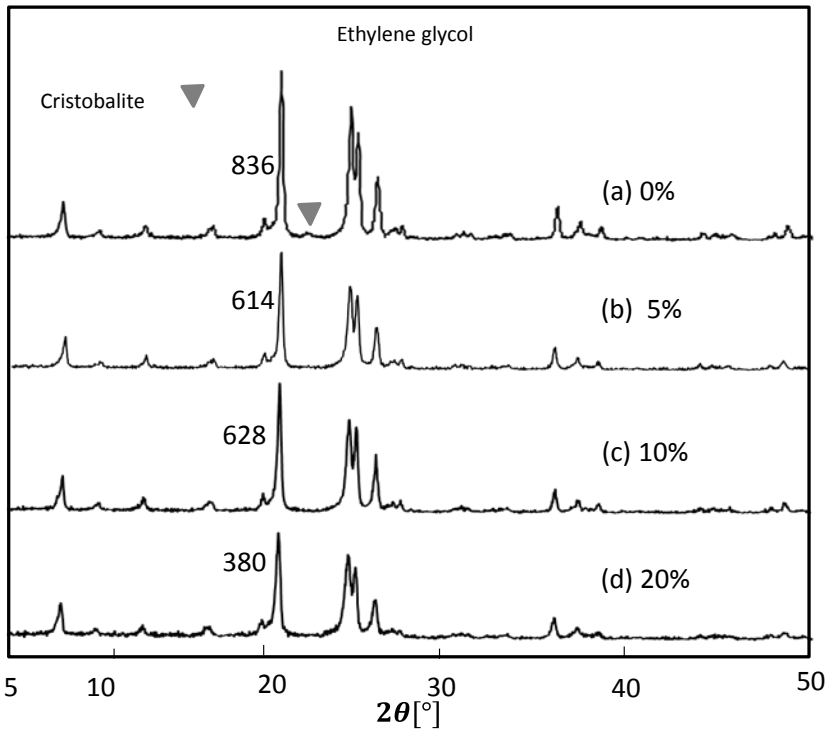

Figure 5-30. XRD patterns of ZSM-22 synthesized with different weight percent (wt.%) ethylene glycol.

Tri-ethylene glycol showed the strongest effect on the agglomeration rate as noticed in Figure 5-31 crystals was intensively agglomerated.

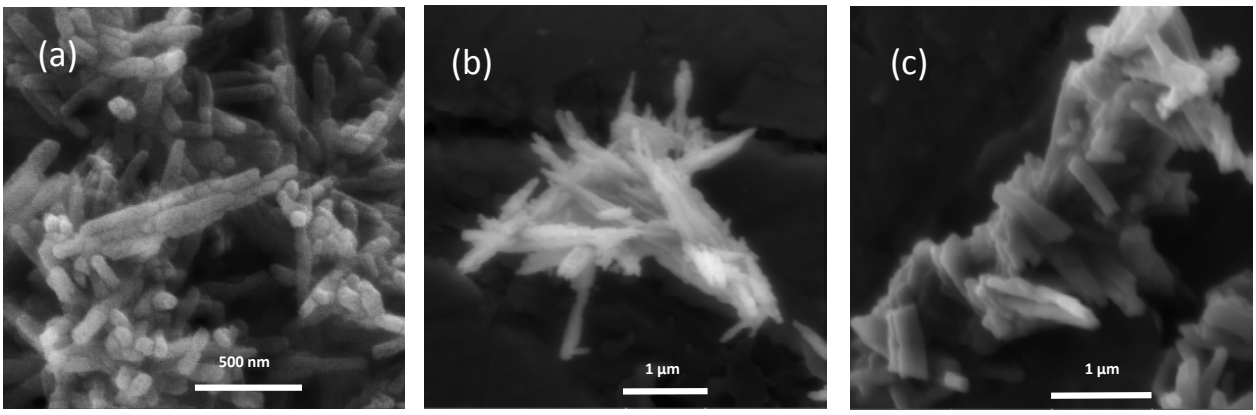

Figure 5-31. SEM micrographs of ZSM-22 synthesized with different concentration of tri-ethylene glycol (in wt.%): (a) 0, (b) 5 and (c) 10.

5.2.10 Effect of co-solvent concentration on the agglomeration rate

By adding more co-solvent in the synthesis mixture, the resulted ZSM-22 crystals tend to be longer. It is worth to mention that the higher rate of agglomeration was observed with higher concentrations of co-solvents in the solution-gel mixture. As clearly shown in Figure 5-25 and Figure 5-32, this kind of orientation or agglomeration will end up with larger individual crystals.

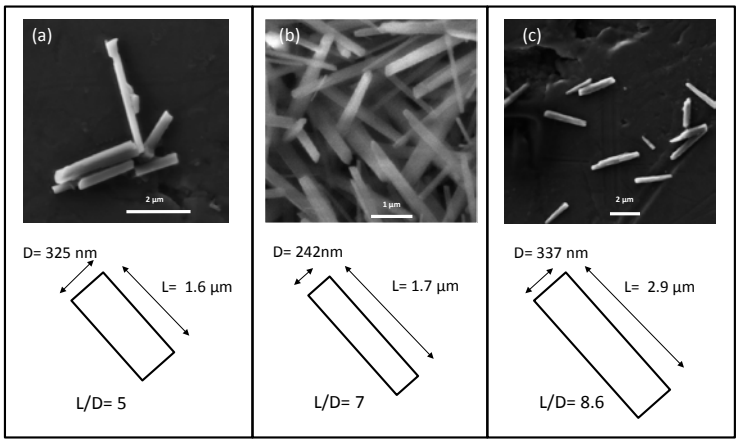

Figure 5-32. SEM micrographs of ZSM-22 synthesized in the presence of different co-solvents with 20 wt.% of co-solvents: (a) 2-propanol, (b) ethanol, (c) ethylene glycol.

5.2.11 Effect of co-solvent on the co-crystallization

Some zeolite phases such as MFI, cristobalite and MEL may appear as a competing phase in the synthesis of ZSM-22 as reported elsewhere [33, 77, 88, 143].

Table 5-8. Effect of ethylene glycol on TON synthesis.

Co-solvent	Si /Al (-)	Co-solvent /Al (-)	H_2O/Al (-)	DAH /Al (-)	T (℃)	t (h)	Morphology	Ref.
ethylene glycol	47	0	1890	29	160	24	ZSM-22	[76, 77]
ethylene glycol	48	53	1884	29	160	48	ZSM-22	[76, 77]
ethylene glycol	48	0	1921	57	143	96	**ZSM-5** +ZSM-22	[76, 77]
ethylene glycol	48	54	1921	29	143	72	ZSM-22	[76, 77]

Reactant ratios: molar ratio with respect to Al.
2-Conventional heating in PTFE-lined autoclaves was applied to all experiments.
3-Collodical silica (30%).
4- For the all experiments, KOH/Al= 11.9.
5-DAH: 1,6-diaminohexane
6-Bold type is the major phase

In the absence of co-solvent, we observed that very small traces of cristobalite phase as shown in Figure 5-23. The XRD patterns show that neither ZSM-5 (MFI) nor ZSM-11 (MEL) was present. In Table 5.2.11-1, we make a brief comparison among some co-solvents used in synthesis ZSM-22 [76, 77]. By using 2-propanol as co-solvent, co-crystallization of cristobalite phase identified as shown in Figure 5-28. On the other hand, addition of ethylene glycol suppressed the growth of impurities as showed in Figure 5-27. From these observations we can conclude that 2-propanol as co-solvent will favor and

stabilize cristobalite phase while ethylene glycol act as an excellent stabilizer for ZSM-22.

Table 5-9. Effect of different co-solvents on TON synthesis.

co-solvent	Si/Al (-)	co-solvent /Al (-)	co-solvent (wt.%)	T (℃)	time (h)	morphology
-	46	-	-	180	48	**ZSM-22**+cristobalite
ethylene glycol	46	218	20	180	48	**ZSM-22**
2-propanol	46	225	20	180	48	**ZSM-22**+cristobalite
ethanol	46	322	20	180	48	**ZSM-22+**cristobalite
1-propanol	46	225	20	180	48	**ZSM-22**+cristobalite

1-Reactants ratios: molar ratio with respect to Al.
2-For the all experiments Source of heat was autoclave.
3-Collodical silica (40%).
4- KOH/Al=26.5,H_2O/Al= 3203 and DAH/Al= 27.4.
5-DAH: 1,6-diaminohexane.
6-Bold type is the major phase.

From our observations, it seems that ethylene glycol stabilize nuclei of TON and from thermodynamic point of view this reduce energy barrier for TON formation, subsequently this lead to a better synthesis technique via reducing TON crystallization time and temperature which is similar to the other reports [76, 77].

The stabilization TON nuclei can be originated from the strong bond emerges between the diols and zeolite precursors, because of the additional hydroxyl group (OH) and ether groups (O) that are exist in the diols, as shown in Table 3. Similar phenomena were observed when LTL and MFI zeolites were synthesized in the presence diols as co-solvent [90, 111].

5.2.12 Mechanism of co-solvents as a crystallization modifier in the synthesis of ZSM-22 zeolite

The formation of zeolites crystals starts by the formation of zeolites nuclei followed by subsequent growth of zeolites precursors at higher crystallization temperature [79]. After the nuclei formed, an intervention is required to tune the growth process of zeolites crystals in order to get the required size and morphology. Many additives were used to achieve this goal. However, our objective here was to investigate the effect and mechanism of adding co-solvent as a modifier of zeolite crystal growth. To understand the role of co-solvents, it is important to investigating the interactions among the co-solvent, the structure directing agent and zeolite precursor surface [144]. A co-solvent, which is an alcohol such as ethanol or propanol, or a diol like ethylene glycol, provides a confined space that works as damper for zeolite growth, meantime changing the type co-solvent will directly effects the morphology of the produced zeolites [79]. Co-solvent adsorbs on the surfaces of the zeolites precursors, depending on the molecular structures of the co-solvent and zeolite precursors restrictions will form by attaching co-solvents molecules on the surface of nuclei. The key point in using co-solvent is choosing the right co-solvent that will result in the required size and shape. In case of co-solvent which adsorbs selectively on surfaces [100] that will lead to hinder these surfaces and the crystals will grow in [001] direction and this will result in elongation of the zeolites crystals. The other case of co-solvent which adsorbs selectively on surfaces [001] so crystals will grow in [100] direction and this will result in reducing the aspect ratio

(length/diameter) the third case is co-solvent adsorb on the all crystals surfaces making confined spaces to shape and reduce or increase the crystal size.

In the case of ZSM-22 zeolite, which has rod-like shapes [47, 49], we observed that adding co-solvent will stimulate crystal growth in c-direction [001] resulted in larger aspect ratio (length/diameter). From this finding, we propose that alcohols adsorbs more on [100] surfaces as described in Figure 5-33 for general co-solvents.

A potential explanation for this trend may be originated from hydroxyl groups density on the TON surfaces. It seems that hydroxyl groups are higher on surfaces [001], which lead to preferential adsorption of solvent with longer hydrocarbon chain such as propanol and butanol rather than the shorter ones like ethanol [142]. Similar observations were reported elsewhere for other zeolite frameworks. For instance, Chen and co-workers found that diols can be used as co-solvent to increase the crystal length of ZSM-5 crystals [90]. Ethanol also can stimulate zeolite L crystals growth in c-direction (elongation) when aging time is increased [111, 145]. These finding coincide with our results using co-solvents resulted in larger unified crystals.

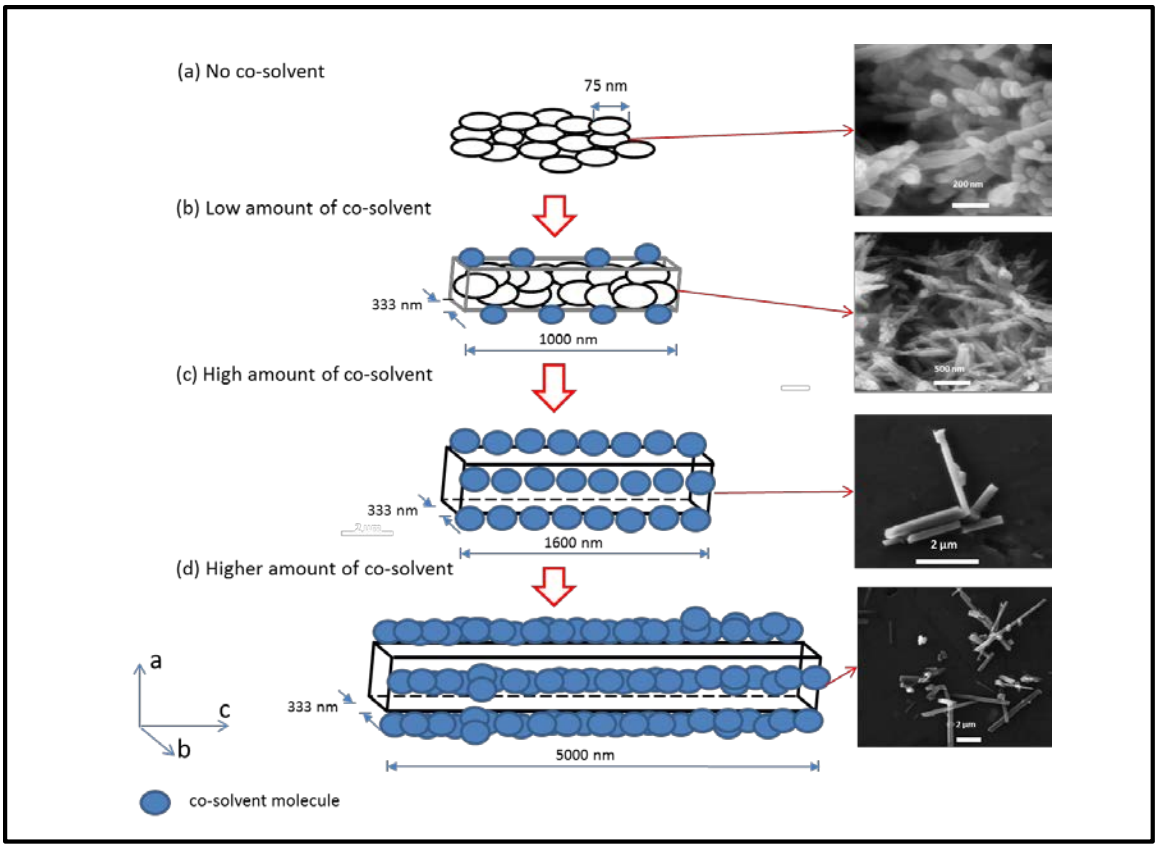

Figure 5-33. Proposed mechanism for the effect of adding co-solvent on ZSM-22 crystal size and morphology.

Figure 5-33 shows a proposed mechanism for the effect of co-solvent addition on ZSM-22 size and morphology. Without adding co-solvent, the as-synthesized ZSM-22 were separated nanocrystals with size of 76 nm and an aspect ratio of 1 (Figure 5-33.a). By adding a small amount of co-solvent (< 10 wt.%), those crystals were orienteded to form agglomerates and elongated large crystals in c-direction (needle shape, Figure 5-33.b). High concentration of co-solvent (10 - 20 wt.%), resulted in unified large crystals. Adding more co-solvent will increase the length of the unified crystals.

5.3 Methanol conversion to light olefins reaction over H-ZSM-22 zeolite crystals

The three different-sized H-ZSM-22 zeolite crystals were examined for the catalytic conversion of methanol; the crystal sizes were ca. 1000, 300 and 100 nm.

Table 5-10. BET surface areas of ZSM-22 zeolites with different crystal sizes.

Crystal length [nm]	**Si/Al [-]**	**S_{BET} [m^2 g^{-1}]**
100	46	150
300	46	100
1000	46	75

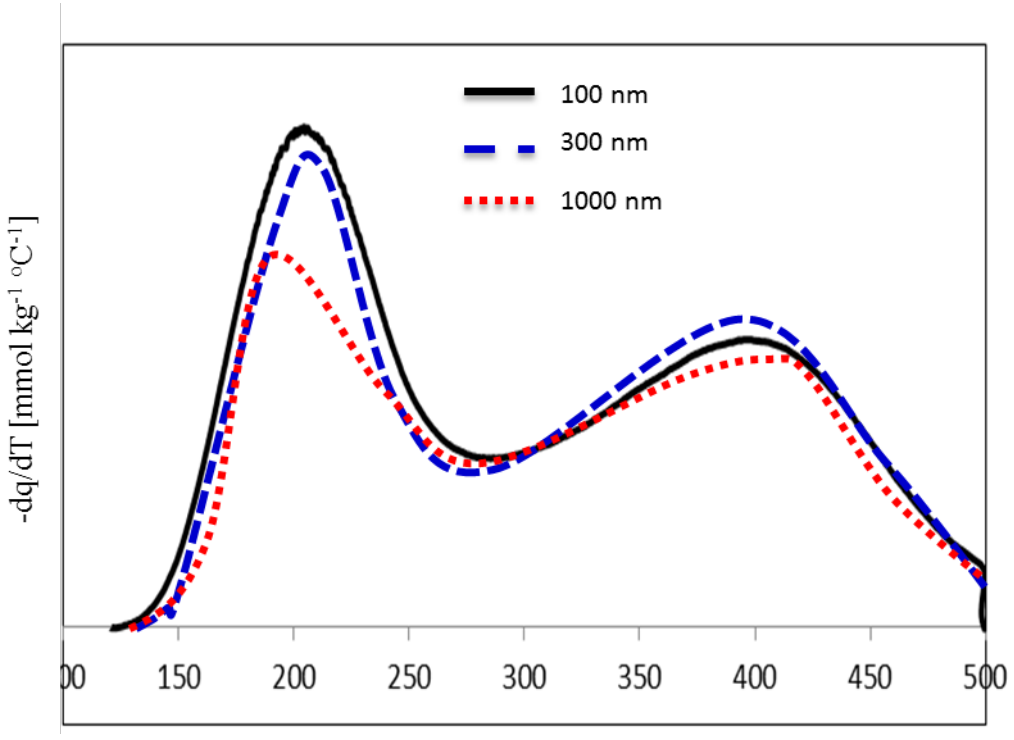

Figure 5-34. NH_3-TPD profiles of ZSM-22 zeolite with different crystal lengths.

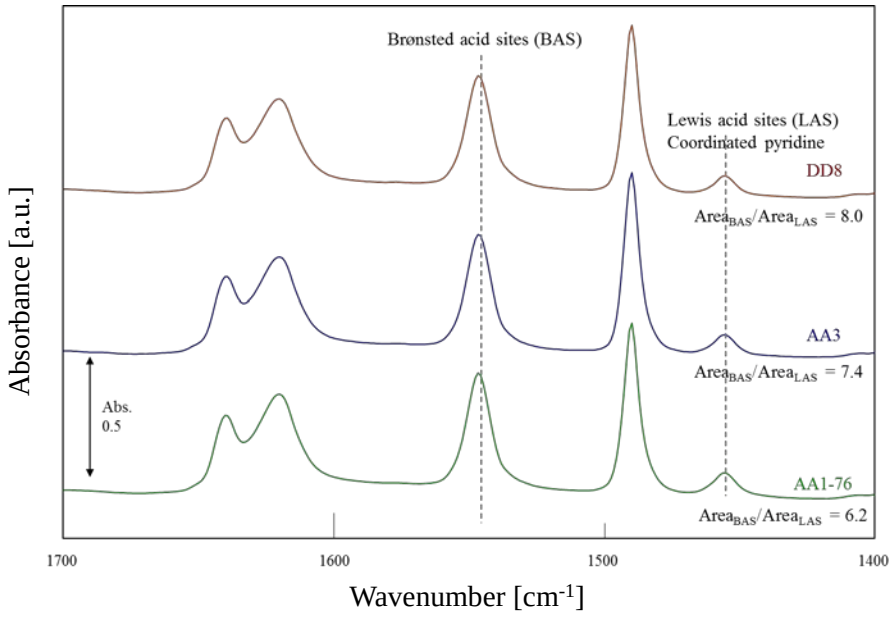

Figure 5-35. Pyridine FTIR analysis of ZSM-22 zeolite with different crystals sizes.

To investigate the effect of the crystal size of the ZSM-22 zeolites on the product selectivity and yield, ZSM-22 zeolites with Si/Al of 46 and different crystal sizes (100,300 and 1000 nm) were applied in methanol to olefins. Nanoscale ZSM-22 crystals were prepared via microwave-assisted hydrothermal synthesis with agglomeration controlled by using surfactant; another method was via using rotating autoclave as explained earlier (see Table 5.3-1). Different sizes of ZSM-22 zeolite were prepared using crystal growth modifiers. The phase purity was verified using the X-ray diffraction. Pure ZSM-22 zeolites were achieved and confirmed without any observed impurity peaks. The crystal sizes were measured using FE-SEM micrographs and confirmed by TEM.

As can be seen in Table 5.3-1, the BET surface area increased with decreasing crystal size. The Si/Al ratios of the resulted ZSM-22 zeolite crystals were nearly the same for the initial Si/Al ratio as confirmed by XRF analysis. The acid strength distribution of ZSM-

22 zeolite crystals were investigated using ammonia temperature-programmed desorption (NH_3-TPD) as shown in Figure 5-34. The Brönsted and Lewis acid sites of the ZSM-22 zeolite crystals were investigated by FTIR based on pyridine adsorption as shown in Figure 5-35. Even though the crystal sizes for the ZSM-22 zeolites were different the acidity properties were almost similar.

First, the influence of the reaction temperature on the catalytic performances was investigated. Figure 5-36 shows the effect of reaction temperature on the methanol conversion and the product selectivity. Unless the temperature is very low, diffusion of molecules inside the catalyst pellets is the responsible from obstructing the reaction rate [52]. High temperature stimulates pressure difference across pore insuring satisfying mass flow [52].

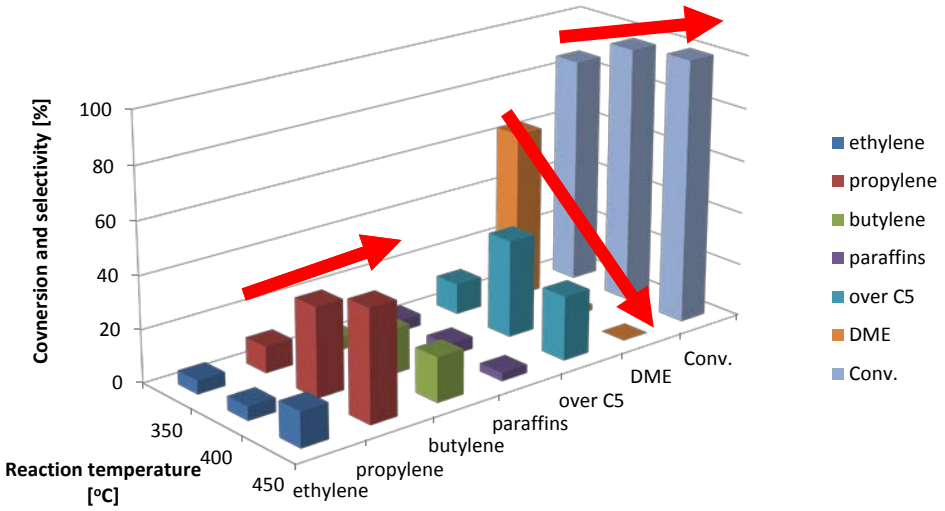

Figure 5-36. Effect of temperature on the conversion of the methanol and selectivity of the products over H-ZSM-22 zeolite with WHSV of 1.03 $gg^{-1}h^{-1}$.

It should be noted the methanol conversion was increased by increasing temperature and the same for the selectivity to olefins. Dimethyl ether was the major product at low

temperature (350 ℃). However, it was completely converted to olefins at higher temperatures (400 - 450 ℃). Temperature is essential for conversion of DME to olefins (further dehydration reaction) [14, 146]. Below 300 ^{o}C, there was no any dehydration of DME as can be seen in Figure 5-36.

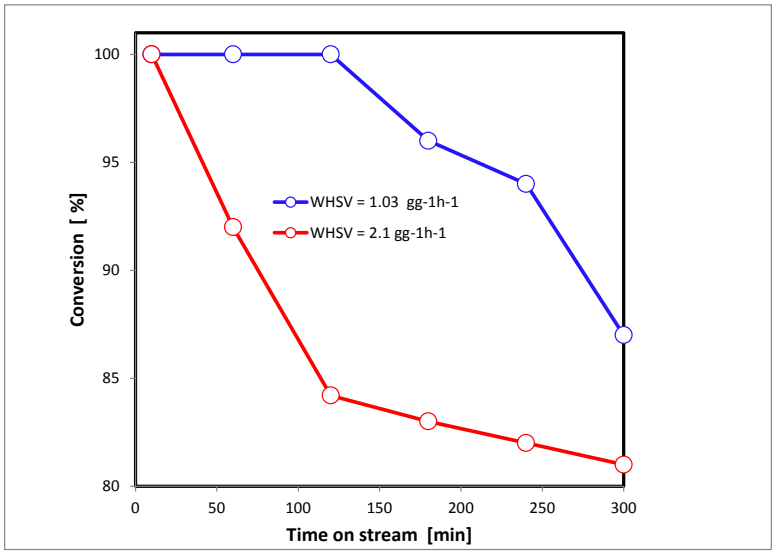

Figure 5-37. Results of methanol conversion reaction over the H-ZSM-22 zeolite catalysts at 450 ^{o}C with the different WHSV.

Changing feeding rate affected the catalyst life severely. At the same temperature, increasing feeding rate decreased the deactivation rate as shown in Figure 5-37.

5.3.1 Methanol conversion and Propylene selectivity over nano-sized H-ZSM-22 zeolite crystal

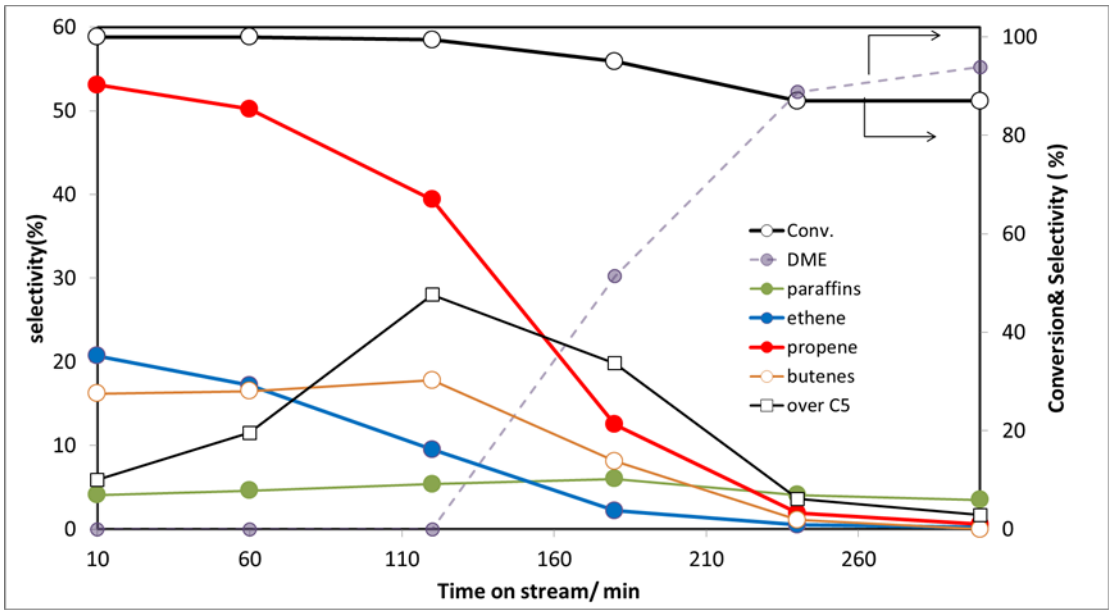

Figure 5-38. Methanol conversion and selectivity over the H-ZSM-22 catalysts at 450 ^{o}C with the WHSV = 1.03 $gg^{-1}h^{-1}$.

As shown in Figure 5-38. Firstly, propylene was formed as the major product with high percentage (53%), this percentage was higher than the highest reported percentage (35%) [72]. However, the selectivity to the desired propylene was decreased with the increase of time on stream. The selectivity to paraffins was almost constant. An explanation for this selectivity, the propylene was prodcued inside the pores by methylation and cracking cycle with little contribution from the hydrocarbon pool mechanism and hence the product contained higher amounts of aromatics such as polymethylbenzenes, naphthalenes, and phenanthrenes [72]. However, as coke species covered the surface of zeolite crystals inner pores, the strong acidity inside the pores is covered and hence more methylation reaction occurred [72]. The selectivity to C5 increased with increasing of

time from 10 to 120 min, and then the selectivity of C5 decreased which can be explained by the methylation of light olefins [64, 69]. After 110 min (see Figure 5-38), the methanol was increasingly converted to DME. At this stage, probably crystals pores were blocked and the reaction was carried out on the crystal surface. Finally, after 240 min the main product was DME, whcih formed from methylation of methanol on the deactivated ZSM-22 zeolite crystal surface [146].

5.3.2 Olefins selectivity and propylene/ethylene ratio over different crystal sizes

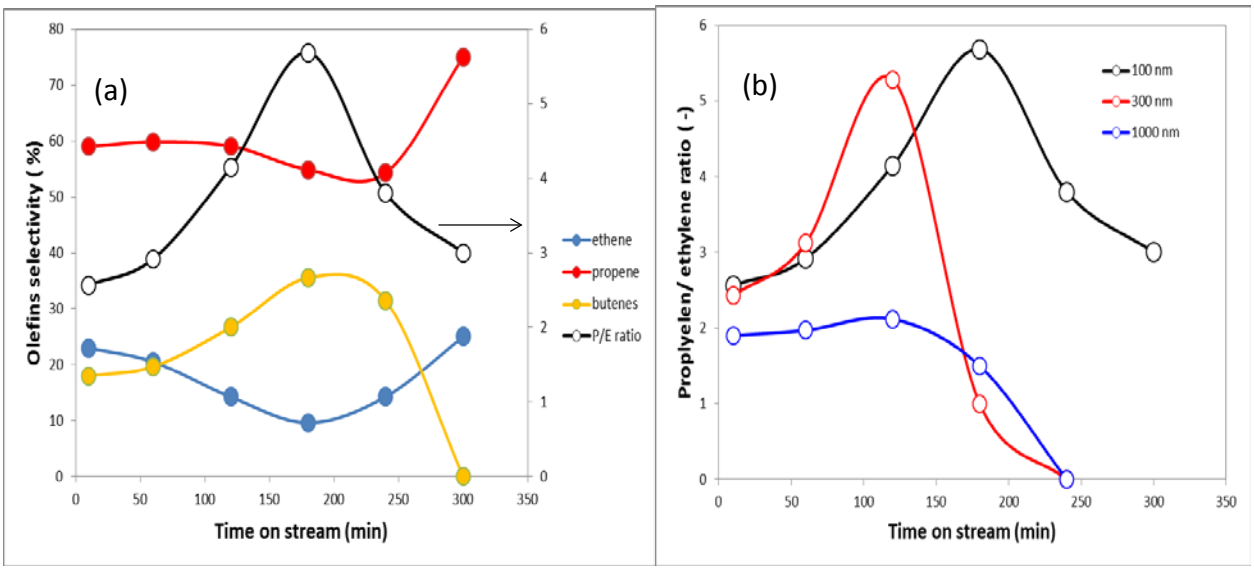

Figure 5-39. (a) Olefins selectivity over nanosized H-ZSM-22 (100 nm) (b) Effect of crystal size on the propylene over ethylene ratio at 450 ^{o}C, WHSV = 1.03 $gg^{-1}h^{-1}$.

Propylene and was the primary product, followed by heavier olefins formed probably by methylation reactions of the light olefins (propylene, ethylene), indicating that strong acid sites were covered by coke [64]. As shown in Figure 5-39 (a), propylene selectivity was the major product among the light olefins produced over the nanosized ZSM-22.

Generally, the propylene/ ethylene were the very high in comparisons with commercialized zeolites (ZSM-5 and SAPO-34) [14]. Propylene / ethylene ratio was affected by the ZSM-22 crystal size as shown in Figure 5-39 (b), the nanosized ZSM-22 crystals (100 nm) were the most stable catalyst with highest ratio of (5.5) at 200 min and still high (3) until 300 min. While, the medium (300 nm) and large (1000 nm) ZSM-22 crystals deactivated completely at 250 min. the worse results was for the the large crystals with the highest propylene / ethylene ratio of (2).

5.3.3 Stability of nanosized ZSM-22 zeolite crystal in methanol to propylene

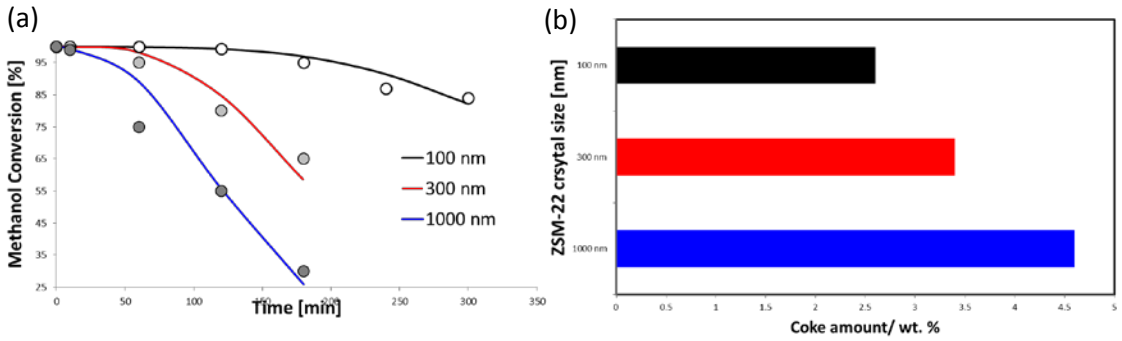

Figure 5-40. Effect of crystal size on: (a) Conversion of the methanol, (b) amount of coke after 180 min. Reaction carried out over H-ZSM-22 with WHSV = 1.03 $gg^{-1}h^{-1}$.

The effect of zeolite crystal size on catalytic stability and olefins selectivity were investigated. As shown in Figure 5-40, the conversion of methanol to hydrocarbons over ZSM-22 zeolites, conventional ZSM-22 zeolite crystallites were deactivated quickly by the pore blocking as mentioned earlier. Interestingly, by scaling down the crystal length, the deactivation rate decreased noticeably therefore the lowest deactivation rate was observed over the nanocrystals. The same trends were noticed for the coke deposition (see Figure 5-40.b).

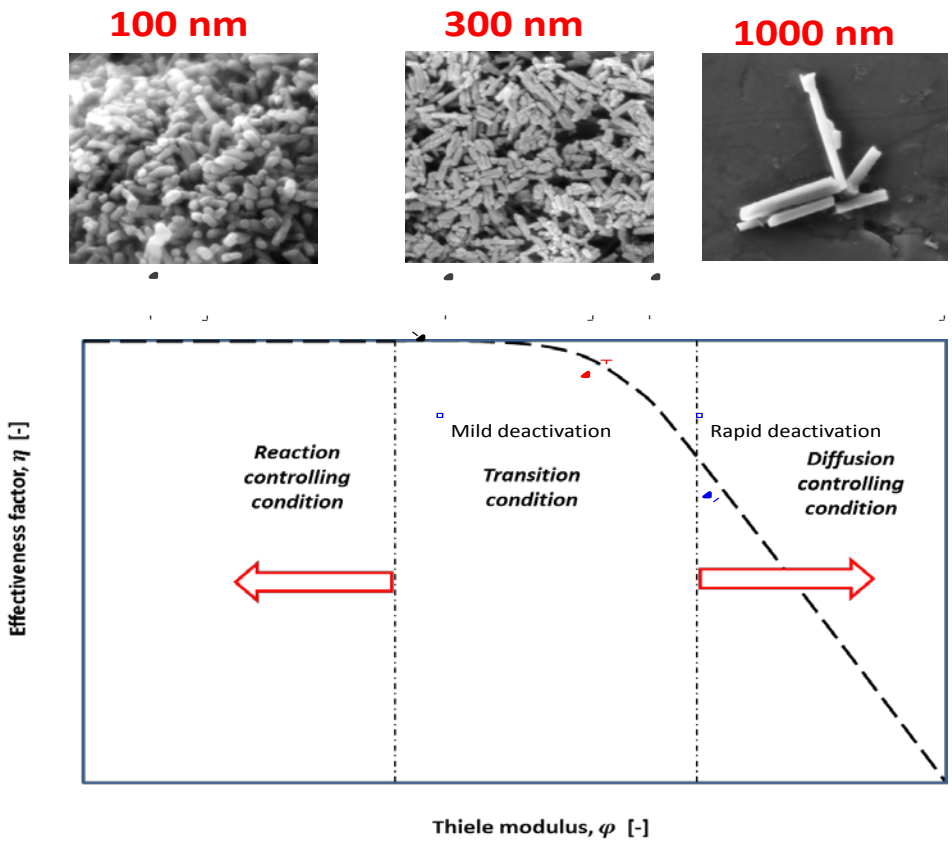

Figure 5-41. Thiele modulus and effectiveness factor in methanol to light olefins reaction at 450 ^{o}C over ZSM-22 zeolites (Si/Al =46) with different crystal sizes.

To investigate the effect of crystal sizes on the catalyst activity, the Thiele modulus and the effectiveness factor for methanol conversion on ZSM-22 zeolite crystals were calculated and investigated in details as shown in Figure 5-41 and Table 5.3.3-1 and Appendix C. Small Thiele modulus leads to low diffusional resistance ($\varphi \rightarrow 0, \eta \rightarrow 1$) while the large value of Thiele modulus means low effectiveness factor and then high resistance to the molecular diffusion in the crystal pores ($\varphi \rightarrow \infty, \eta \rightarrow {}^{1}/_{\varphi}$).

For the large crystal size (1000 nm) the catalytic performance was highly affected by interacristalline diffusion reflected in large Thiele modulus number and low effectiveness factor (φ = 2.3, η = 0.1) as shown in Table 5.3.3-1. The large crystal performance was in

the region of diffusion controlling condition (see Figure 5-41). While the medium size crystal (300 nm) were in the transition region (φ = 1.2, η = 0.71). The small crystal (100 nm) was free of diffusion obstacles as confirmed by Thiele modulus and effectiveness factor (φ = 0.15, η = 0.95). More details on calculations of Thiele modulus and effectiveness factor are shown in Appendix C

Table 5-11. Deactivation calculations results for different ZSM-22 zeolite crystal sizes

Size (nm)	**Φ** **[-]**	$\boldsymbol{\eta}$ **[-]**	$\mathbf{k_d}$ $[\mathbf{s^{-1}}]$	**k`** $[\boldsymbol{m^3 . kg^{-1} . s^{-1}}]$
100 nm	0.15	0.95	0.0061	0.078
300 nm	1.2	0.71	0.0242	0.075
1000 nm	2.3	0.11	0.0334	0.43

CHAPTER 6

CONCLUSIONS AND RECOMMENDATIONS

6.1 Conclusions

Decreasing the size of ZSM-22 zeolite crystal to the nanometer scale crystals (< 100 nm) with low-aspect-ratio has been achieved by using microwave radiation as a heating source. The reduced agglomeration rate was observed in small concentration of the nonionic surfactant (Brij-76). The polyoxyethylene surfactant acted as a promoter in crystallization without stimulating the nucleation of unwanted phases. Increasing Si/Al in the initial solution increased the ZSM-22 zeolite crystal length. Nanosized ZSM-22 zeolites have been applied as an effective catalyst for methanol to olefins with high selectivity to propylene.

We also demonstrated the effects of co-solvents as crystal growth modifier in the synthesis of ZSM-22. We were able to synthesize ZSM-22 zeolite with different sizes and morphologies, while the nanosized of ZSM-22 zeolite crystals were not reported previously. Low aspect ratio of ZSM-22 zeolite crystals (length/width = 1) was achieved. In the presence of co-solvent, we obtained wide range aspect ratios up to 9. After the formation of zeolite nuclei, intervention by co-solvent is required to tune the growth process of zeolites crystals. Co-solvents were added as a modifier of zeolite crystal growth. Addition of co-solvents to ZSM-22 zeolite synthesis solution may stimulate crystal growth in the c-direction [001] resulted in a higher aspect-ratio. The nucleation of

unwanted cristobalite phase in the synthesis of ZSM 22 zeolite was suppressed by addition of co-solvents especially by using ethylene glycol. This study explored the applicability of co-solvents can be used as effective, flexible and cheap platform to control crystal size of zeolites, which are crucial in refining and petrochemicals.

It was found that controlling zeolite crystal sizes are important in reaction like MTO reaction. Nano-crystal size of ZSM-22 zeolite showed better propylene selectivity, higher catalytic activity and more deactivation resistance as it is confirmed by effectiveness factor and Thiele modulus calculations. The conversion of methanol to light olefins over nanosized ZSM-22 zeolite (100 nm) was under reaction limiting condition as calculated by Thiele modulus and effectiveness factor ($\varphi = 0.15$, $\eta = 0.95$).

6.2 Recommendations

The application of ZSM-22 as a catalyst in MTO can be improved by doping the crystals using heteroatoms metals. The high-selectivity to propylene may be enhanced by acid treatment of ZSM-22 crystals, which is also helpful in increasing catalyst lifetime.

NOMENCLATURE

AlPO4	Aluminophosphate (zeolitic material composed of Al, P and O)
BET	Braunauer-Emmet-Teller
W	Catalyst weigth
K	Dimensionless adsorption equilibrium constant
DME	Dimethyl ether
D_{eff}	Effective diffusivity
ke	Effective reaction constant
EDS	Energy dispersive x-ray spectroscopy
FAU	Faujasite
FESEM	Field Emission Scanning Electron Microscope
FTIR	Fourier transform infrared spectroscopy
GC	Gas chromatography
C_{Ao}	Initial methanol concentration (mol/m^3)
IUPAC	International Union of Pure and Applied Chemistry
D	Intracrystalline diffusivity
k	Intrinsic rates constant
AEI	IZA code for the framework of AlPO4-18 and SAPO-18
AFI	IZA code for the framework of AlPO4-5 and SAPO-5
CHA	IZA code for the framework of Chabazite, SSZ-13 and SAPO-34
MFI	IZA code for the framework of ZSM-5

LTA	Linde type A
LTL	Linde type l
L	Mean diffusion path length
MeOH	Methanol
C_A	Methanol concentration (mol/m^3)
MTG	Methanol-to-gasoline
MTH	Methanol-to-hydrocarbons
MTO	Methanol-to-olefins
MTP	Methanol-to-propene
MAHyS	Microwave-assisted hydrothermal synthesis
MTT	Mobil Twenty Three, IZA code for the framework of ZSM-12
MW	Molecular weight
MFI	Mordenite Framework Inverted
OSDA	Organic Structural Directing Agent
am	Outer surface area of the zeolite crystal
H	Partition factor
Brij-76	Polyoxyethylene surfactant with chain length of 10
P/E	Propylene / ethylene ratio
T	Reaction temperature
t	Reaction time
SAPO	Silicoaluminophosphate (zeolitic material consisting of Si, Al, P and O)
TPD	Temperature-programmed desorption

M_t	The amount adsorbed at time t
TON	Theta-One, IZA code for the framework of ZSM-22
TOS	Time on stream
R	Universal gas constant (kJ/kmol K)
M_e	Value of M_t at equilibrium
V	Volume of the vapor phase
WHSV	Weight hourly space velocity (often referred to simply as space velocity)
XRD	X-ray diffraction
dp	Zeolite pore diameter
ZSM	Zeolite Socony Mobil

Greek Letters

$\tilde{\tau}$	Tortusity
ϕ_p	Pellet porosity
σ_c	Constriction factor
η	Effectiveness factor
ϕ	Thiele modulus
ϕ_s	Intracrystalline Thiele modulus

Appendices

Appendix A. One dimensional zeolites

Table A. One dimensional zeolites with different topology and ring structure [45].

Topology	Zeolite	Direction	Ring structure	Main channel (nm)
VFI	VPI-5	[001]	18	1.27 x 1.27
AET	AlPO-8	[001]	14	0.79 x 0.87
CFI	CIT-5	[010]	14	0.72 x 0.75
DON	UTD-1F	[010]	14	0.81 x 0.82
SFH	SSZ-53	[001]	14	0.64 x 0.87
SFN	SSZ-59	[001]	14	0.62 x 0.85
AFI	AlPO-5	[001]	12	0.73 x .73
ASV	ASU-7	[001]	12	0.41 x 0.41
ATO	AlPO-31	[001]	12	0.54 x 0.54
ATS	MAPO-36	[001]	12	0.65 x 0.75
CAN	Cancrinite	[001]	12	0.59 x 0.59
CZP	Chiral $ZnPO_4$	[001]	12	0.38 x 0.72 (highly distorted 12-ring)
EZT	EMM-3	[100]	12	0.65 x 0.74
GON	GUS-1	[001]	12	0.54 x 0.68
IFR	ITQ-4	[001]	12	0.62 x 0.72

LTL	Linde Type L	[001]	12	0.71 x 0.71
MTW	ZSM-12	[010]	12	0.56 x 0.60
NPO	Nitridophosphate-1	[100]	12	0.33 x 0.44
OSI	UiO-6	[001]	12	0.52 x 0.60
-RON	Roggianite	[001]	12	0.43 x 0.43
SFE	SSZ-48	[010]	12	0.54 x 0.76
SSY	SSZ-60	[001]	12	0.50 x 0.76
VET	VPI-8	[001]	12	0.59 x 0.59
AEL	AlPO-11	[001]	10	0.40 x 0.60
AFO	AlPO-41	[001]	10	0.43 x 0.70
AHT	AlPO-H2	[001]	10	0.33 x 0.68
EUO	EU-1	[100]	10	0.41 x 0.54 with large side pockets
LAU	Laumontite	[100]	10	0.40 x 0.53 (contracts upon dehydration)
MTT	ZSM-23	[001]	10	0.45 x 0.52
-PAR	Partheite	[001]	10	0.35 x 0.69
PON	IST-1	[100]	10	0.50 x 0.53
SFF	SSZ-44	[001]	10	0.54 x 0.57
STF	SSZ-35	[001]	10	0.54 x 0.57
TON	Theta-1	[001]	10	0.46 x 0.57
-CHI	Chiavennite	[001]	9	0.39 x 0.43
ABW	Li-A ACP-1	[001]	8	0.34 x 0.38

ATN	MAPO-39	[001]	8	0.40 x 0.40
ATV	AlPO-25	[001]	8	0.30 x 0.49
AWO	AlPO-21	[100]	8	0.27 x 0.55
AWW	AlPO-22	[001]	8	0.39 x 0.39
BCT	Mg-BCTT	[001]	8	0.24 x 0.24
BIK	Bikitaite	[010]	8	0.28 x 0.37
CAS	Cs luminosilicate	[001]	8	0.24 x 0.47
ESV	ERS-7	[010]	8	0.35 x 0.47
JBW	Na-J	[001]	8	0.37 x 0.48
MTF	MCM-35	[001]	8	0.36 x 0.39
RTE	RUB-3	[001]	8	0.37 x 0.44

Appendix B. Kinetic molecular diameter of selected compounds

Table B. Kinetic molecular diameter of selected compounds, adopted from (http://www.sigmaaldrich.com/chemistry.htmlhttp://www.sigmaaldrich.com/chemistry/chemical-synthesis/learning-center/technical-bulletins/al-1430/molecular-sieves.html) [115].

Molecule	Critical Diameter [nm]	Molecule	Critical Diameter [nm]
Helium	0.2	Propane	0.49
Hydrogen	0.24	n-Butane to n-Docosane	0.49
Acetylene	0.24	Propylene	0.5
Oxygen	0.28	1-Butene	0.51
Carbon Monoxide	0.28	Trans-2-Butene	0.51
Carbon Dioxide	0.28	1,3-Butadiene	0.52
Nitrogen	0.3	Isobutane to Isodocosane	0.56
Water	0.32	Dimethyl ether	0.585
Ammonia	0.36	Cyclohexane	0.61
Argon	0.38	Benzene	0.67
Methane	0.4	Toluene	0.67
Ethylene	0.42	p-Xylene	0.67
Ethylene Oxide	0.42	m-Xylene	0.71
methanol	0.44	o-Xylene	0.74
methanol	0.44		

Appendix C. Thiele modulus and effectiveness factor calculations

1st order reaction rate with respect to methanol [14]

- $-r'_A = \acute{k} \, . C_A . a . \eta$ *"Deactivation with diffusion resistance"*
- $\varphi = L\sqrt{\frac{k' \rho}{D_e}}, \eta = \frac{\tanh \varphi}{\varphi}$ *"Slab shape"*, $-\frac{da}{dt} = k_d \, a$
- $\frac{W}{F} = \int \frac{dx}{-r'_A}$ "plug flow reactor"
- $\ln\left(\frac{C_{A0}}{C_A}\right) = \frac{k' \tau'}{\varphi} \, e^{(\frac{-k_d \, t}{2})}$
- $\ln\left(\ln\left(\frac{1}{1-X}\right)\right) = \ln\left(\frac{k' \tau'}{\varphi}\right) - \frac{k_d \, t}{2}$ **(C-1)**
- $D_{eff} = 1 * 10^{-9} \, \frac{m^2}{s}, \rho = 630 \, kg.m^{-3}, \tau' = 1300.76 \, kg.s.m^{-3}$

Diffusivity of methanol can be measured via experiments. Volumetric method is one of the methods used [147]:

$$\frac{M_t}{M_e} = 1 - \sum_{n=1} \frac{2\alpha(1+\alpha)}{1+\alpha+\alpha^2 q_n^2} exp\left(-\frac{D q_n^2 t}{L^2}\right)$$

$\alpha = V/(\alpha_m WHL), tanq_n = -\alpha q_n.$

Based on the approximation done for one dimensional zeolites with wide diameters (> 0.73 nm) [148] and ZSM-5 zeolite 3D pore system, which its 10 ring pore structure is similar to ZSM-22 (TON) zeolite the intracrystalline diffusivity (D_{eff}) for methanol diffusion under MTO reaction conditions was estimated to be $D_e = 1 * 10^{-9} \, \frac{m^2}{s}$ [149].

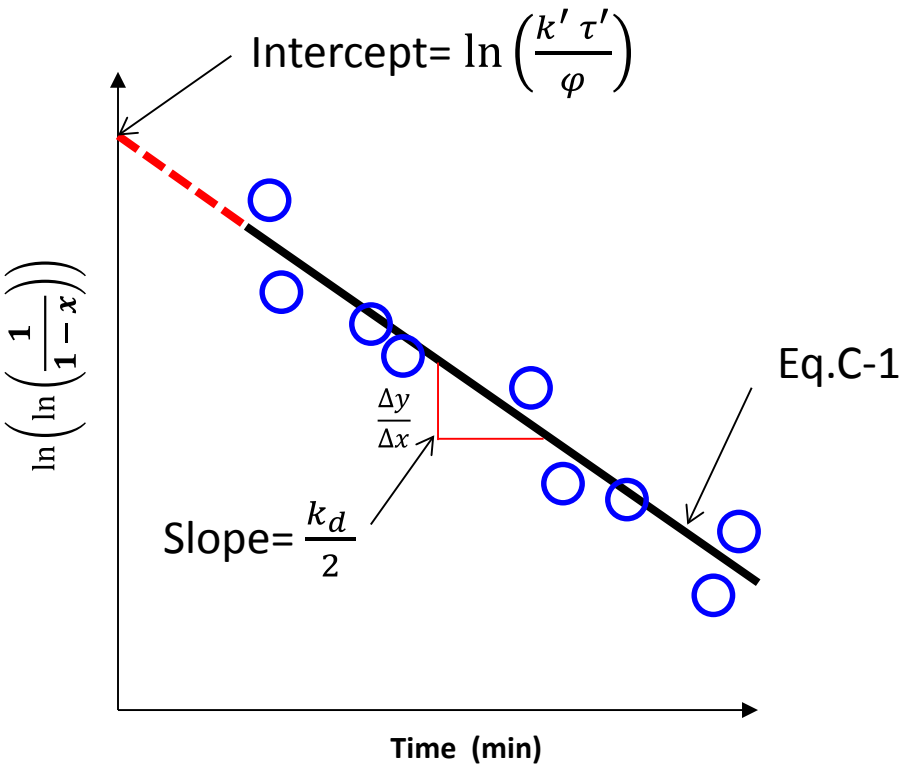

Figure C-1. Kinetic expressions of Equation (C-1) in the presence of the deactivation and pore diffusional resistance.

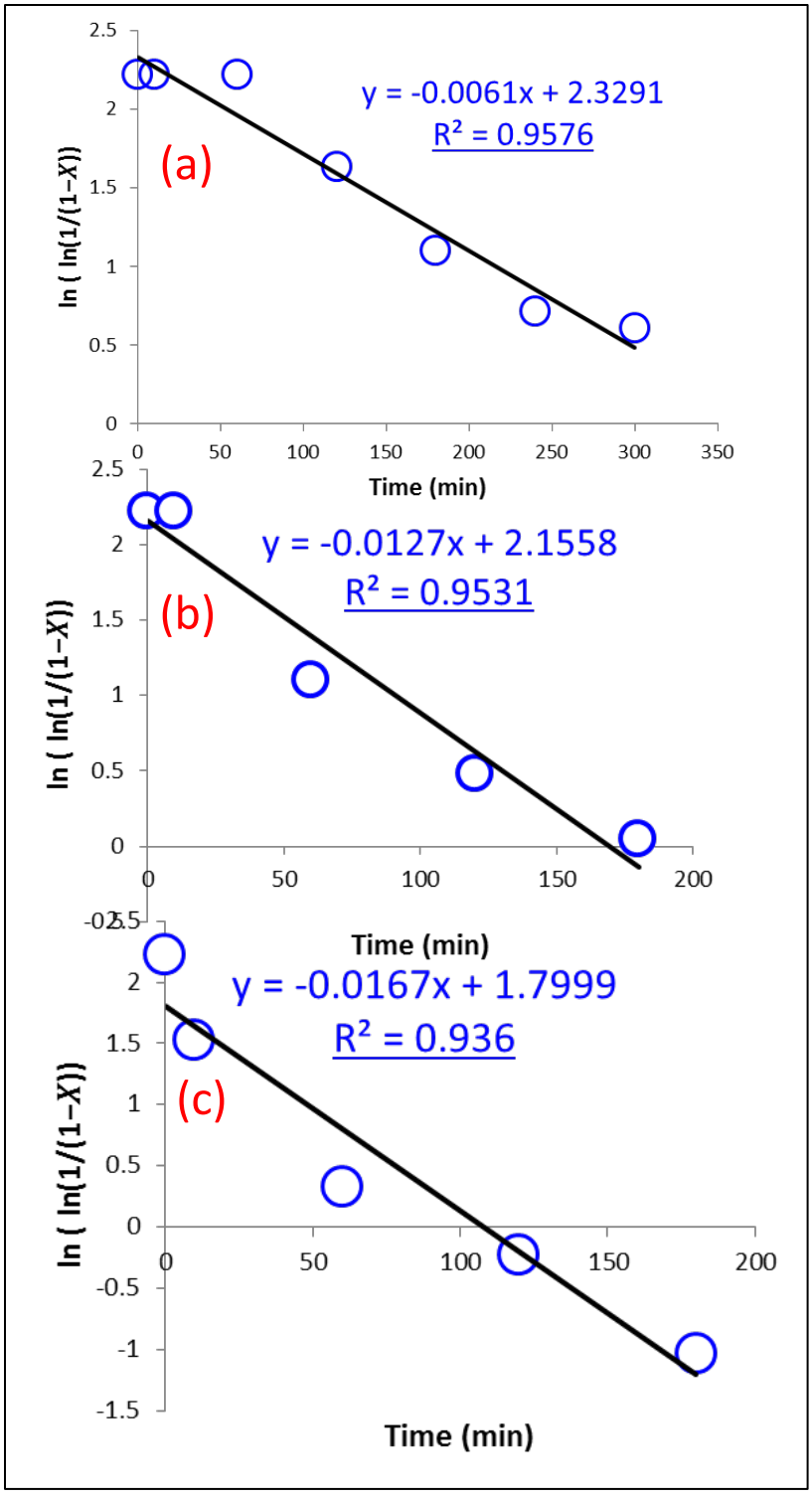

Figure C-2.Calculated deactivation constant and observed reaction constant for different ZSM-22 crystal sizes: (a) 100 nm,(b) 300 nm, and (c)1000 nm.

REFERENCES

[1] M. Stöcker, Methanol-to-hydrocarbons: catalytic materials and their behavior, Microporous and Mesoporous Materials, 29 (1999) 3-48.
[2] Americas Light Olefins Market is Expected to Grow Over Forecast Period at a CAGR of 3.4%, in, ASDReports, The Netherlands, 2012.
[3] 2009 world light Olefins analysis, in, 2008.
[4] L.A. Pellegrini, G. Soave, S. Gamba, S. Langè, Economic analysis of a combined energy–methanol production plant, Applied Energy, 88 (2011) 4891-4897.
[5] H. Koempel, W. Liebner, Lurgi's Methanol To Propylene (MTP®) Report on a successful commercialisation, Studies in Surface Science and Catalysis, 167 (2007) 261-267.
[6] J.D. Sherman, Synthetic zeolites and other microporous oxide molecular sieves, Proceedings of the National Academy of Sciences, 96 (1999) 3471-3478.
[7] F. Grinberg, P. Heitjans, Diffusion Fundamentals Leipzig 2005, Leipziger Universitätsverlag, 2005.
[8] S.M. Auerbach, K.A. Carrado, P.K. Dutta, Handbook of zeolite science and technology, CRC press, 2003.
[9] S. Taylor, Abundance of chemical elements in the continental crust: a new table, Geochimica et Cosmochimica Acta, 28 (1964) 1273-1285.
[10] K. Byrappa, M. Yoshimura, Handbook of hydrothermal technology, Access Online via Elsevier, 2001.
[11] J. Weitkamp, Zeolites and catalysis, Solid State Ionics, 131 (2000) 175-188.
[12] A. De Araujo, V. Fernandes, G.J. Fernandes, Determination of Ca/NaY zeolite acidity by TG and DSC, Journal of Thermal Analysis and Calorimetry, 49 (1997) 567-572.
[13] A. Aerts, M. Haouas, T.P. Caremans, L.R. Follens, T.S. van Erp, F. Taulelle, J. Vermant, J.A. Martens, C.E. Kirschhock, Investigation of the Mechanism of Colloidal Silicalite-1 Crystallization by Using DLS, SAXS, and 29Si NMR Spectroscopy, Chemistry-A European Journal, 16 (2010) 2764-2774.
[14] G. Froment, W. Dehertog, A. Marchi, Zeolite catalysis in the conversion of methanol into olefins, Catalysis, 9 (1992).
[15] S.H. Brown, D. Levin, R. Shinnar, W.A. Weber, Single stage process for converting oxygenates to gasoline and distillate in the presence of undimensional ten member ring zeolite, in, Google Patents, 2002.
[16] P. Meriaudeau, V. Tuan, V.T. Nghiem, S. Lai, L. Hung, C. Naccache, SAPO-11, SAPO-31, and SAPO-41 Molecular Sieves: Synthesis, Characterization, and Catalytic Properties in< i> n</i>-Octane Hydroisomerization, Journal of Catalysis, 169 (1997) 55-66.
[17] L. Vial, P. Dumy, Artificial enzyme-based biosensors, New Journal of Chemistry, 33 (2009) 939-946.
[18] R.J. Argauer, Crystalline zeolite zsm-s and method, in, Google Patents, 1972.
[19] P. Chu, ZSM-II, in, Google Patents, 1973.

[20] H. Furuta, N. Matsuzawa, A. Tachi, T. Tomoshige, Epoxy-modified polyolefin wax, process for preparation thereof and thermosetting resinous composition comprising said wax, in, Google Patents, 1981.
[21] E.W. Valyocsik, Synthesis of zeolite ZSM-22 with a heterocyclic organic compound, in, Google Patents, 1984.
[22] C.J. Plank, E.J. Rosinski, M.K. Rubin, Crystalline zeolite ZSM-23 and synthesis thereof, in, Google Patents, 1978.
[23] C.J. Plank, E.J. Rosinski, M.K. Rubin, Crystalline zeolite and method of preparing same, in, Google Patents, 1977.
[24] C.T. Chu, N.M. Page, E.W. Valyocsik, Zeolite ZSM-57, in, Google Patents, 1989.
[25] G.C. Edwards, D.E.W. Vaughan, Synthetic ferrierite synthesis, in, Google Patents, 1976.
[26] E.W. Valyocsik, Synthesis of crystalline silicate ZSM-48, in, Google Patents, 1986.
[27] R. Byggningsbacka, L.-E. Lindfors, N. Kumar, Catalytic activity of ZSM-22 zeolites in the skeletal isomerization reaction of 1-butene, Industrial & engineering chemistry research, 36 (1997) 2990-2995.
[28] R. Kumar, P. Ratnasamy, Isomerization and formation of xylenes over ZSM-22 and ZSM-23 zeolites, Journal of Catalysis, 116 (1989) 440-448.
[29] J.A. Martens, W. Souverijns, W. Verrelst, R. Parton, G.F. Froment, P.A. Jacobs, Selective isomerization of hydrocarbon chains on external surfaces of zeolite crystals, Angewandte Chemie International Edition in English, 34 (1995) 2528-2530.
[30] M.W. Simon, S.L. Suib, C.-L. Oyoung, Synthesis and characterization of ZSM-22 zeolites and their catalytic behavior in 1-butene isomerization reactions, Journal of Catalysis, 147 (1994) 484-493.
[31] W. Souverijns, J. Martens, G. Froment, P. Jacobs, Hydrocracking of Isoheptadecanes on Pt/H–ZSM-22: An Example of Pore Mouth Catalysis, Journal of catalysis, 174 (1998) 177-184.
[32] F.G. Dwyer, Highly siliceous porous crystalline material ZSM-22 and its use in catalytic dewaxing of petroleum stocks, in, Google Patents, 1985.
[33] S. Ernst, J. Weitkamp, J.A. Martens, P.A. Jacobs, Synthesis and shape-selective properties of ZSM-22, Applied catalysis, 48 (1989) 137-148.
[34] X. Zhu, S. Liu, Y. Song, L. Xu, Catalytic cracking of C4 alkenes to propene and ethene: Influences of zeolites pore structures and Si/Al< sub> 2</sub> ratios, Applied Catalysis A: General, 288 (2005) 134-142.
[35] D. Ji, B. Wang, G. Qian, Q. Gao, G. Lü, L. Yan, J. Suo, A highly efficient catalytic C4 alkane cracking over zeolite ZSM-23, Catalysis Communications, 6 (2005) 297-300.
[36] C.T. Kresge, J.P. McWilliams, M.P. Nicoletti, J.C. Vartuli, Catalyst for alkylation of aromatic hydrocarbons, in, Google Patents, 1985.
[37] R.S. Bridges, R.B. Halsey, D.H. Powers, Method of producing olefins from petroleum residua, in, Google Patents, 2001.
[38] P. Mériaudeau, V.A. Tuan, V.T. Nghiem, G. Sapaly, C. Naccache, Comparative Evaluation of the Catalytic Properties of SAPO-31 and ZSM-48 for the Hydroisomerization of< i> N-Octane</i>: Effect of the Acidity, Journal of Catalysis, 185 (1999) 435-444.
[39] T.E. Helton, W.F. Lai, D.N. Mazzone, High activity ZSM-48 and methods for dewaxing, in, Google Patents, 2009.

[40] H.P. Wang, K.S. Lin, Y. Huang, M. Li, L. Tsaur, Synthesis of zeolite ZSM-48 from rice husk ash, Journal of hazardous materials, 58 (1998) 147-152.
[41] G. Zhao, J. Teng, Y. Zhang, Z. Xie, Y. Yue, Q. Chen, Y. Tang, Synthesis of ZSM-48 zeolites and their catalytic performance in C< sub> 4</sub>-olefin cracking reactions, Applied Catalysis A: General, 299 (2006) 167-174.
[42] J.L. Casci, B.M. Lowe, T.V. Whittam, Zeolite EU-1 and a method of making zeolite EU-1, in, Google Patents, 1985.
[43] P. Raybaud, A. Patrigeon, H. Toulhoat, The Origin of the C< sub> 7</sub>-Hydroconversion Selectivities on Y, β, ZSM-22, ZSM-23, and EU-1 Zeolites, Journal of Catalysis, 197 (2001) 98-112.
[44] G. Rao, R. Kumar, P. Ratnasamy, Shape selectivity of zeolite EU-1 in reactions of aromatic hydrocarbons, Applied catalysis, 49 (1989) 307-318.
[45] C. Baerlocher, L.B. McCusker, D.H. Olson, Atlas of zeolite framework types, Elsevier, 2007.
[46] F.G. Dwyer, E.W. Valyocsik, Highly siliceous porous crystalline material, in, Google Patents, 1994.
[47] C.A. Fyfe, G.T. Kokotailo, H. Strobl, C. Pasztor, G. Barlow, S. Bradley, Combined use of nuclear magnetic resonance, electron microscopy, and diffraction techniques as a probe of the uniqueness of zeolite structures: zeolites KZ-2, Theta-1, ZSM-22, and NU-10, Zeolites, 9 (1989) 531-534.
[48] G. Kokotailo, P. Chu, S. Lawton, W. Meier, Synthesis and structure of synthetic zeolite ZSM-11, (1978).
[49] G. Kokotailo, J. Schlenker, F. Dwyer, E. Valyocsik, The framework topology of ZSM-22: A high silica zeolite, Zeolites, 5 (1985) 349-351.
[50] S.A.I. Barri, D.A. Kidd, Process for the preparation of branched olefins, in, EP Patent 0,485,145, 1992.
[51] M.E. Davis, R.J. Davis, Fundamentals of chemical reaction engineering, Courier Dover Publications, 2012.
[52] J.M. Thomas, W.J. Thomas, J. Anderson, M. Boudart, Principles and practice of heterogeneous catalysis, VCH Weinheim, 1997.
[53] O. Levenspiel, Chemical reaction engineering, Wiley New York etc., 1972.
[54] C.D. Chang, C.T. Chu, P.D. Perkins, E.W. Valyocsik, Olefins from methanol and/or dimethyl ether, in, Google Patents, 1984.
[55] S. Teketel, U. Olsbye, K.-P. Lillerud, P. Beato, S. Svelle, Selectivity control through fundamental mechanistic insight in the conversion of methanol to hydrocarbons over zeolites, Microporous and Mesoporous Materials, 136 (2010) 33-41.
[56] W. Song, D.M. Marcus, H. Fu, J.O. Ehresmann, J.F. Haw, An oft-studied reaction that may never have been: Direct catalytic conversion of methanol or dimethyl ether to hydrocarbons on the solid acids HZSM-5 or HSAPO-34, Journal of the American Chemical Society, 124 (2002) 3844-3845.
[57] R. Dessau, On the H-ZSM-5 catalyzed formation of ethylene from methanol or higher olefins, Journal of Catalysis, 99 (1986) 111-116.
[58] R. Dessau, R. LaPierre, On the mechanism of methanol conversion to hydrocarbons over HZSM-5, Journal of Catalysis, 78 (1982) 136-141.
[59] K. Hemelsoet, A. Nollet, M. Vandichel, D. Lesthaeghe, V. Van Speybroeck, M. Waroquier, The Effect of Confined Space on the Growth of Naphthalenic Species in a

Chabazite-Type Catalyst: A Molecular Modeling Study, ChemCatChem, 1 (2009) 373-378.
[60] W. Song, H. Fu, J.F. Haw, Selective synthesis of methylnaphthalenes in HSAPO-34 cages and their function as reaction centers in methanol-to-olefin catalysis, The Journal of Physical Chemistry B, 105 (2001) 12839-12843.
[61] B.P. Hereijgers, F. Bleken, M.H. Nilsen, S. Svelle, K.-P. Lillerud, M. Bjørgen, B.M. Weckhuysen, U. Olsbye, Product shape selectivity dominates the Methanol-to-Olefins (MTO) reaction over H-SAPO-34 catalysts, Journal of catalysis, 264 (2009) 77-87.
[62] S. Svelle, U. Olsbye, F. Joensen, M. Bjørgen, Conversion of methanol to alkenes over medium-and large-pore acidic zeolites: steric manipulation of the reaction intermediates governs the ethene/propene product selectivity, The Journal of Physical Chemistry C, 111 (2007) 17981-17984.
[63] M. Bjørgen, S. Svelle, F. Joensen, J. Nerlov, S. Kolboe, F. Bonino, L. Palumbo, S. Bordiga, U. Olsbye, Conversion of methanol to hydrocarbons over zeolite H-ZSM-5: On the origin of the olefinic species, Journal of Catalysis, 249 (2007) 195-207.
[64] Z.M. Cui, Q. Liu, W.G. Song, L.J. Wan, Insights into the mechanism of methanol-to-olefin conversion at zeolites with systematically selected framework structures, Angewandte Chemie International Edition, 45 (2006) 6512-6515.
[65] Z.-M. Cui, Q. Liu, Z. Ma, S.-W. Bian, W.-G. Song, Direct observation of olefin homologations on zeolite ZSM-22 and its implications to methanol to olefin conversion, Journal of Catalysis, 258 (2008) 83-86.
[66] Z.-M. Cui, Q. Liu, S.-W. Bain, Z. Ma, W.-G. Song, The role of methoxy groups in methanol to olefin conversion, The Journal of Physical Chemistry C, 112 (2008) 2685-2688.
[67] Q. Wang, Z.-M. Cui, C.-Y. Cao, W.-G. Song, 0.3 Å Makes the Difference: Dramatic Changes in Methanol-to-Olefin Activities between H-ZSM-12 and H-ZSM-22 Zeolites, The Journal of Physical Chemistry C, 115 (2011) 24987-24992.
[68] J. Li, Y. Qi, Z. Liu, G. Liu, D. Zhang, Co-reaction of Ethene and Methylation Agents over SAPO-34 and ZSM-22, Catalysis Letters, 121 (2008) 303-310.
[69] S. Teketel, S. Svelle, K.P. Lillerud, U. Olsbye, Shape-Selective Conversion of Methanol to Hydrocarbons Over 10-Ring Unidirectional-Channel Acidic H-ZSM-22, ChemCatChem, 1 (2009) 78-81.
[70] J. Li, Y. Wei, G. Liu, Y. Qi, P. Tian, B. Li, Y. He, Z. Liu, Comparative study of MTO conversion over SAPO-34, H-ZSM-5 and H-ZSM-22: Correlating catalytic performance and reaction mechanism to zeolite topology, Catalysis Today, 171 (2011) 221-228.
[71] S. Teketel, W. Skistad, S. Benard, U. Olsbye, K.P. Lillerud, P. Beato, S. Svelle, Shape Selectivity in the Conversion of Methanol to Hydrocarbons: The Catalytic Performance of One-Dimensional 10-Ring Zeolites: ZSM-22, ZSM-23, ZSM-48, and EU-1, ACS Catalysis, 2 (2011) 26-37.
[72] J. Li, Y. Wei, Y. Qi, P. Tian, B. Li, Y. He, F. Chang, X. Sun, Z. Liu, Conversion of methanol over H-ZSM-22: The reaction mechanism and deactivation, Catalysis Today, 164 (2011) 288-292.
[73] F.-F. Wei, Z.-M. Cui, X. Meng, C.-Y. Cao, F.-S. Xiao, W.-G. Song, Origin of the low olefin production over HZSM-22 and HZSM-23 Zeolites: External Acid Sites and Pore Mouth Catalysis, ACS Catalysis, (2013).

[74] T. Behrsing, H. Jaeger, J. Sanders, Coke deposits on H-ZSM-5 zeolite, Applied catalysis, 54 (1989) 289-302.
[75] L. Palumbo, F. Bonino, P. Beato, M. Bjørgen, A. Zecchina, S. Bordiga, Conversion of methanol to hydrocarbons: Spectroscopic characterization of carbonaceous species formed over H-ZSM-5, The Journal of Physical Chemistry C, 112 (2008) 9710-9716.
[76] D.J. Klocke, J.C. Vartuli, G.W. Kirker, Synthesis of zeolites ZSM-22 and ZSM-23, in, EP Patent 0,220,893, 1987.
[77] G.W. Kirker, D.J. Klocke, J.C. Vartuli, P. Chu, D.O. Marler, J.P. McWilliams, Zeolite synthesis using an alcohol or like molecule, in, Google Patents, 1991.
[78] T.L. Maesen, M. Schenk, T. Vlugt, J.d. Jonge, B. Smit, The shape selectivity of paraffin hydroconversion on TON-, MTT-, and AEL-type sieves, Journal of Catalysis, 188 (1999) 403-412.
[79] K. Hayasaka, D. Liang, W. Huybrechts, B.R. De Waele, K.J. Houthoofd, P. Eloy, E.M. Gaigneaux, G. Van Tendeloo, J.W. Thybaut, G.B. Marin, Formation of ZSM-22 Zeolite Catalytic Particles by Fusion of Elementary Nanorods, Chemistry-A European Journal, 13 (2007) 10070-10077.
[80] T. Tago, T. Masuda, Zeolite nanocrystals-synthesis and applications.
[81] H. Konno, T. Okamura, Y. Nakasaka, T. Tago, T. Masuda, Effects of crystal size and Si/Al ratio of MFI-type zeolite catalyst on n-hexane cracking for light olefin synthesis, Journal of the Japan Petroleum Institute, 55 (2012) 267-274.
[82] G. Calzaferri, S. Huber, H. Maas, C. Minkowski, Host–guest antenna materials, Angewandte Chemie International Edition, 42 (2003) 3732-3758.
[83] M. Veiga-Gutiérrez, M. Woerdemann, E. Prasetyanto, C. Denz, L. De Cola, Assembly: Optical-Tweezers Assembly-Line for the Construction of Complex Functional Zeolite L Structures (Adv. Mater. 38/2012), Advanced Materials, 24 (2012) 5198-5198.
[84] A. Kuperman, S. Nadimi, S. Oliver, G.A. Ozin, J.M. Garcés, M.M. Olken, Non-aqueous synthesis of giant crystals of zeolites and molecular sieves, (1993).
[85] G.A. Tompsett, W.C. Conner, K.S. Yngvesson, Microwave synthesis of nanoporous materials, ChemPhysChem, 7 (2006) 296-319.
[86] S.-E. Park, J.-S. Chang, Y.K. Hwang, D.S. Kim, S.H. Jhung, J.S. Hwang, Supramolecular interactions and morphology control in microwave synthesis of nanoporous materials, Catalysis surveys from Asia, 8 (2004) 91-110.
[87] S. Laha, G. Kamalakar, R. Gläser, Microwave-assisted synthesis of [Cr] APO-5, Microporous and mesoporous materials, 90 (2006) 45-52.
[88] H. Robson, Verified synthesis of zeolitic materials, Access Online via Elsevier, 2001.
[89] P. Chu, F.G. Dwyer, J.C. Vartuli, Crystallization method employing microwave radiation, in, Google Patents, 1988.
[90] X. Chen, W. Yan, X. Cao, J. Yu, R. Xu, Fabrication of silicalite-1 crystals with tunable aspect ratios by microwave-assisted solvothermal synthesis, Microporous and Mesoporous Materials, 119 (2009) 217-222.
[91] X. Chen, W. Yan, W. Shen, J. Yu, X. Cao, R. Xu, Morphology control of self-stacked silicalite-1 crystals using microwave-assisted solvothermal synthesis, Microporous and mesoporous materials, 104 (2007) 296-304.

[92] A. Mitra, Z. Wang, T. Cao, H. Wang, L. Huang, Y. Yan, Synthesis and corrosion resistance of high-silica zeolite MTW, BEA, and MFI coatings on steel and aluminum, Journal of The Electrochemical Society, 149 (2002) B472-B478.
[93] X. Xu, W. Yang, J. Liu, L. Lin, Synthesis of a high-permeance NaA zeolite membrane by microwave heating, Advanced Materials, 12 (2000) 195-198.
[94] O. Muraza, E.V. Rebrov, J. Chen, M. Putkonen, L. Niinistö, M.H. de Croon, J.C. Schouten, Microwave-assisted hydrothermal synthesis of zeolite Beta coatings on ALD-modified borosilicate glass for application in microstructured reactors, Chemical Engineering Journal, 135 (2008) S117-S120.
[95] A. Arafat, J. Jansen, A. Ebaid, H. Van Bekkum, Microwave preparation of zeolite Y and ZSM-5, Zeolites, 13 (1993) 162-165.
[96] N. Esmaeili, H. Kazemian, D. Bastani, Synthesis of Nano Particles of LTA Zeolite by Means of Microemulsion Technique, IRANIAN JOURNAL OF CHEMISTRY AND CHEMICAL ENGINEERING (IJCCE), (2011).
[97] R. Khomane, B. Kulkarni, R. Ahedi, Synthesis and characterization of ferrierite-type zeolite in the presence of nonionic surfactants, Journal of colloid and interface science, 236 (2001) 208-213.
[98] G.J. Myatt, P.M. Budd, C. Price, F. Hollway, S.W. Carr, The influence of surfactants and water-soluble polymers on the crystallization of zeolite NaA, Zeolites, 14 (1994) 190-197.
[99] M.K. Naskar, A. Das, D. Kundu, M. Chatterjee, Emulsion-based synthesis of NaA zeolite nanocrystals and its integration towards NaA membranes, Bulletin of Materials Science, 34 (2011) 651-659.
[100] W.C. Griffin, Classification of surface-active agents by" HLB", J Soc Cosmetic Chemists, 1 (1946) 311-326.
[101] W.C. Griffin, Calculation of HLB values of non-ionic surfactants, Am Perfumer Essent Oil Rev, 65 (1955) 26-29.
[102] F. Arriagada, K. Osseo-Asare, Synthesis of nanosize silica in a nonionic water-in-oil microemulsion: effects of the water/surfactant molar ratio and ammonia concentration, Journal of Colloid and Interface Science, 211 (1999) 210-220.
[103] Z. Chen, S. Li, Y. Yan, Synthesis of template-free zeolite nanocrystals by reverse microemulsion-microwave method, Chemistry of materials, 17 (2005) 2262-2266.
[104] K. Osseo-Asare, F. Arriagada, Growth kinetics of nanosize silica in a nonionic water-in-oil microemulsion: a reverse micellar pseudophase reaction model, Journal of colloid and interface science, 218 (1999) 68-76.
[105] O. Muraza, T. Tago, S. Fujiwara, H. Konno, T. Okamura, Y. Nakasaka, T. Masuda, FABRICATION OF SUBMICRON TON ZEOLITES VIA MICROEMULSION-ASSISTED SYNTHESIS: TOWARDS EFFICIENT 1-D PORE SYSTEM.
[106] J. Yao, L. Zhang, H. Wang, Synthesis of nanocrystalline sodalite with organic additives, Materials Letters, 62 (2008) 4028-4030.
[107] C.J. Plank, E.J. Rosinski, M.K. Rubin, Method for producing zeolites, in, Google Patents, 1979.
[108] A.G. Gomez, G. de Silveira, H. Doan, C.-H. Cheng, A facile method to tune zeolite L crystals with low aspect ratio, Chemical Communications, 47 (2011) 5876-5878.

[109] Y. Huang, J. Yao, X. Zhang, C.C. Kong, H. Chen, D. Liu, M. Tsapatsis, M.R. Hill, A.J. Hill, H. Wang, Role of ethanol in sodalite crystallization in an ethanol–Na2O–Al2O3–SiO2–H2O system, CrystEngComm, 13 (2011) 4714-4722.
[110] W. Song, R. Justice, C. Jones, V. Grassian, S. Larsen, Synthesis, characterization, and adsorption properties of nanocrystalline ZSM-5, Langmuir, 20 (2004) 8301-8306.
[111] A. Gaona-Gómez, C.-H. Cheng, Modification of zeolite L (LTL) morphology using diols,(OH)< sub> 2</sub>(CH< sub> 2</sub>)< sub> 2</sub>< i> n</i>< sub>+ 2</sub> O< i> n</i>(< i> n</i>= 0, 1, and 2), Microporous and Mesoporous Materials, 153 (2012) 227-235.
[112] D. Bibby, M. Dale, Synthesis of silica-sodalite from non-aqueous systems, Nature, 317 (1985) 157-158.
[113] H.G. Karge, J. Weitkamp, Adsorption and Diffusion, Springer, 2008.
[114] K.M. Lewis, H. Wang, Process for the recovery of alkoxysilanes obtained from the direct reaction of silicon with alkanols, in, Google Patents, 2008.
[115] S. Aldrich, Sigma Aldrich Technical Information Bulletin: Mineral Adsorbents, Filter Agents, and Drying Agents, in, Sigma Aldirch, St. Louis, MO, United States of America, 2013.
[116] D. Ginter, A. Bell, C. Radke, The effects of gel aging on the synthesis of NaY zeolite from colloidal silica, Zeolites, 12 (1992) 742-749.
[117] S. Alfaro, C. Rodriguez, M. Valenzuela, P. Bosch, Aging time effect on the synthesis of small crystal LTA zeolites in the absence of organic template, Materials Letters, 61 (2007) 4655-4658.
[118] V.P. Valtchev, A.-C. Faust, J. Lézervant, Rapid synthesis of silicalite-1 nanocrystals by conventional heating, Microporous and mesoporous materials, 68 (2004) 91-95.
[119] B.O. Hincapie, L.J. Garces, Q. Zhang, A. Sacco, S.L. Suib, Synthesis of mordenite nanocrystals, Microporous and mesoporous materials, 67 (2004) 19-26.
[120] Y. LIU, Z. WANG, Y. LING, X. LI, Y. LIU, P. WU, Synthesis of ZSM-23 Zeolite Using Isopropylamine as Template, Chinese Journal of Catalysis, 30 (2009) 525-530.
[121] Y. Hu, C. Liu, Y. Zhang, N. Ren, Y. Tang, Microwave-assisted hydrothermal synthesis of nanozeolites with controllable size, Microporous and Mesoporous Materials, 119 (2009) 306-314.
[122] L. Shirazi, E. Jamshidi, M. Ghasemi, The effect of Si/Al ratio of ZSM-5 zeolite on its morphology, acidity and crystal size, Crystal Research and Technology, 43 (2008) 1300-1306.
[123] R. Zhang, Y. Wang, W. Wu, Dynamic and Static Synthesis of ZSM-22 Zeolite and its Characterization.
[124] H. Yunfeng, W. Xiangsheng, G. Xinwen, L. Silue, H. Sheng, S. Haibo, B. Liang, Effects of channel structure and acidity of molecular sieves in hydroisomerization of n-octane over bi-functional catalysts, Catalysis letters, 100 (2005) 59-65.
[125] E.W. Valyocsik, Synthesis of zeolite ZSM-22, in, Google Patents, 1990.
[126] N. Kumar, L. Lindfors, R. Byggningsbacka, Synthesis and characterization of H-ZSM-22, Zn-H-ZSM-22 and Ga-H-ZSM-22 zeolite catalysts and their catalytic activity in the aromatization of n-butane, Applied Catalysis A: General, 139 (1996) 189-199.
[127] M. Asensi, A. Corma, A. Martínez, M. Derewinski, J. Krysciak, S. Tamhankar, Isomorphous substitution in ZSM-22 zeolite. The role of zeolite acidity and crystal size

during the skeletal isomerization of< i> n</i>-butene, Applied Catalysis A: General, 174 (1998) 163-175.
[128] R. Byggningsbacka, N. Kumar, L.-E. Lindfors, Comparative study of the catalytic properties of ZSM-22 and ZSM-35/ferrierite zeolites in the skeletal isomerization of 1-butene, Journal of Catalysis, 178 (1998) 611-620.
[129] D. Masih, T. Kobayashi, T. Baba, Hydrothermal synthesis of pure ZSM-22 under mild conditions, Chemical Communications, (2007) 3303-3305.
[130] O. Fouad, R. Mohamed, M. Hassan, I. Ibrahim, Effect of template type and template/silica mole ratio on the crystallinity of synthesized nanosized ZSM-5, Catalysis today, 116 (2006) 82-87.
[131] S. Sang, F. Chang, Z. Liu, C. He, Y. He, L. Xu, Difference of ZSM-5 zeolites synthesized with various templates, Catalysis Today, 93 (2004) 729-734.
[132] L. Ding, Y. Zheng, Effect of template concentration and gel dilution on crystallization and particle size of zeolite beta in the absence of alkali cations, Microporous and mesoporous materials, 103 (2007) 94-101.
[133] L. Ding, Y. Zheng, Nanocrystalline zeolite beta: The effect of template agent on crystal size, Materials research bulletin, 42 (2007) 584-590.
[134] J. Martens, P. Jacobs, Synthesis of high-silica aluminosilicate zeolites, Elsevier, 1987.
[135] S.P. Ždanov, S. Khvoshchev, N.N. Feoktistova, S. Zhdanov, S.S. Chvoščev, N.N. Feoktistova, Synthetic Zeolites: Crystallization, Gordon & Breach Science Pub, 1990.
[136] M. Stöcker, H. Karge, J. Jansen, J. Weitkamp, Advanced zeolite science and applications, Access Online via Elsevier, 1994.
[137] M. Derewinski, M. Machowska, Effect of stirring on the selective synthesis of mel or ton zeolites in the presence of 1, 8-diaminooctane, Studies in Surface Science and Catalysis, 154 (2004) 349-354.
[138] J.P. Verduijn, L.R.M. Martens, ZSM-22 zeolite, in, Google Patents, 1998.
[139] J.P. Verduijn, L.R.M. Martens, ZSM-22 zeolite, in, Google Patents, 1999.
[140] R. Finsy, On the critical radius in Ostwald ripening, Langmuir, 20 (2004) 2975-2976.
[141] R. Boistelle, J. Astier, Crystallization mechanisms in solution, Journal of Crystal Growth, 90 (1988) 14-30.
[142] A.I. Lupulescu, M. Kumar, J.D. Rimer, A Facile Strategy To Design Zeolite L Crystals with Tunable Morphology and Surface Architecture, Journal of the American Chemical Society, 135 (2013) 6608-6617.
[143] J. VERDUIJN, L. MARTENS, M. Roger, ZSM-22 ZEOLITE, in, WO Patent 1,993,025,475, 1993.
[144] T. Tago, H. Konno, M. Sakamoto, Y. Nakasaka, T. Masuda, Selective synthesis for light olefins from acetone over ZSM-5 zeolites with nano- and macro-crystal sizes, Applied Catalysis A: General, 403 (2011) 183-191.
[145] J. Yu, Synthesis of zeolites, Studies in Surface Science and Catalysis, 168 (2007) 39-103.
[146] L. Travalloni, A.C. Gomes, A.B. Gaspar, M.A. da Silva, Methanol conversion over acid solid catalysts, Catalysis Today, 133 (2008) 406-412.

[147] H. Konno, T. Okamura, T. Kawahara, Y. Nakasaka, T. Tago, T. Masuda, Kinetics of< i> n</i>-hexane cracking over ZSM-5 zeolites–Effect of crystal size on effectiveness factor and catalyst lifetime, Chemical Engineering Journal, 207 (2012) 490-496.
[148] C. Chmelik, E. Lehmann, S. Vasenkov, B. Staudte, J. Kärger, Application of Interference and IR Microscopy for Studies of Intracrystalline Molecular Transport in AFI Type Zeolites, in: Fluid Transport in Nanoporous Materials, Springer, 2006, pp. 575-581.
[149] F.J. Keil, J. Hinderer, A.R. Garayhi, Diffusion and reaction in ZSM-5 and composite catalysts for the methanol-to-olefins process, Catalysis today, 50 (1999) 637-650.

VITAE

Name :Anas Karrar Jamil Abdelrahman

Nationality :Sudanese

Date of Birth March 13, 1987

Email :anas200007@hotmail.com

anasjamil20007@gmail.com

Address

:LinkedIn: sa.linkedin.com/pub/anas-jamil/48/75b/350/

Mobile Numbers: +966 056 5376 599.

Department of Chemical Engineering P.O. Box 8675KFUPM campus, Dhahran 31261Saudi Arabia

Academic Background

:MS Chemical Engineering, April 2014

King Fahd University of Petroleum and Minerals, Dhahran, Saudi Arabia.

BSc Chemical Engineering, September 2010

University of Khartoum, Khartoum, Sudan.